Electronic Supporting Information

Reactions of [$(dmpe)_2MnH(C_2H_4)$] with Hydrogermanes to Form Germylene, Germyl, Hydrogermane, and Germanide Complexes

Jeffrey S. Price, Ignacio Vargas-Baca, David J. H. Emslie,* and James F. Britten

Department of Chemistry, McMaster University, 1280 Main Street West, Hamilton, Ontario, L8S 4M1, Canada. Fax: (905)-522-2509; Tel: (905)-525-9140 x 23307

E-mail: emslied@mcmaster.ca

Website: https://emsliegroup.mcmaster.ca/

The supplemental file Cartesian_coordinates_for_calculated_structures.xyz contains the computed Cartesian coordinates of all of the molecules reported in this study. The file may be opened as a text file to read the coordinates, or opened directly by a molecular modeling program such as Mercury (version 3.3 or later, http://www.ccdc.cam.ac.uk/pages/Home.aspx) for visualization and analysis.

Contents **Pages**

Selected Abbreviations;

Dmpe = 1,2-bis(dimethylphosphino)ethane
sat. = satellite

Selected NMR Spectra for Complexes 2a-b, 3a-b, 4a-b, 5a-b, and 6.

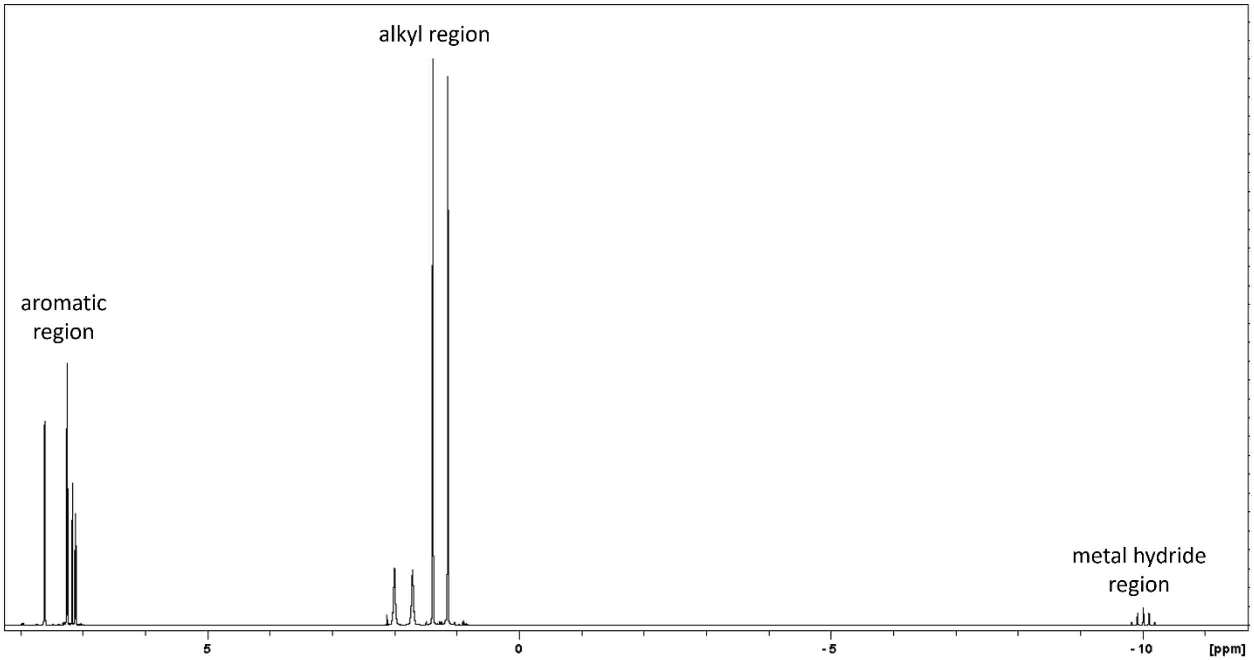

Figure S1. ^1H NMR spectrum of $[(dmpe)_2MnH(=GePh_2)]$ (**2a**) in C_6D_6 (600 MHz, 298 K).

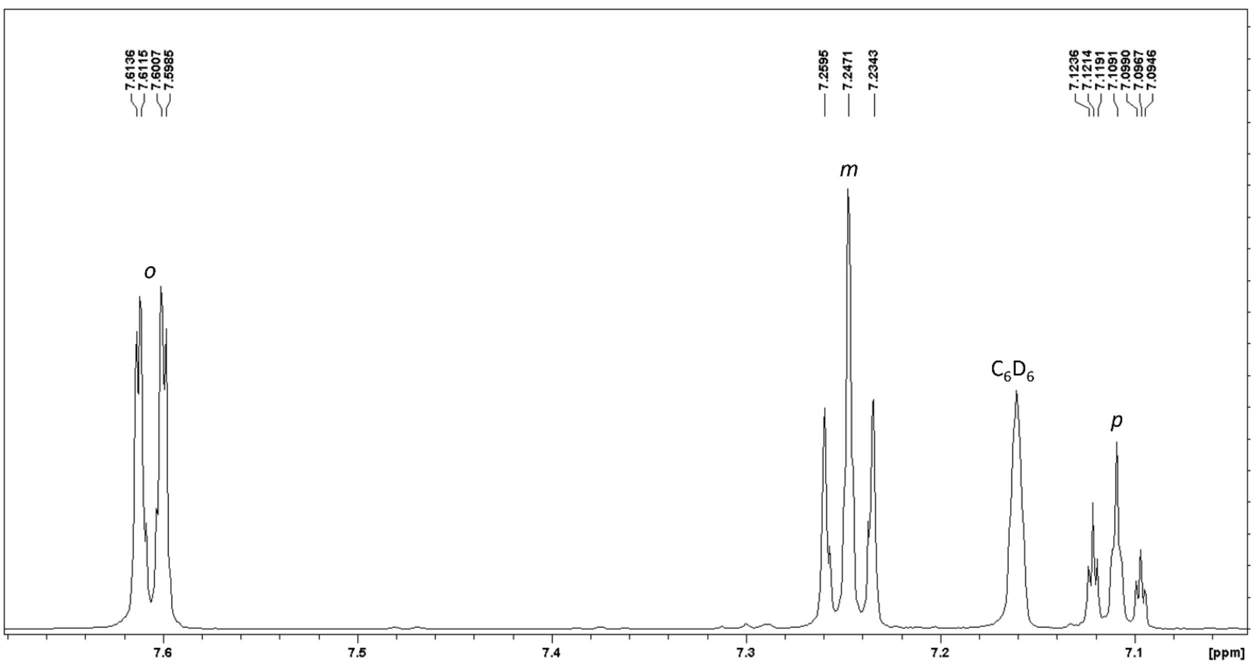

Figure S2. Expanded aromatic region of the ^1H NMR spectrum of $[(dmpe)_2MnH(=GePh_2)]$ (**2a**) in C_6D_6 (600 MHz, 298 K).

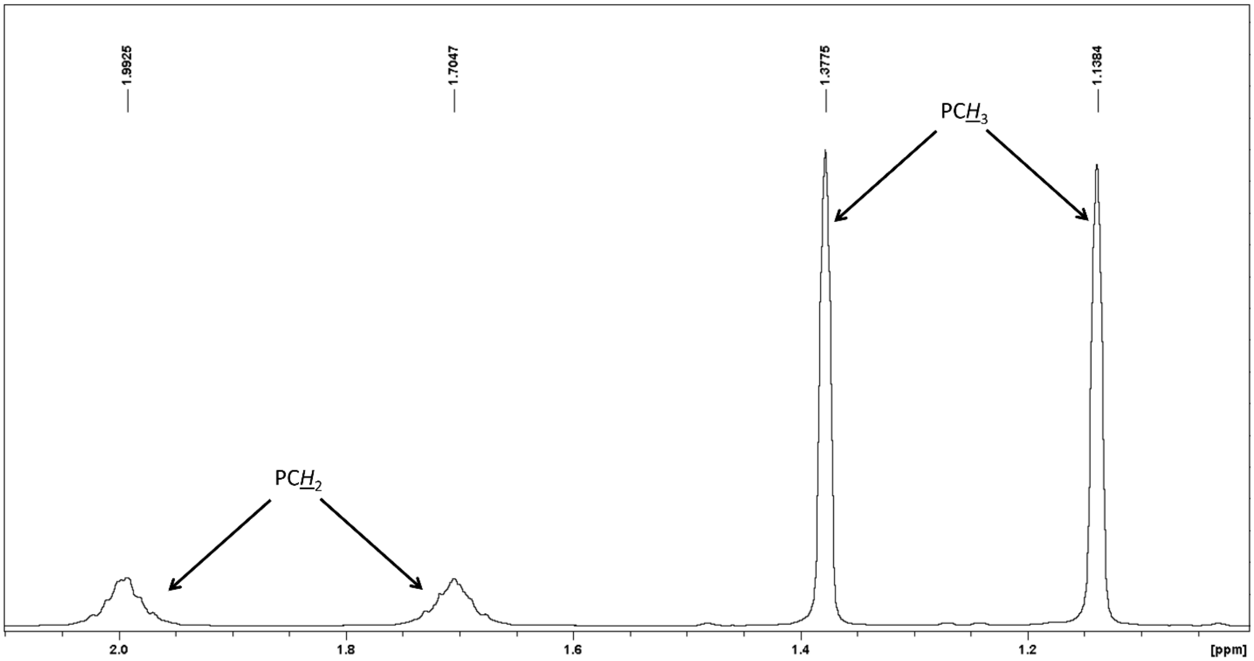

Figure S3. Expanded alkyl region of the ^{1}H NMR spectrum of [(dmpe)$_2$MnH(=GePh$_2$)] (**2a**) in C_6D_6 (600 MHz, 298 K).

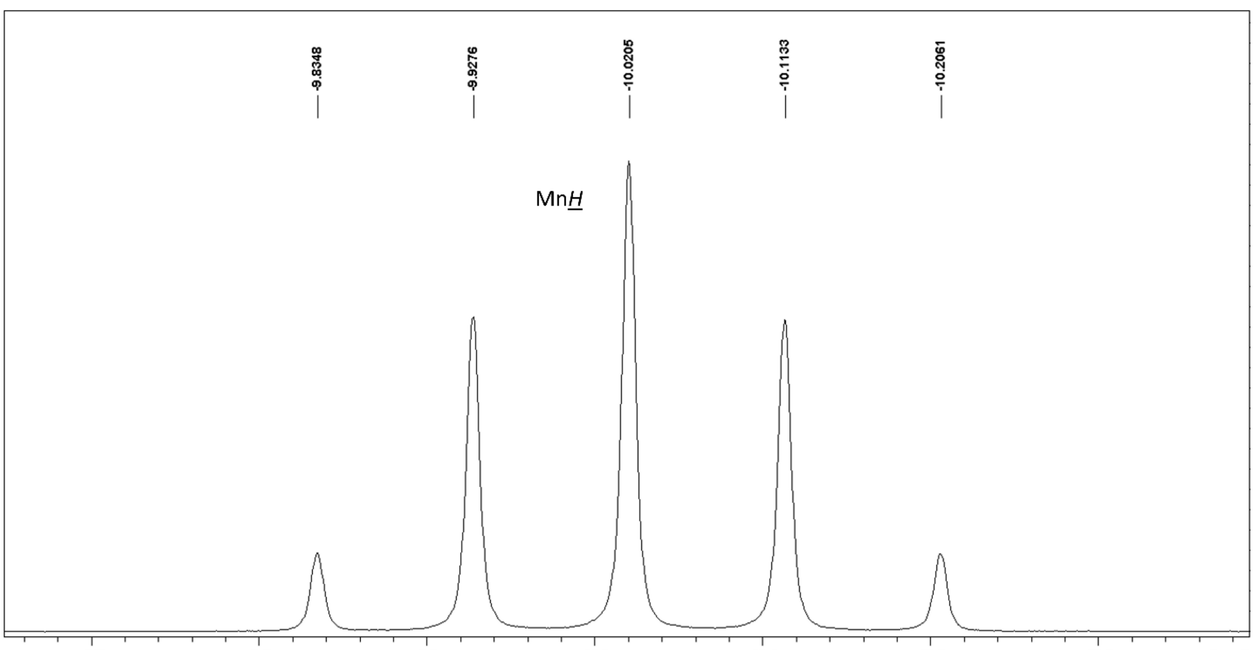

Figure S4. Expanded metal hydride region of the ^{1}H NMR spectrum of [(dmpe)$_2$MnH(=GePh$_2$)] (**2a**) in C_6D_6 (600 MHz, 298 K).

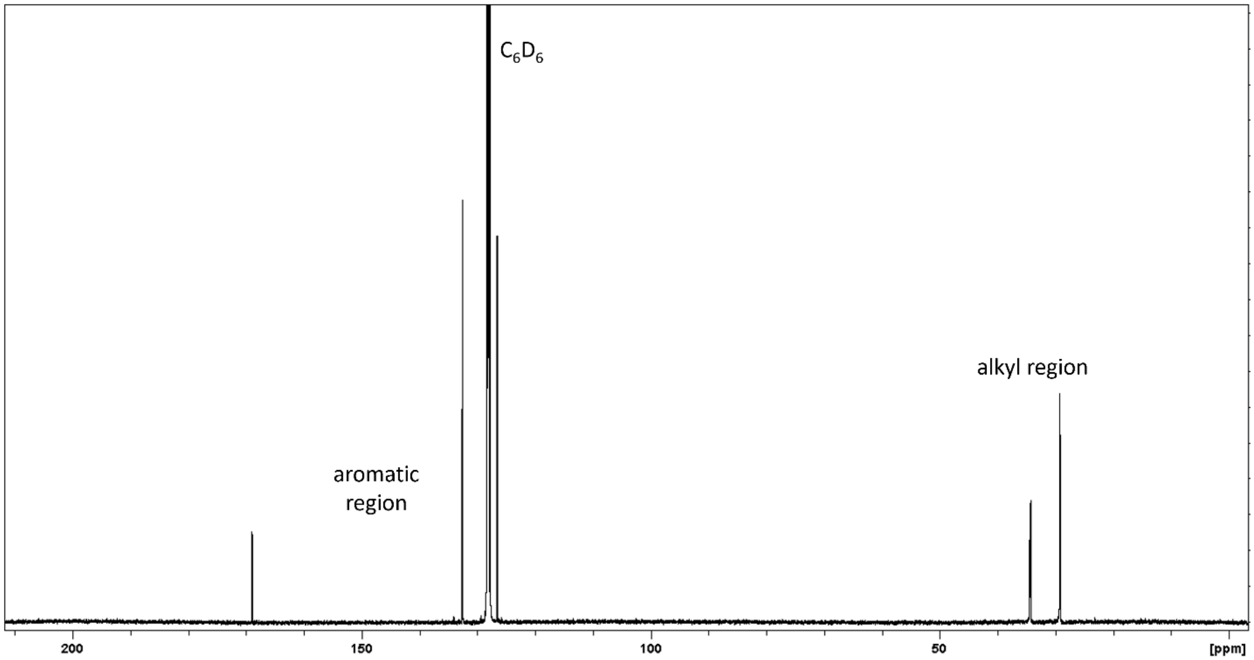

Figure S5. $^{13}C\{^1H\}$ NMR spectrum of $[(dmpe)_2MnH(=GePh_2)]$ (**2a**) in C_6D_6 (151 MHz, 298 K).

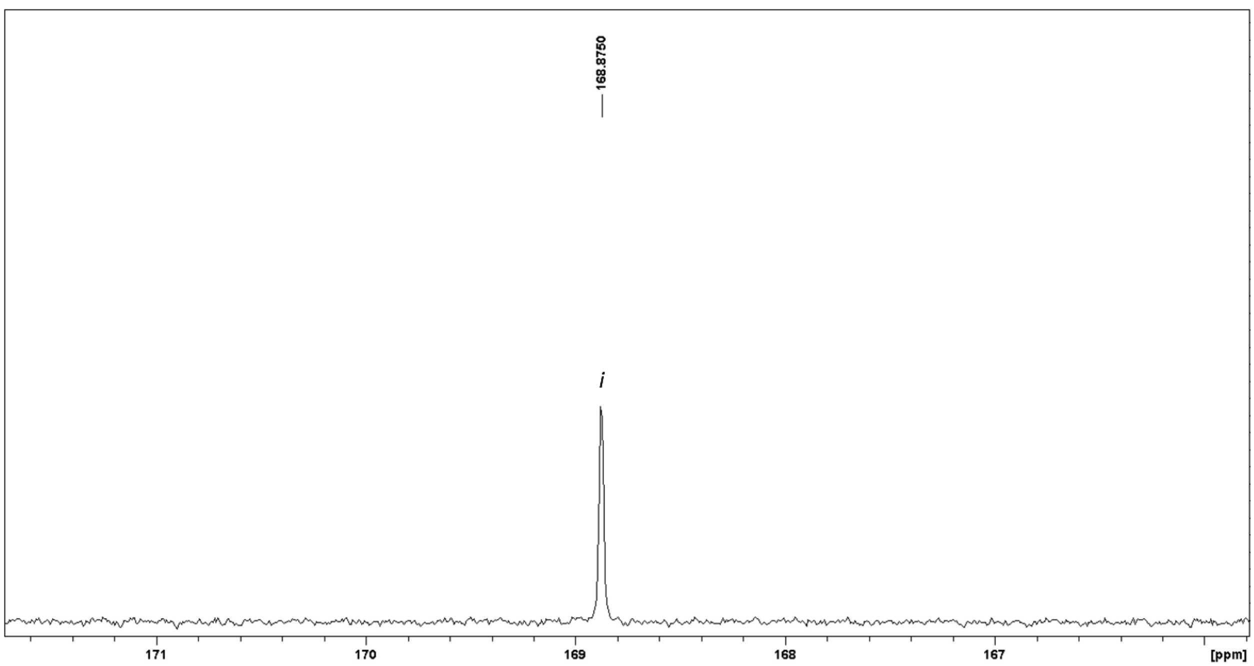

Figure S6. Expanded higher frequency aromatic region of the $^{13}C\{^1H\}$ NMR spectrum of $[(dmpe)_2MnH(=GePh_2)]$ (**2a**) in C_6D_6 (151 MHz, 298 K).

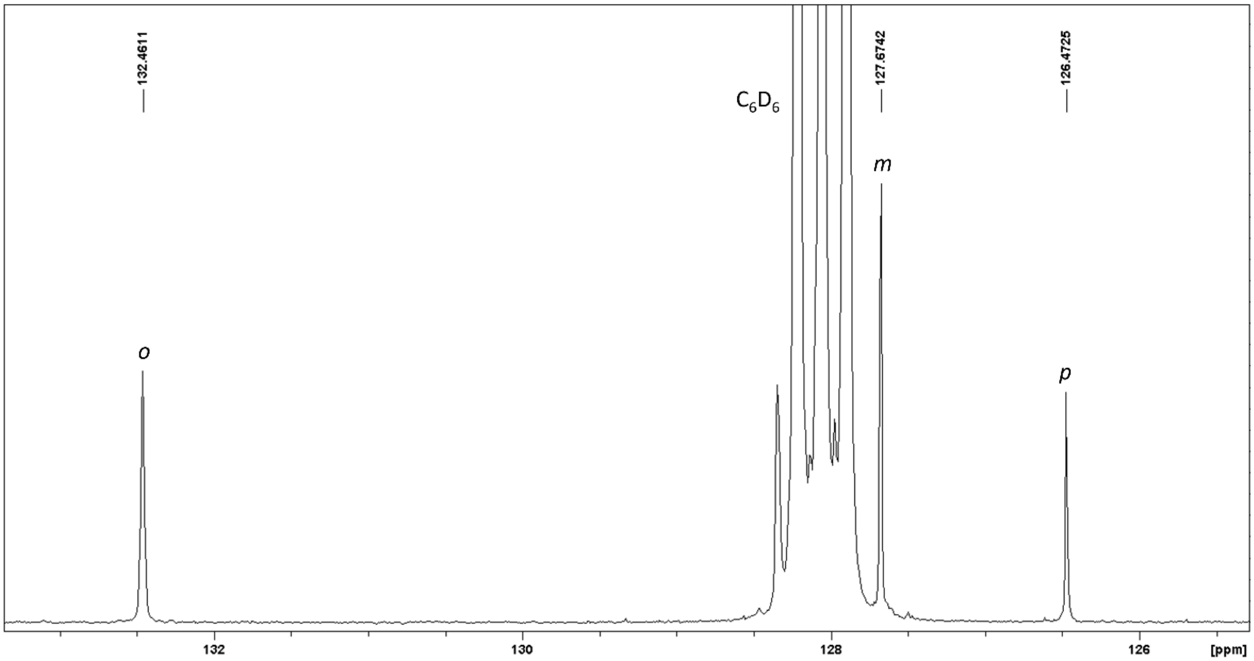

Figure S7. Expanded lower frequency aromatic region of the $^{13}C\{^1H\}$ NMR spectrum of $[(dmpe)_2MnH(=GePh_2)]$ (**2a**) in C_6D_6 (151 MHz, 298 K).

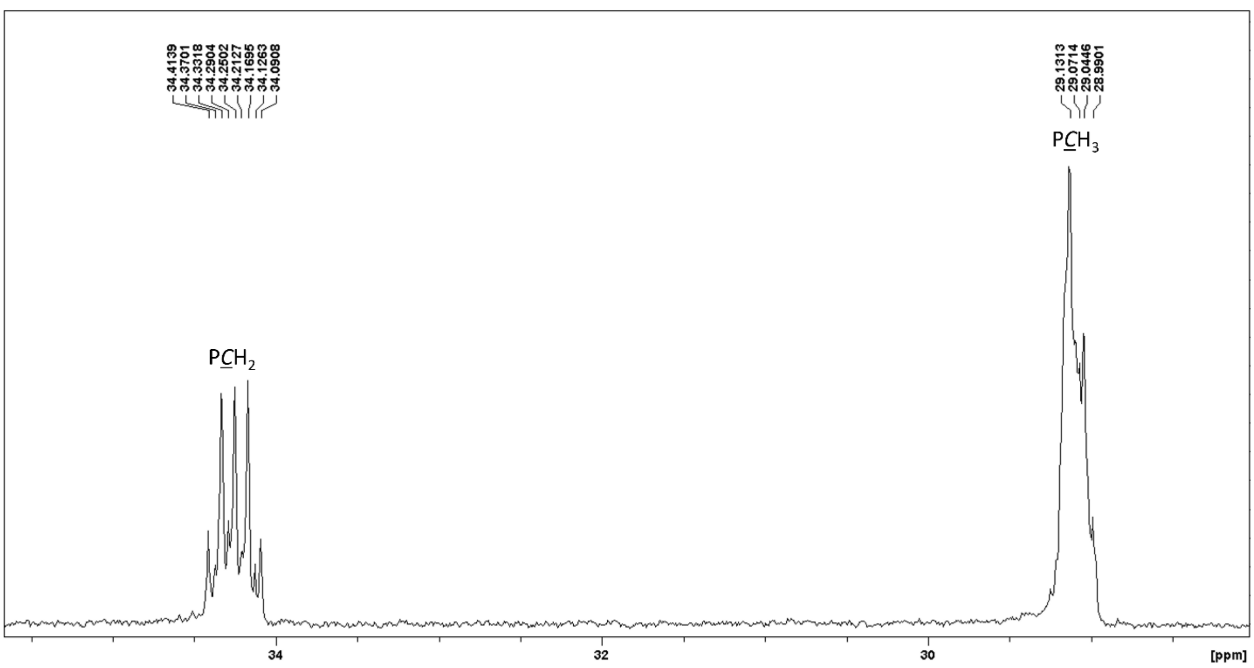

Figure S8. Expanded alkyl region of the $^{13}C\{^1H\}$ NMR spectrum of $[(dmpe)_2MnH(=GePh_2)]$ (**2a**) in C_6D_6 (151 MHz, 298 K).

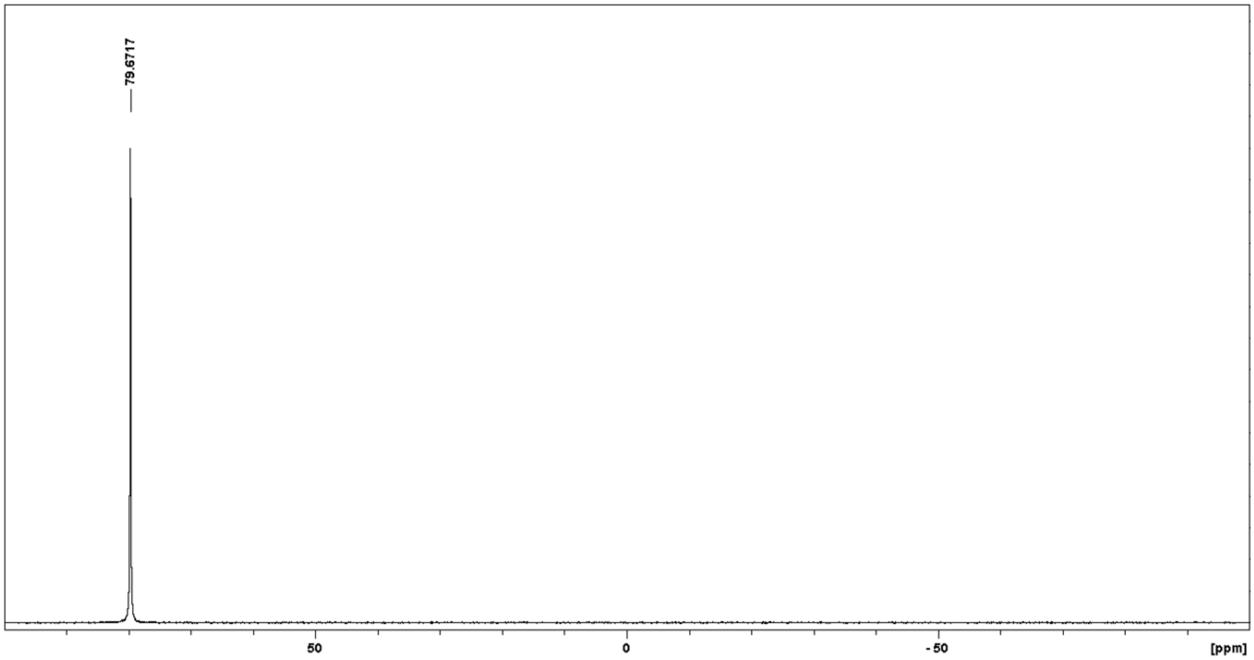

Figure S9. $^{31}P\{^{1}H\}$ NMR spectrum of [(dmpe)$_2$MnH(=GePh$_2$)] (**2a**) in C_6D_6 (243 MHz, 298 K).

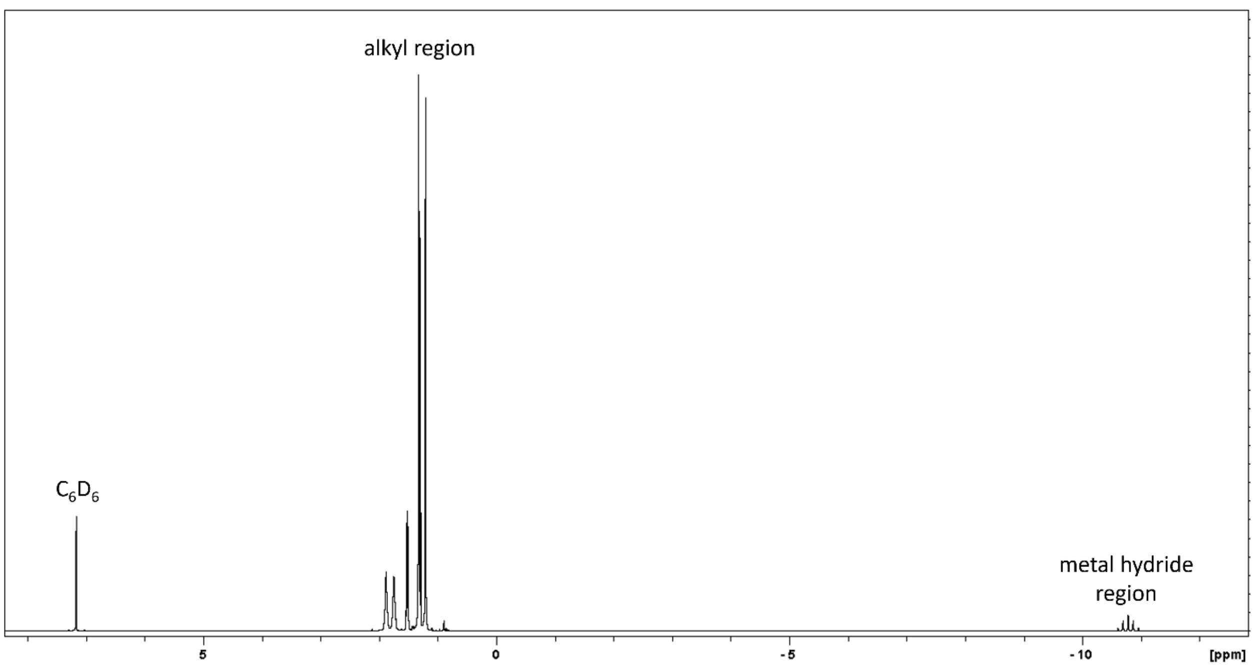

Figure S10. ^{1}H NMR spectrum of [(dmpe)$_2$MnH(=GeEt$_2$)] (**2b**) in C_6D_6 (600 MHz, 298 K).

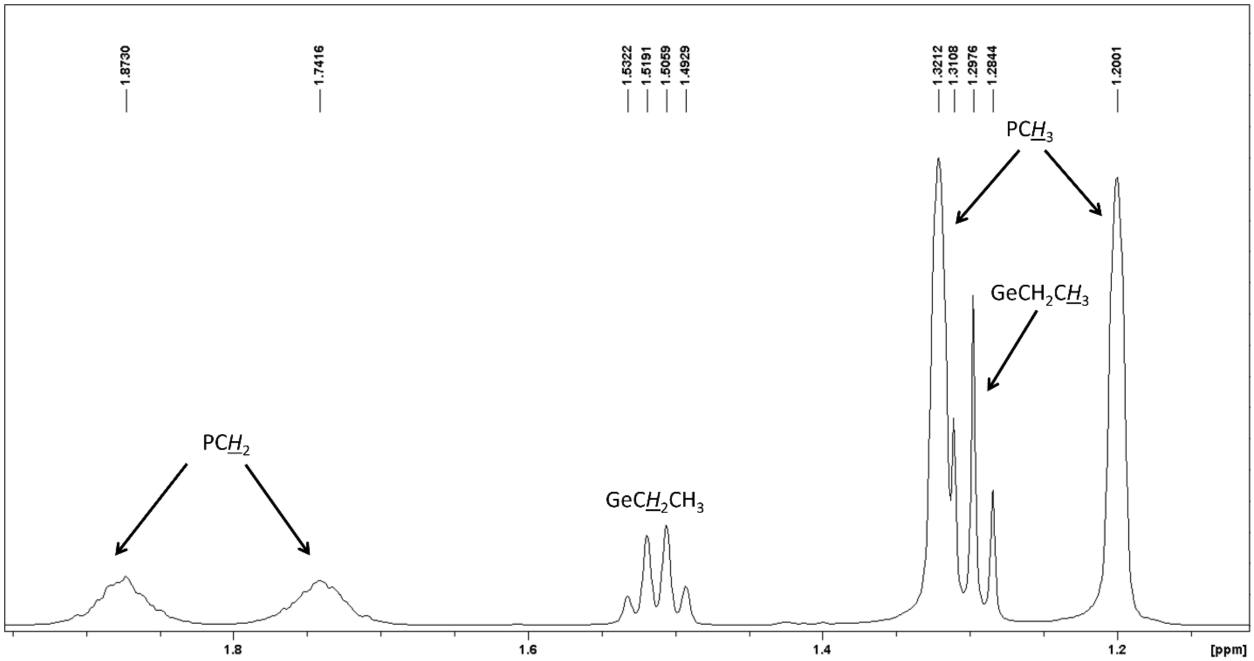

Figure S11. Expanded alkyl region of the ^{1}H NMR spectrum of [(dmpe)$_2$MnH(=GeEt$_2$)] (**2b**) in C_6D_6 (600 MHz, 298 K).

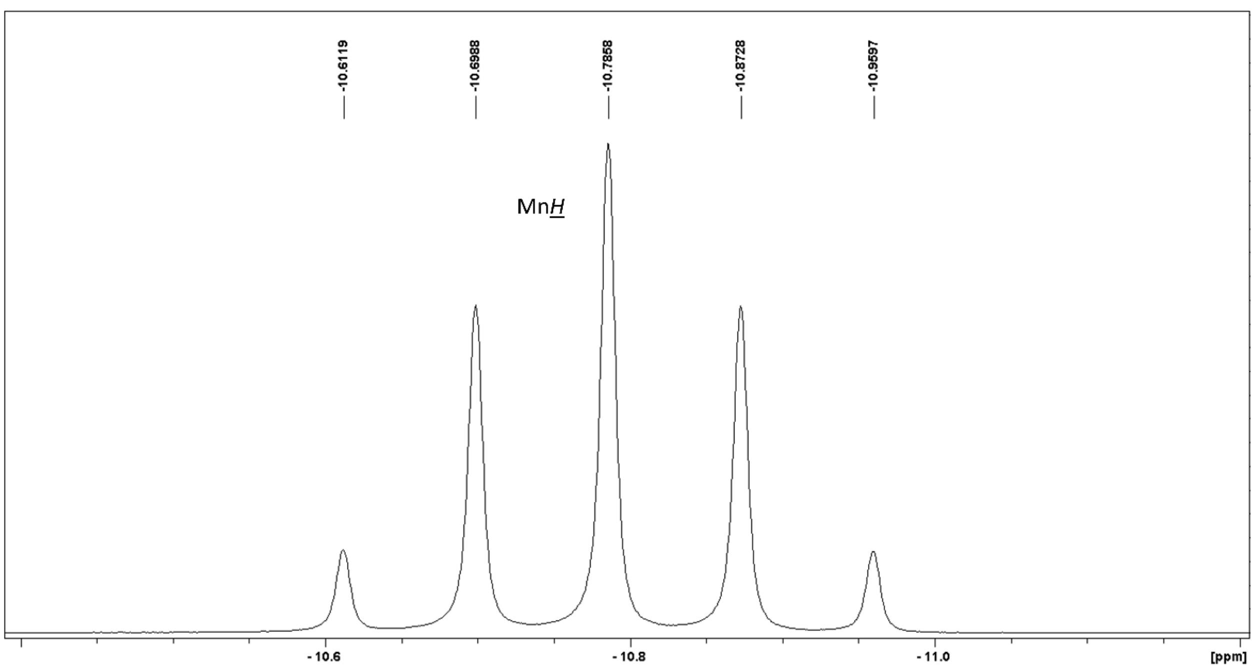

Figure S12. Expanded metal hydride region of the ^{1}H NMR spectrum of [(dmpe)$_2$MnH(=GeEt$_2$)] (**2b**) in C_6D_6 (600 MHz, 298 K).

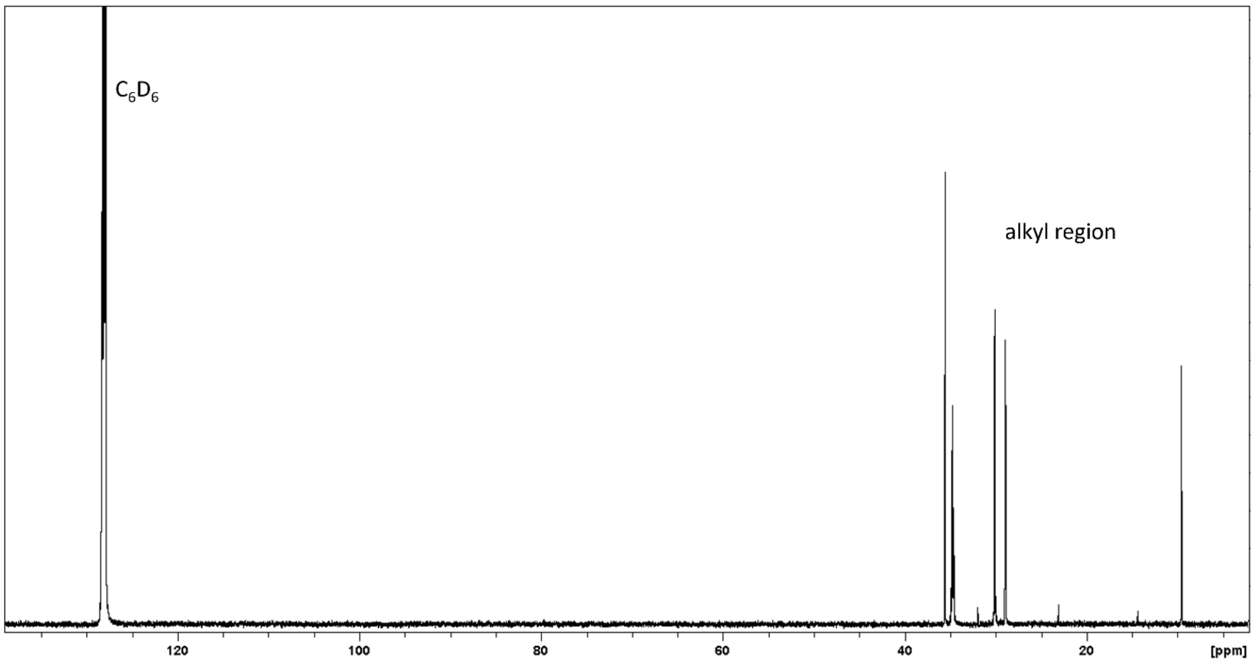

Figure S13. $^{13}C\{^1H\}$ NMR spectrum of [(dmpe)$_2$MnH(=GeEt$_2$)] (**2b**) in C_6D_6 (151 MHz, 298 K).

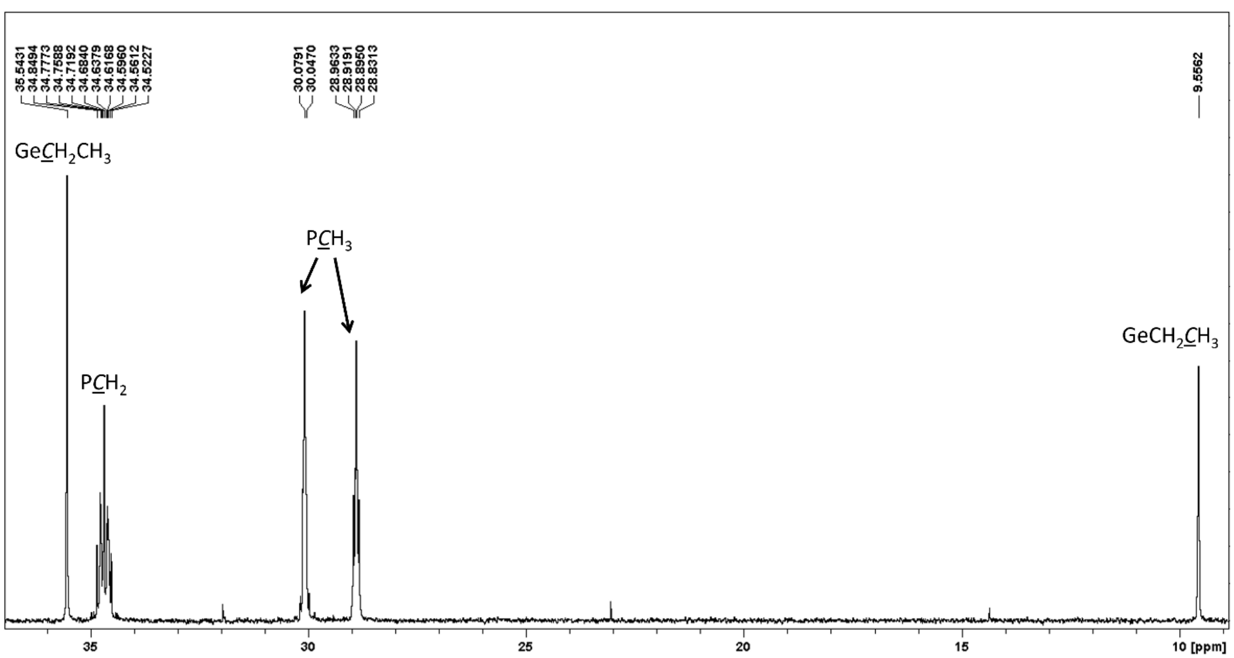

Figure S14. Expanded alkyl region of the $^{13}C\{^1H\}$ NMR spectrum of [(dmpe)$_2$MnH(=GeEt$_2$)] (**2b**) in C_6D_6 (151 MHz, 298 K).

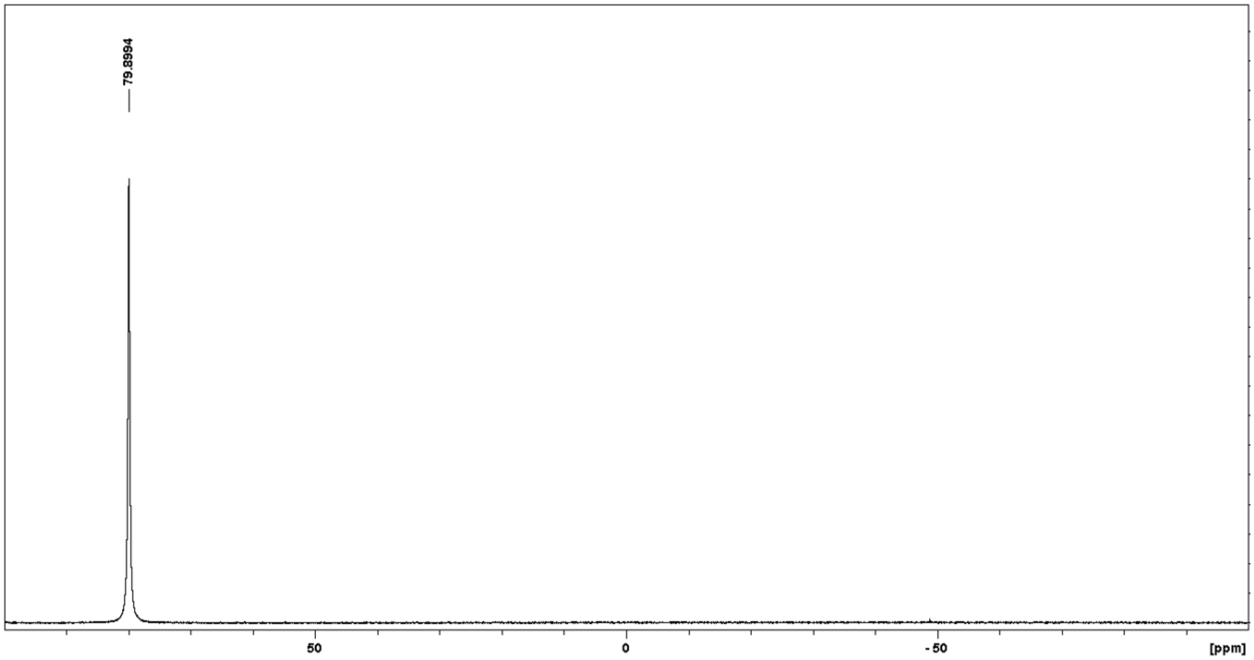

Figure S15. $^{31}P\{^{1}H\}$ NMR spectrum of [(dmpe)$_2$MnH(=GeEt$_2$)] (**2b**) in C_6D_6 (243 MHz, 298 K).

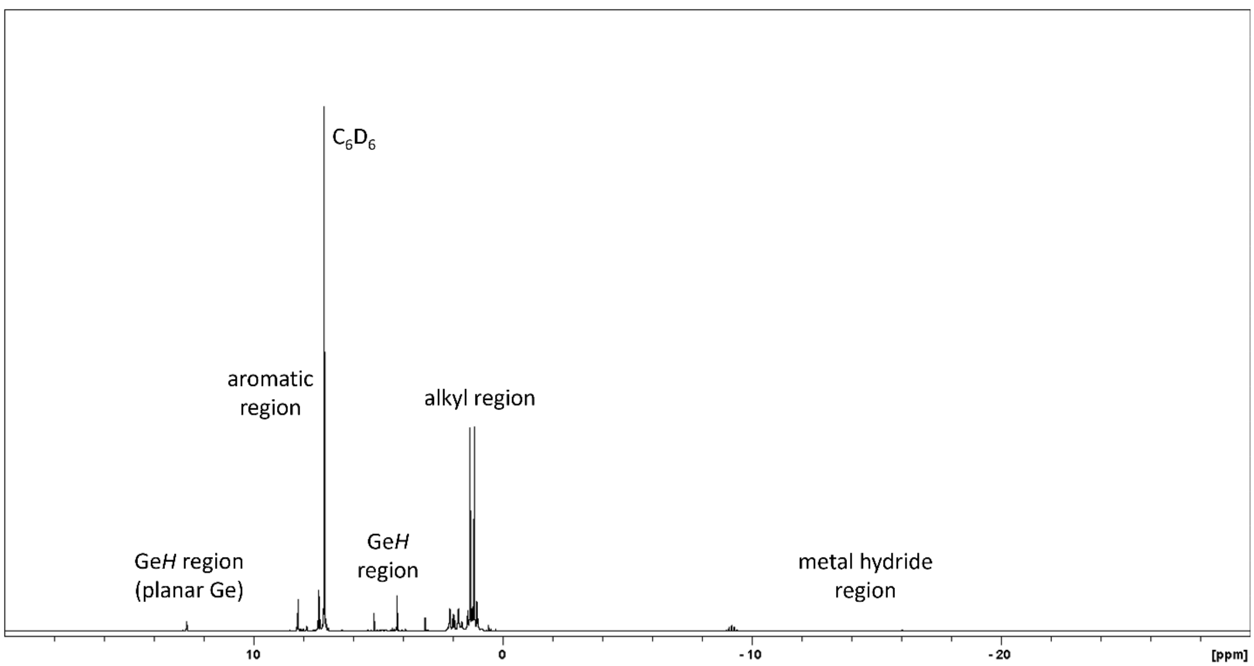

Figure S16. ^{1}H NMR spectrum of [(dmpe)$_2$MnH(=GeHPh)] (**3a**) in C_6D_6 (500 MHz, 298 K). Various decomposition products are also detectable in the spectrum.

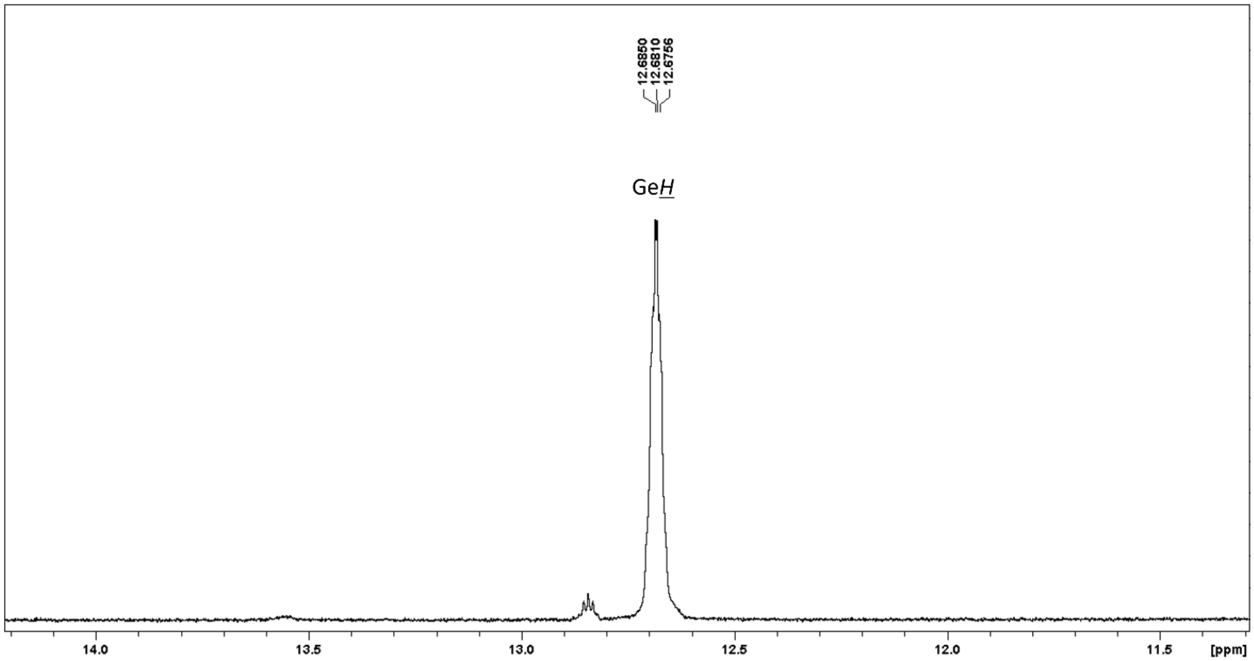

Figure S17. Expanded high frequency region associated with Ge*H* environments on planar Ge atoms of the ^{1}H NMR spectrum of [(dmpe)$_2$MnH(=GeHPh)] (**3a**) in C_6D_6 (500 MHz, 298 K). Various decomposition products are also detectable in the spectrum; only peaks from **3a** are labelled.

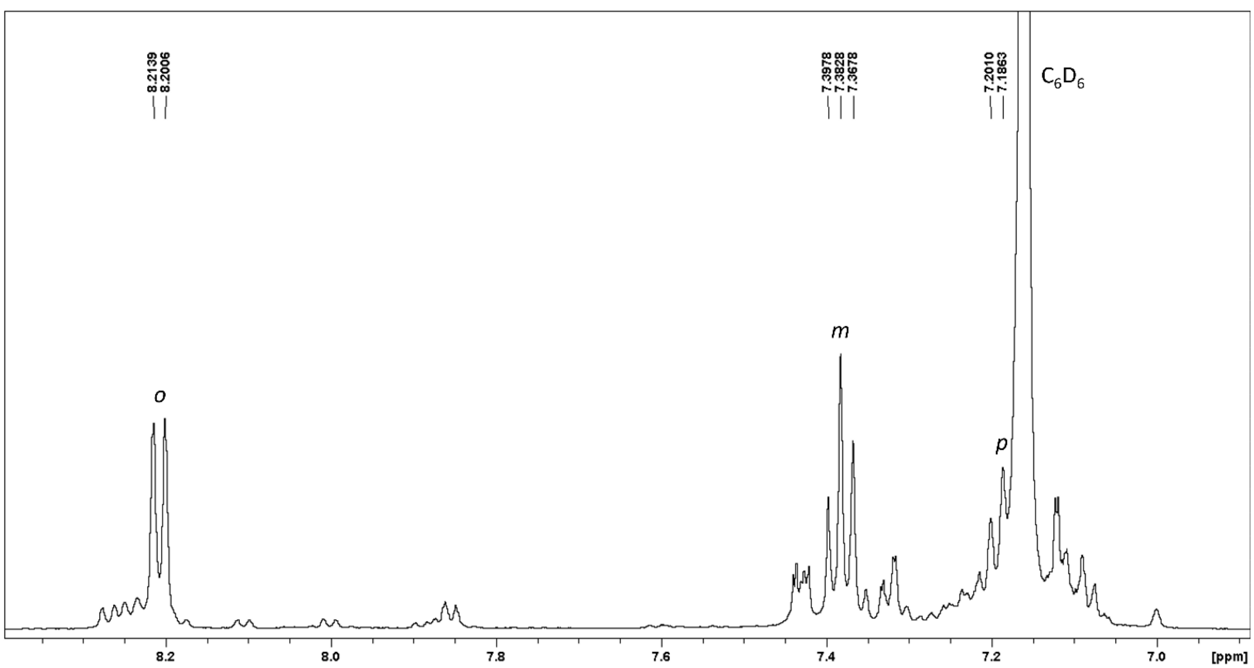

Figure S18. Expanded aromatic region of the ^{1}H NMR spectrum of [(dmpe)$_2$MnH(=GeHPh)] (**3a**) in C_6D_6 (500 MHz, 298 K). Various decomposition products are also detectable in the spectrum; only peaks from **3a** are labelled.

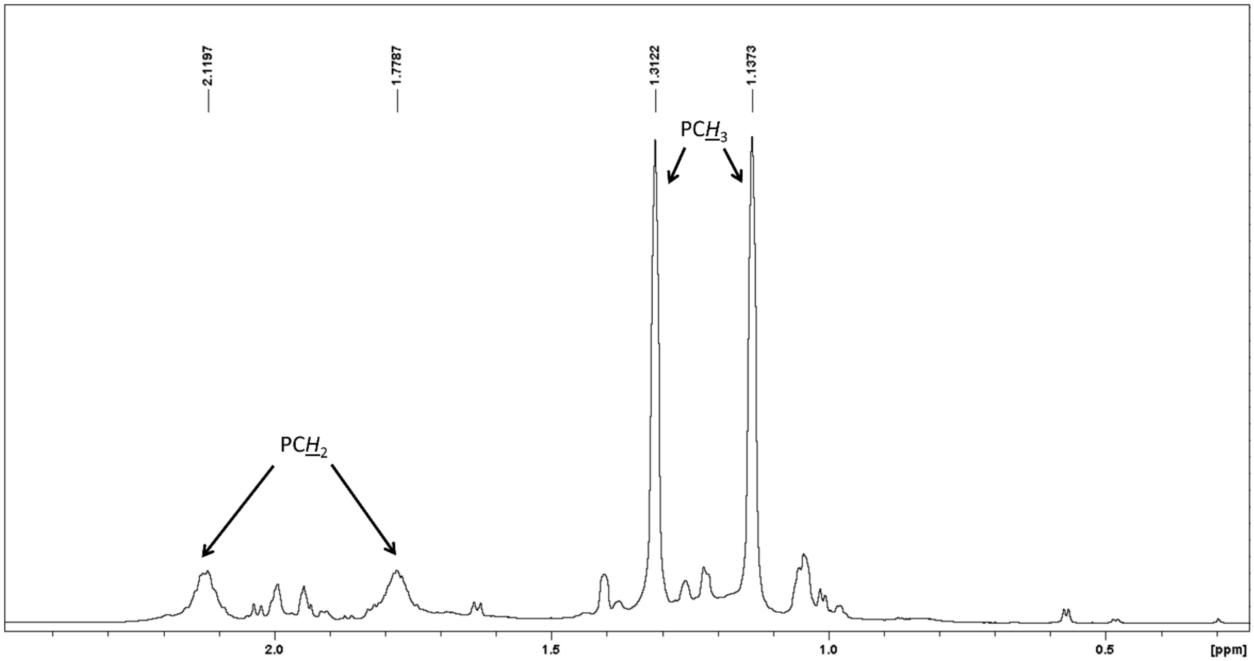

Figure S19. Expanded alkyl region of the ^{1}H NMR spectrum of [(dmpe)$_2$MnH(=GeHPh)] (**3a**) in C_6D_6 (500 MHz, 298 K). Various decomposition products are also detectable in the spectrum; only peaks from **3a** are labelled.

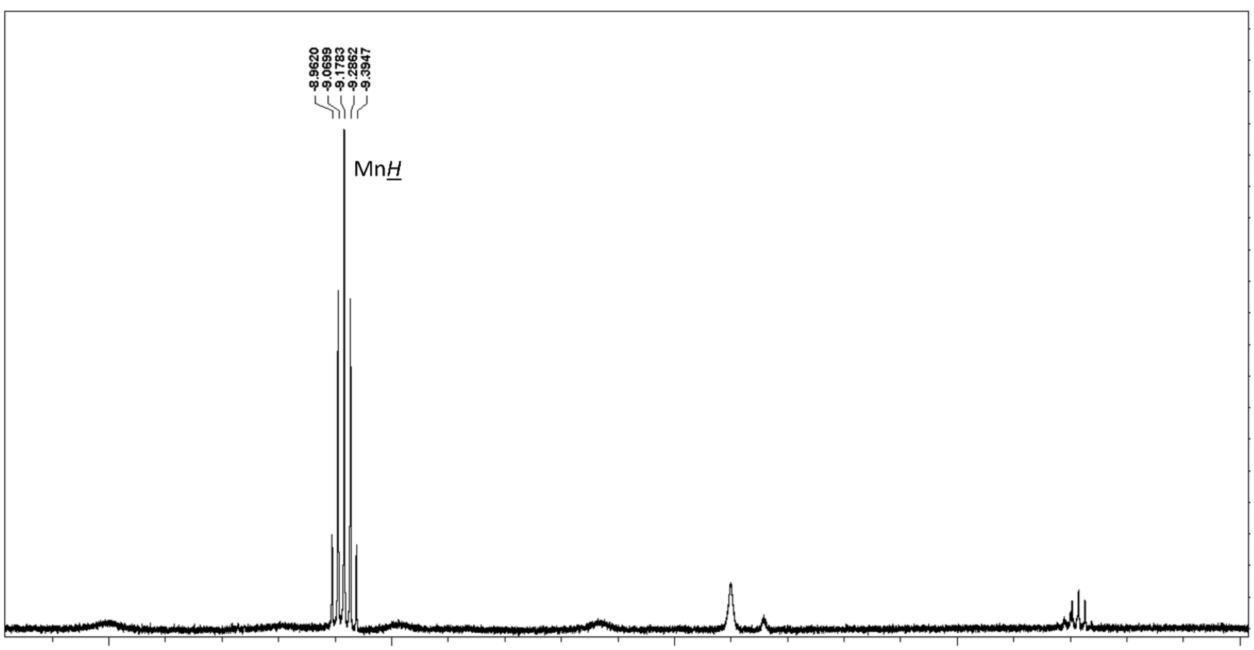

Figure S20. Expanded metal hydride region of the ^{1}H NMR spectrum of [(dmpe)$_2$MnH(=GeHPh)] (**3a**) in C_6D_6 (500 MHz, 298 K). Various decomposition products are also detectable in the spectrum; only peaks from **3a** are labelled.

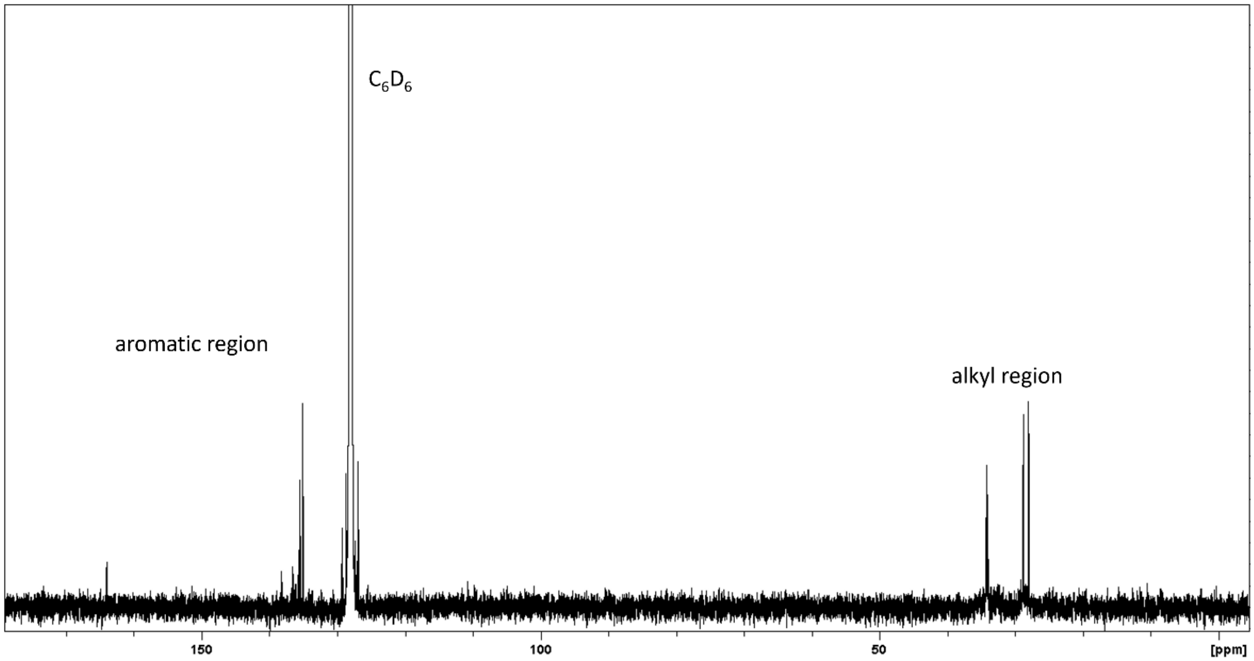

Figure S21. $^{13}C\{^1H\}$ NMR spectrum of [(dmpe)$_2$MnH(=GeHPh)] (**3a**) in C_6D_6 (126 MHz, 298 K). Various decomposition products are also detectable in the spectrum.

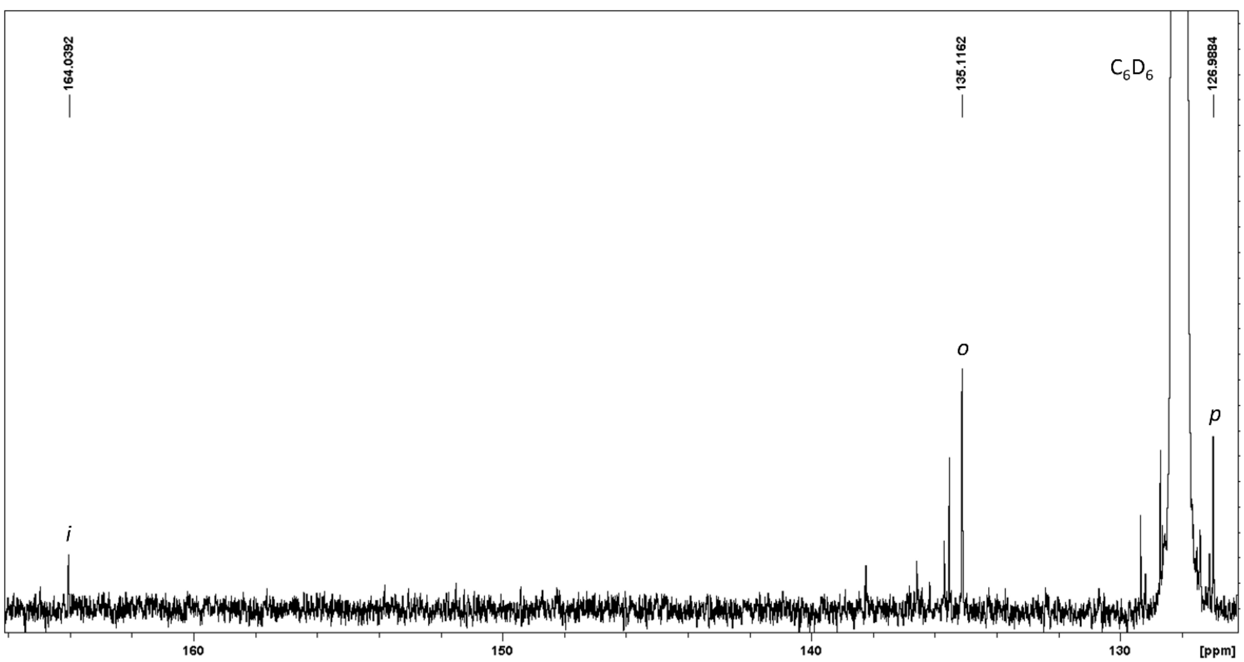

Figure S22. Expanded aromatic region of the $^{13}C\{^1H\}$ NMR spectrum of [(dmpe)$_2$MnH(=GeHPh)] (**3a**) in C_6D_6 (126 MHz, 298 K). Various decomposition products are also detectable in the spectrum; only peaks from **3a** are labelled.

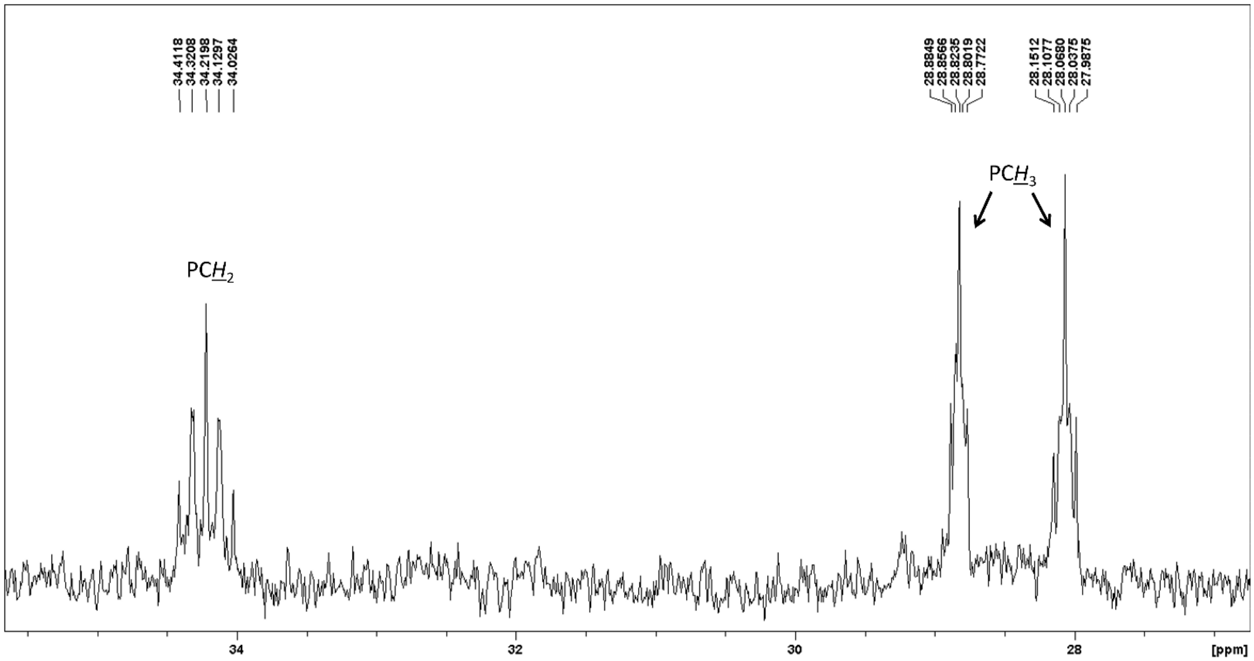

Figure S23. Expanded alkyl region of the $^{13}C\{^1H\}$ NMR spectrum of [(dmpe)$_2$MnH(=GeHPh)] (**3a**) in C_6D_6 (126 MHz, 298 K). Various decomposition products are also detectable in the spectrum; only peaks from **3a** are labelled.

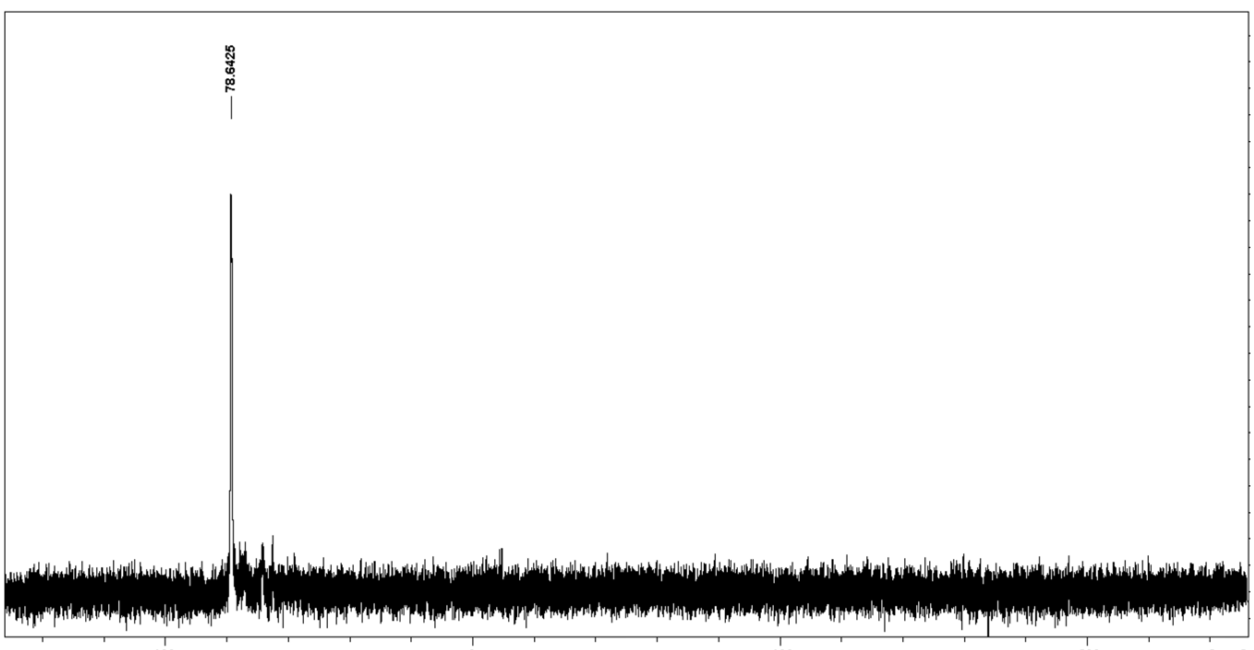

Figure S24. $^{31}P\{^1H\}$ NMR spectrum of [(dmpe)$_2$MnH(=GeHPh)] (**3a**) in C_6D_6 (202 MHz, 298 K). Various decomposition products are also detectable in the spectrum. Only the peak from **3a** has been peak-picked.

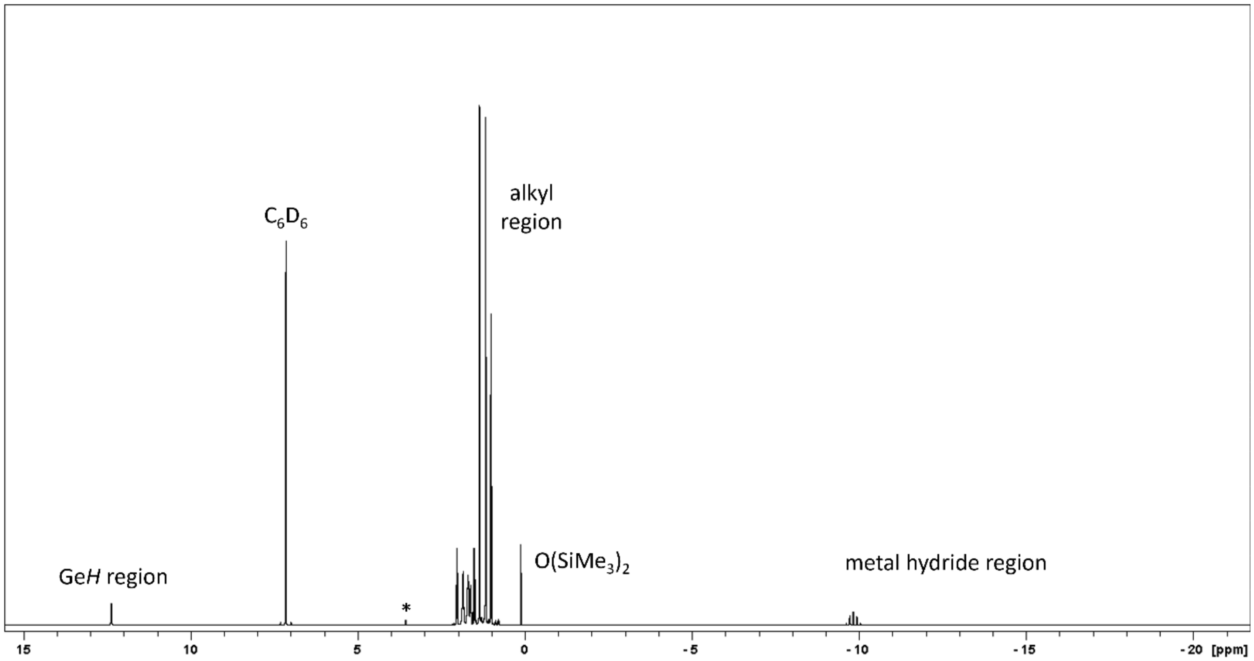

Figure S25. ^{1}H NMR spectrum of [(dmpe)$_2$MnH(=GeH^{n}Bu)] (**3a**) in C_6D_6 (500 MHz, 298 K).

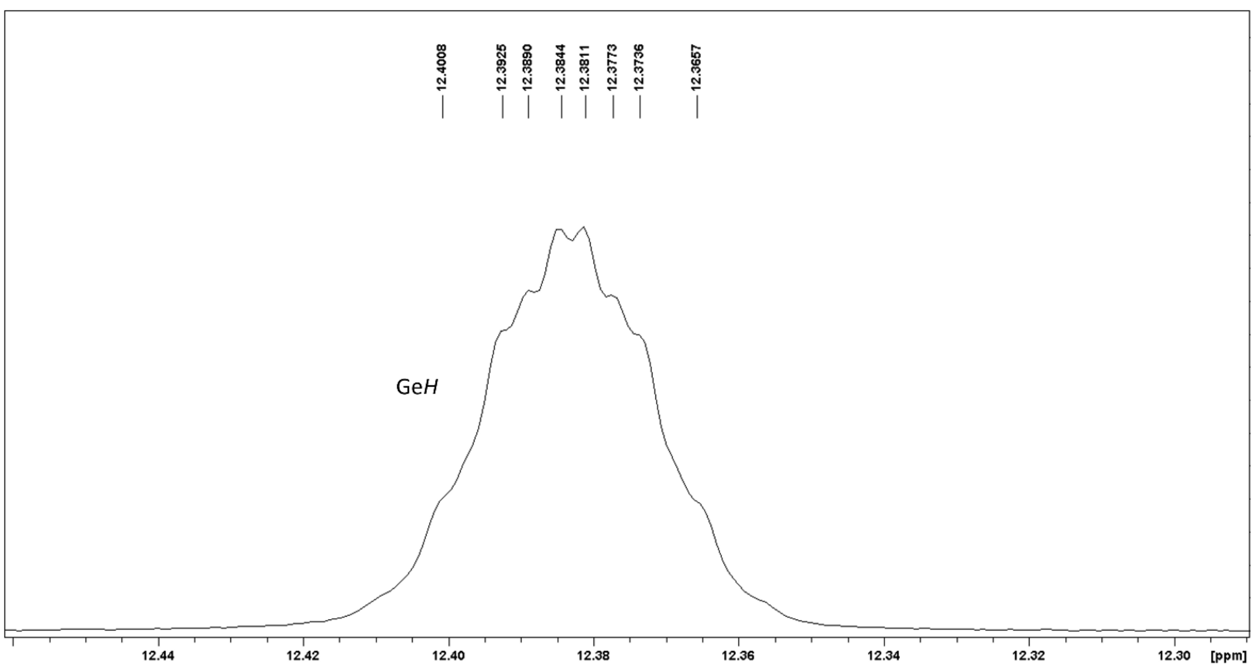

Figure S26. Expanded high frequency region associated with Ge*H* environments on planar Ge atoms of the ^{1}H NMR spectrum of [(dmpe)$_2$MnH(=GeH^{n}Bu)] (**3a**) in C_6D_6 (500 MHz, 298 K).

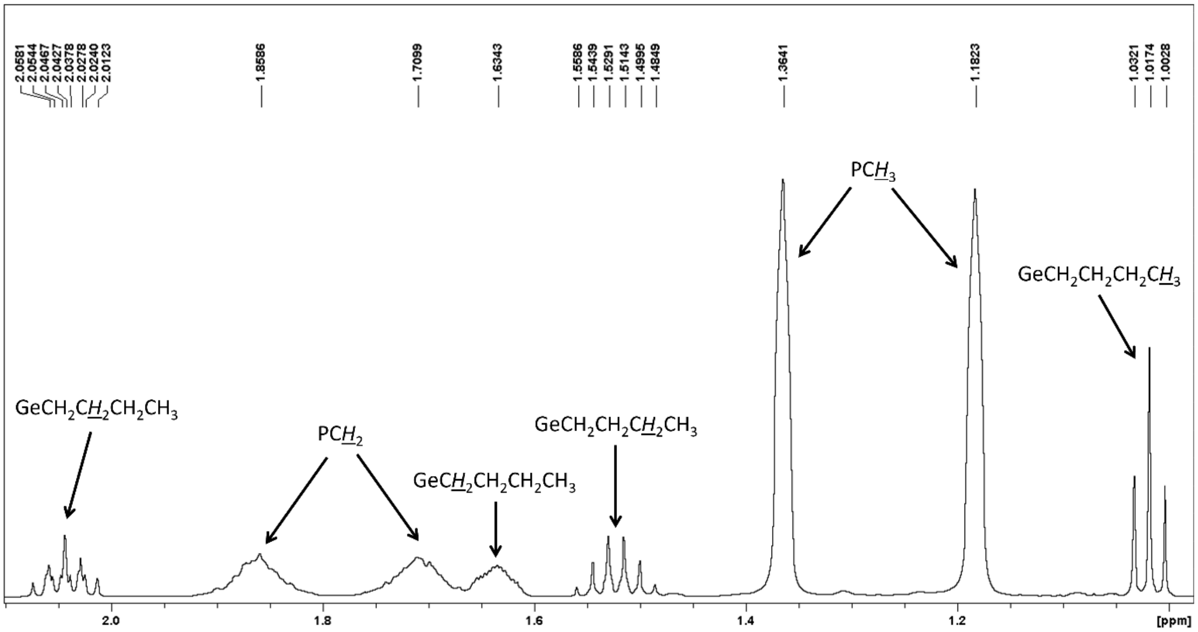

Figure S27. Expanded alkyl region of the ^{1}H NMR spectrum of [(dmpe)$_2$MnH(=GeH^{n}Bu)] (**3a**) in C_6D_6 (500 MHz, 298 K).

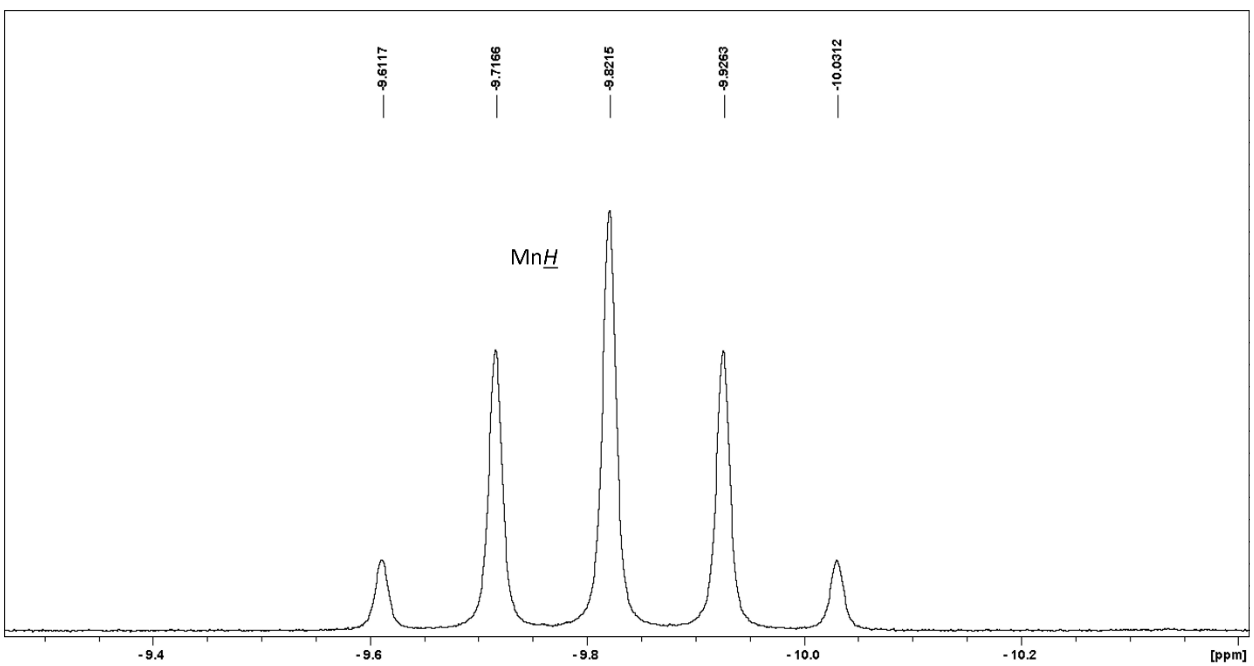

Figure S28. Expanded metal hydride region of the ^{1}H NMR spectrum of [(dmpe)$_2$MnH(=GeH^{n}Bu)] (**3a**) in C_6D_6 (500 MHz, 298 K).

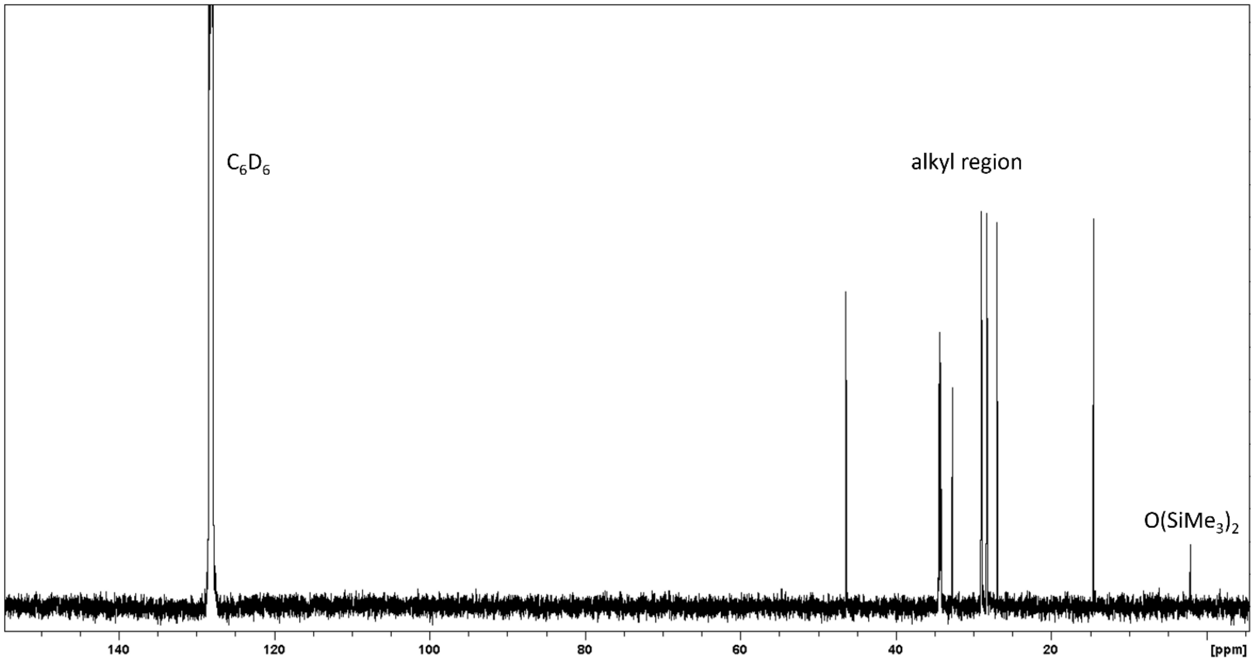

Figure S29. $^{13}C\{^1H\}$ NMR spectrum of [(dmpe)$_2$MnH(=GeH^{n}Bu)] (**3a**) in C_6D_6 (126 MHz, 298 K).

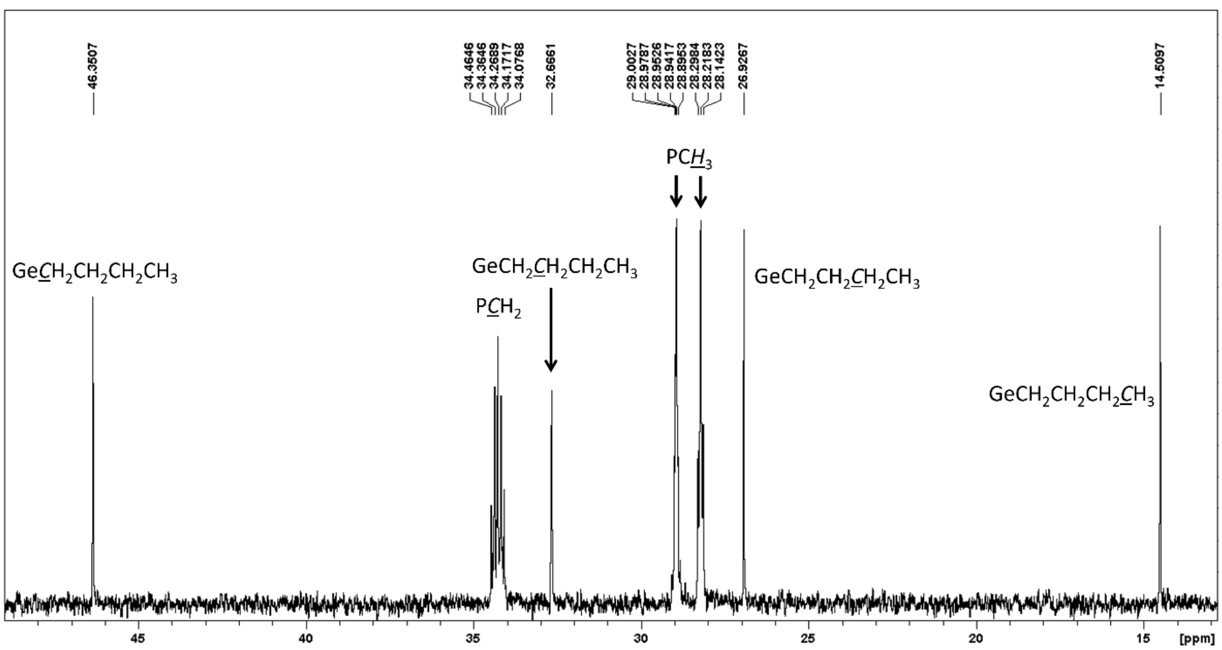

Figure S30. Expanded alkyl region of the $^{13}C\{^1H\}$ NMR spectrum of [(dmpe)$_2$MnH(=GeH^{n}Bu)] (**3a**) in C_6D_6 (126 MHz, 298 K).

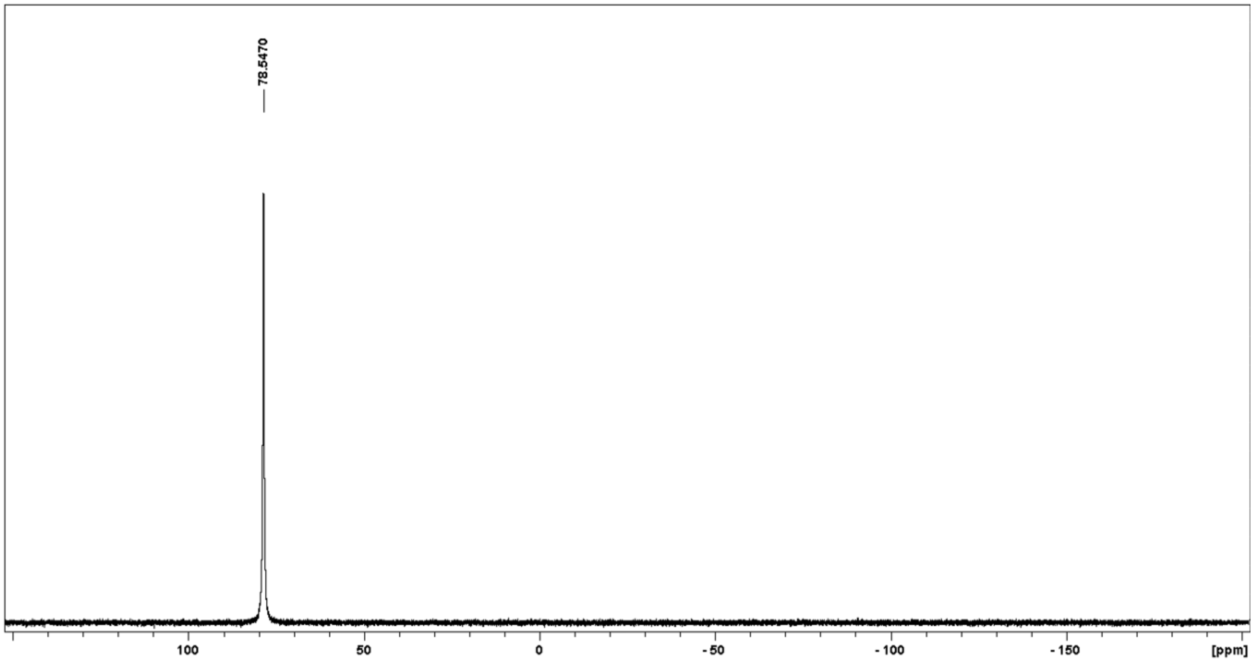

Figure S31. $^{31}P\{^{1}H\}$ NMR spectrum of [(dmpe)$_2$MnH(=GeH^{n}Bu)] (**3a**) in C_6D_6 (202 MHz, 298 K).

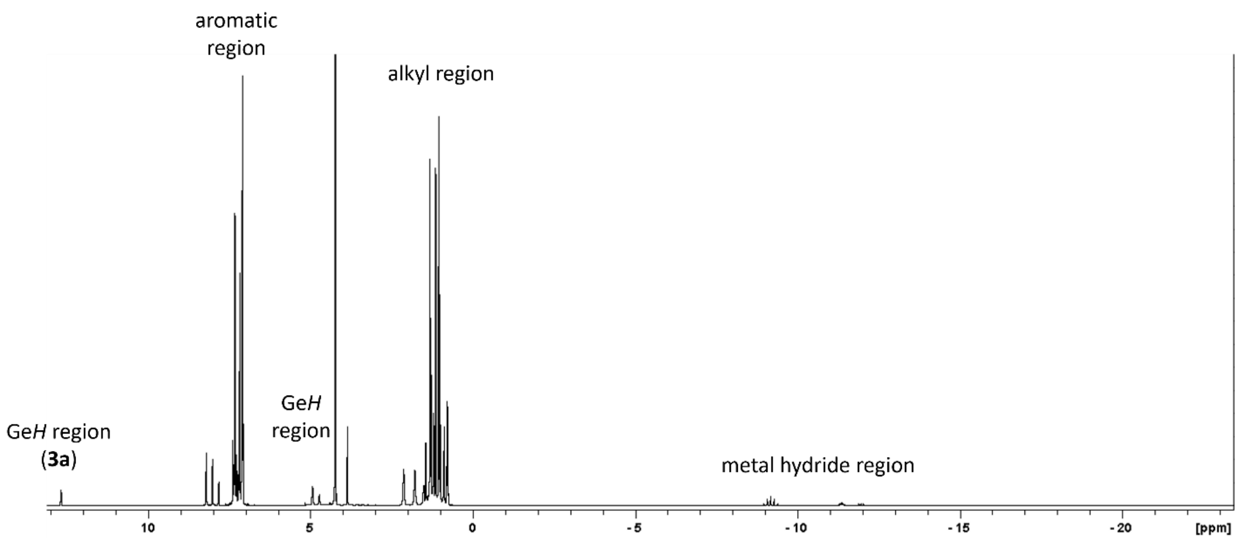

Figure S32. ^{1}H NMR spectrum of a mixture formed from the reaction of [(dmpe)$_2$MnH(=GeEt$_2$)] (**2b**) and an excess of H_3GePh in C_6D_6 (500 MHz, 298 K), containing H_3GePh, H_2GeEt_2, [(dmpe)$_2$MnH(=GeHPh)] (**3a**), *mer*-[(dmpe)$_2$MnH(GeH$_2$Ph)$_2$] (**4a**), and *trans*-[(dmpe)$_2$Mn(GeH$_2$Ph)(HGeH$_2$Ph)] (**5a**).

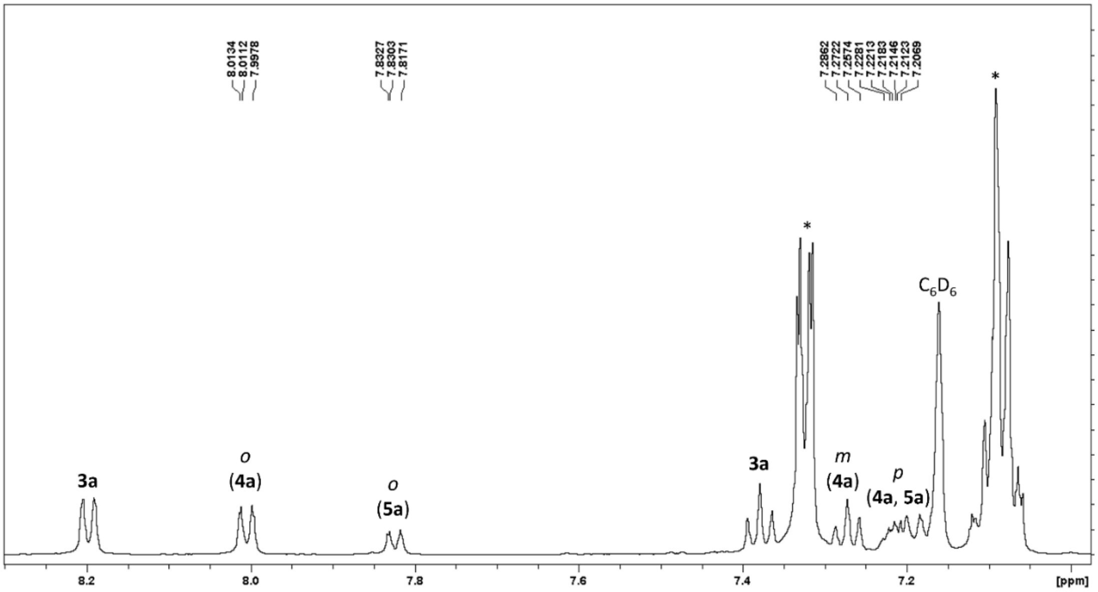

Figure S33. Expanded aromatic region of the ^{1}H NMR spectrum of a mixture formed from the reaction of [(dmpe)$_2$MnH(=GeEt$_2$)] (**2b**) and an excess of H_3GePh in C_6D_6 (500 MHz, 298 K), containing H_3GePh, H_2GeEt_2, [(dmpe)$_2$MnH(=GeHPh)] (**3a**), *mer*-[(dmpe)$_2$MnH(GeH$_2$Ph)$_2$] (**4a**), and *trans*-[(dmpe)$_2$Mn(GeH$_2$Ph)(HGeH$_2$Ph)] (**5a**). * indicates peaks from H_3GePh.

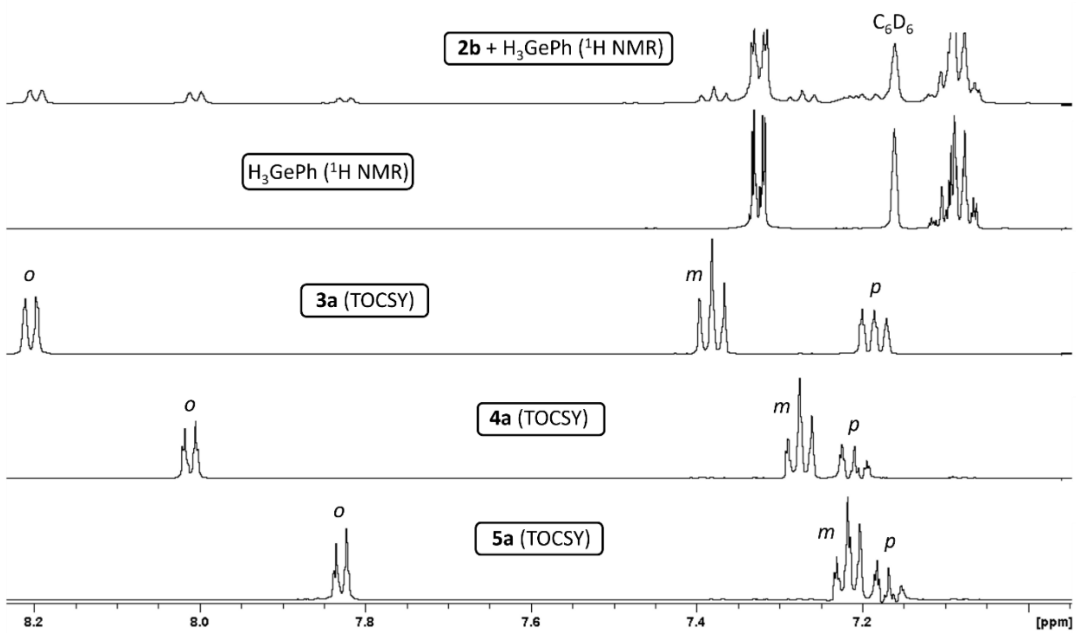

Figure S34. Top; expanded aromatic region of the ^{1}H NMR spectrum of a mixture formed from the reaction of [(dmpe)$_2$MnH(=GeEt$_2$)] (**2b**) and an excess of H_3GePh in C_6D_6 (500 MHz, 298 K), containing H_3GePh, H_2GeEt_2, [(dmpe)$_2$MnH(=GeHPh)] (**3a**), *mer*-[(dmpe)$_2$MnH(GeH$_2$Ph)$_2$] (**4a**), and *trans*-[(dmpe)$_2$Mn(GeH$_2$Ph)(HGeH$_2$Ph)] (**5a**). Second from the top; ^{1}H NMR spectrum of H_3GePh shown for reference. Bottom three; 1D TOCSY NMR spectra of the reaction mixture used to obtain the top ^{1}H NMR spectrum, with excitation of the *ortho* peaks of (middle) **3a**, (second from the bottom) **4a**, or (bottom) **5a**, illustrating the ^{1}H NMR environments associated with the phenyl groups of these complexes.

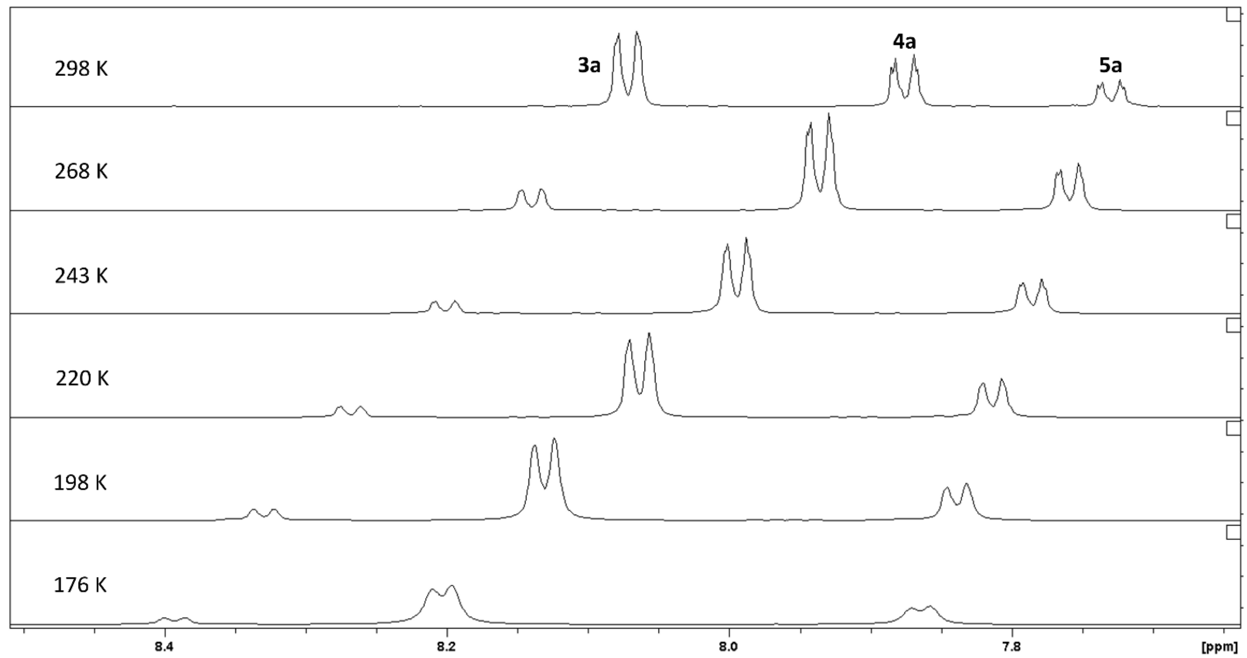

Figure S35. Expanded *ortho* region of variable temperature ^{1}H NMR spectra of a mixture formed from the reaction of [(dmpe)$_2$MnH(=GeEt$_2$)] (**2b**) and an excess of H_3GePh in d_8-toluene (500 MHz), containing H_3GePh, H_2GeEt_2, [(dmpe)$_2$MnH(=GeHPh)] (**3a**), *mer*-[(dmpe)$_2$MnH(GeH$_2$Ph)$_2$] (**4a**), and *trans*-[(dmpe)$_2$Mn(GeH$_2$Ph)(HGeH$_2$Ph)] (**5a**).

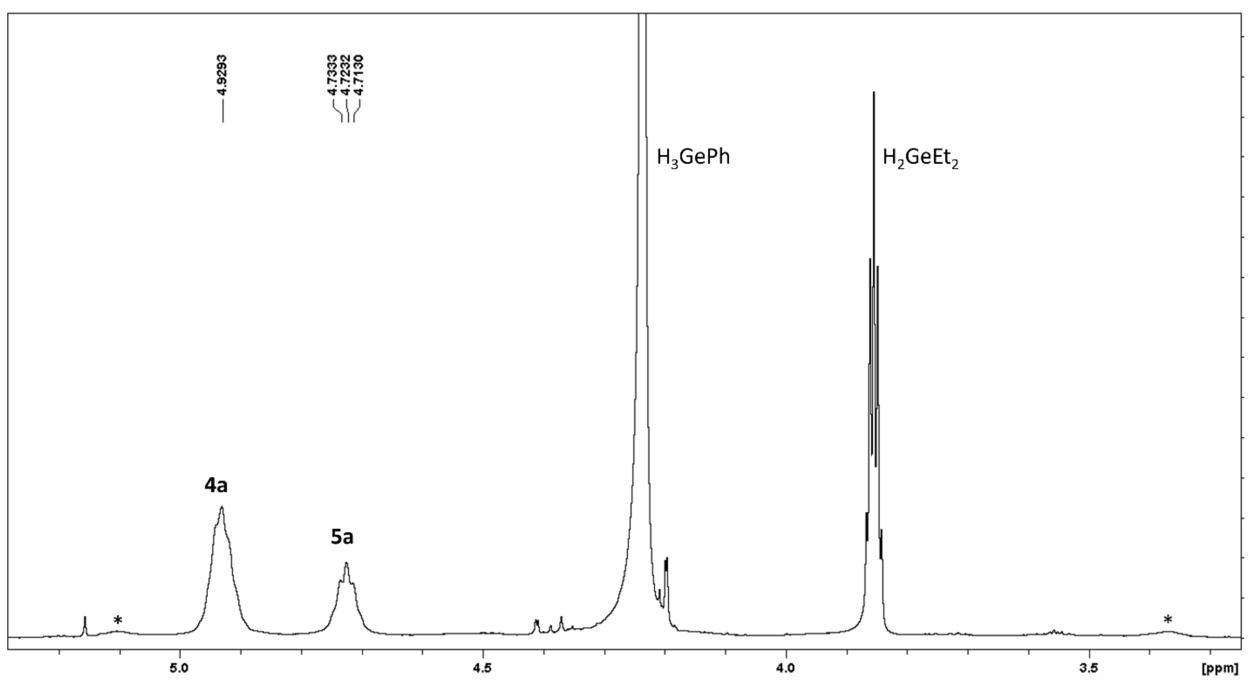

Figure S36. Expanded germyl hydride region of the ^{1}H NMR spectrum of a mixture formed from the reaction of [(dmpe)$_2$MnH(=GeEt$_2$)] (**2b**) and an excess of H_3GePh in C_6D_6 (500 MHz, 298 K), containing H_3GePh, H_2GeEt_2, [(dmpe)$_2$MnH(=GeHPh)] (**3a**), *mer*-[(dmpe)$_2$MnH(GeH$_2$Ph)$_2$] (**4a**), and *trans*-[(dmpe)$_2$Mn(GeH$_2$Ph)(HGeH$_2$Ph)] (**5a**). Labelled peaks arise from Ge*H* environments.

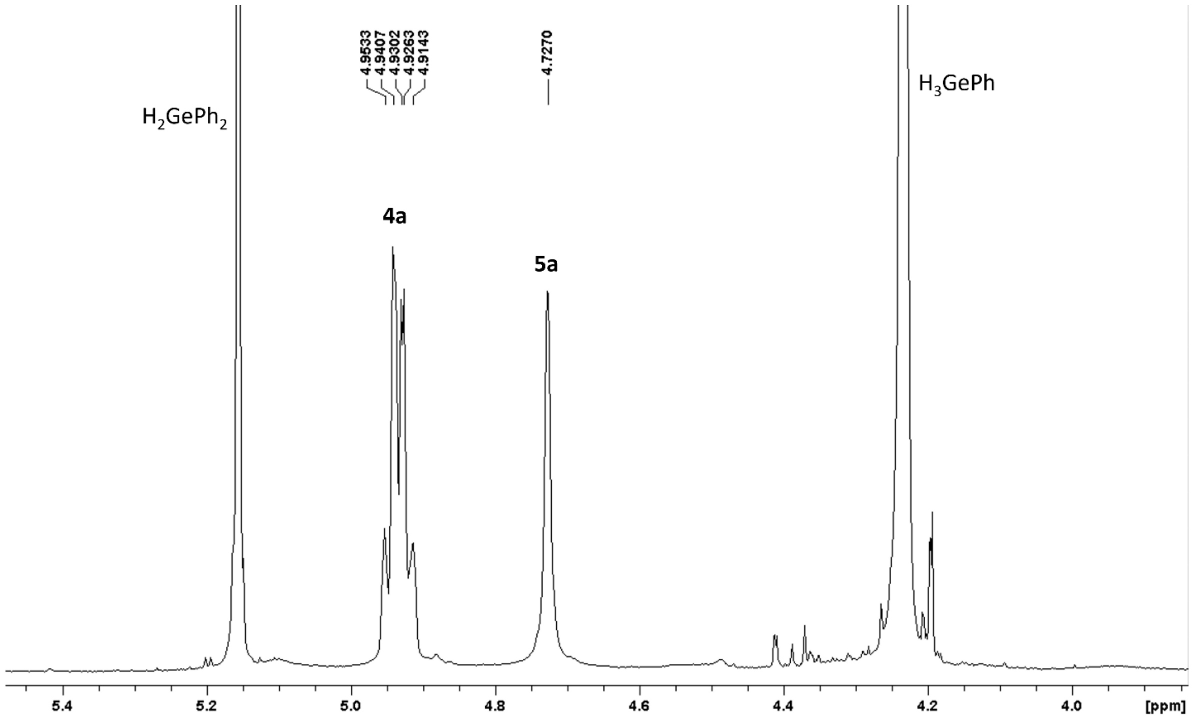

Figure S37. Expanded germyl hydride region of the $^{1}H\{^{31}P\}$ NMR spectrum of a mixture formed from the reaction of [(dmpe)$_2$MnH(=GePh$_2$)] (**2a**) and an excess of H_3GePh in C_6D_6 (500 MHz, 298 K), containing H_3GePh, H_2GePh_2, [(dmpe)$_2$MnH(=GeHPh)] (**3a**), *mer*-[(dmpe)$_2$MnH(GeH$_2$Ph)$_2$] (**4a**), and *trans*-[(dmpe)$_2$Mn(GeH$_2$Ph)(HGeH$_2$Ph)] (**5a**). Labelled peaks arise from Ge*H* environments.

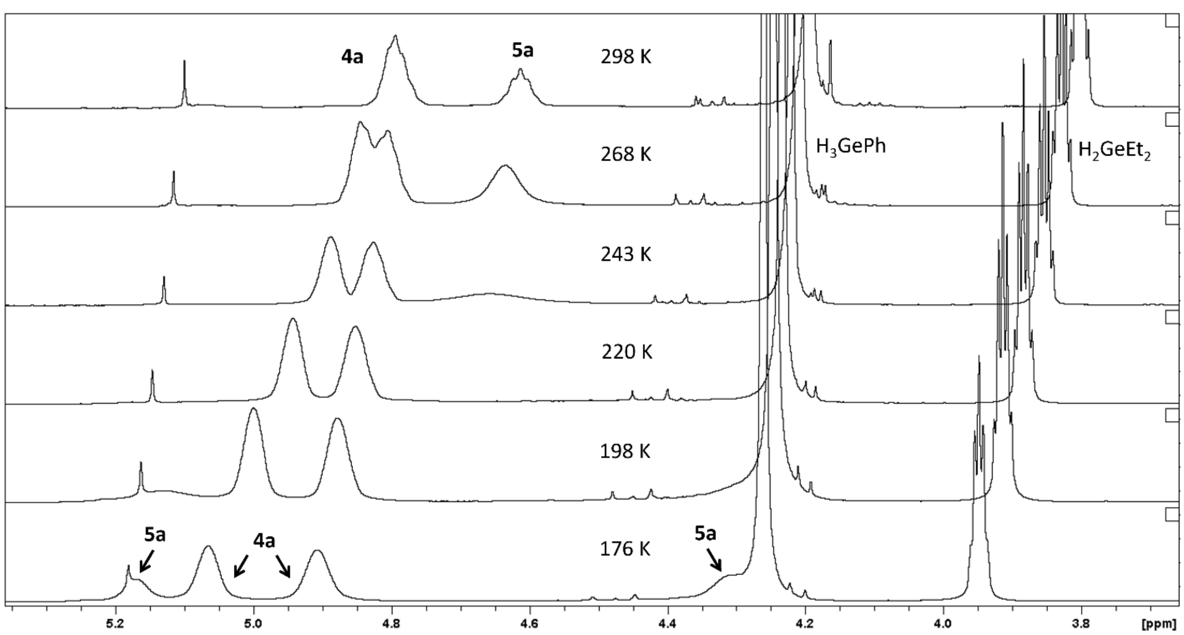

Figure S38. Expanded germyl hydride region of variable temperature ^{1}H NMR spectra of a mixture formed from the reaction of [(dmpe)$_2$MnH(=GeEt$_2$)] (**2b**) and an excess of H_3GePh in d_8-toluene (500 MHz), containing H_3GePh, H_2GeEt_2, [(dmpe)$_2$MnH(=GeHPh)] (**3a**), *mer*-[(dmpe)$_2$MnH(GeH$_2$Ph)$_2$] (**4a**), and *trans*-[(dmpe)$_2$Mn(GeH$_2$Ph)(HGeH$_2$Ph)] (**5a**). Labelled peaks arise from Ge*H* environments.

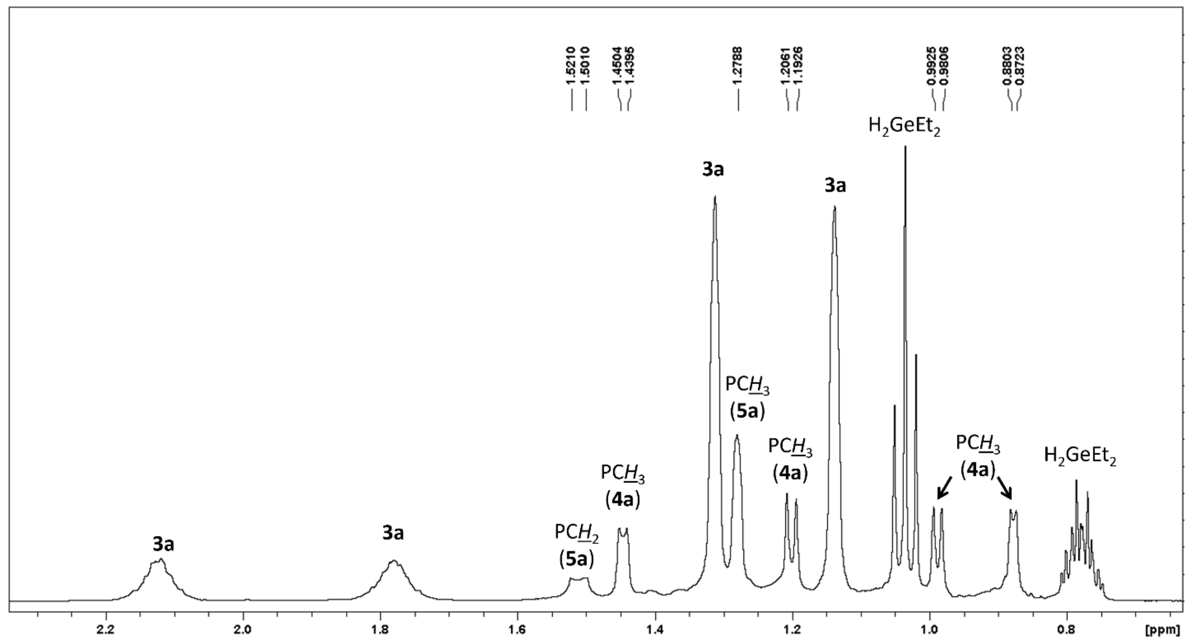

Figure S39. Expanded alkyl region of the [1]H NMR spectrum of a mixture formed from the reaction of [(dmpe)$_2$MnH(=GeEt$_2$)] (**2b**) and an excess of H_3GePh in C_6D_6 (500 MHz, 298 K), containing H_3GePh, H_2GeEt_2, [(dmpe)$_2$MnH(=GeHPh)] (**3a**), *mer*-[(dmpe)$_2$MnH(GeH$_2$Ph)$_2$] (**4a**), and *trans*-[(dmpe)$_2$Mn(GeH$_2$Ph)(HGeH$_2$Ph)] (**5a**).

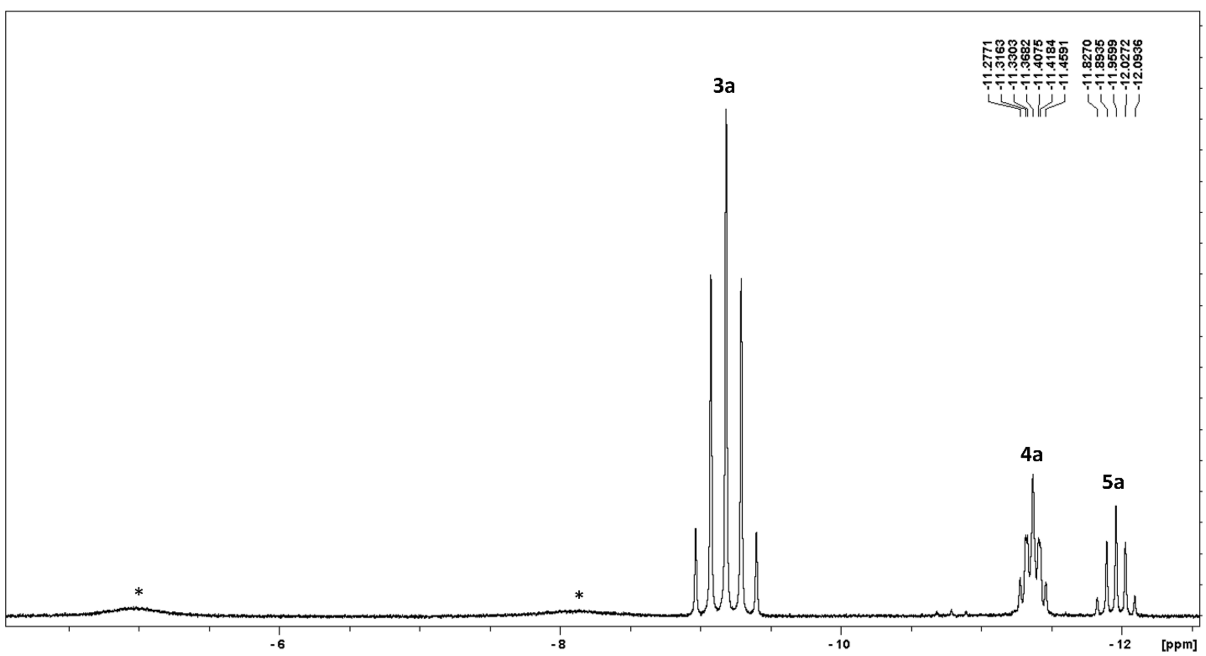

Figure S40. Expanded metal hydride region of the [1]H NMR spectrum of a mixture formed from the reaction of [(dmpe)$_2$MnH(=GeEt$_2$)] (**2b**) and an excess of H_3GePh in C_6D_6 (500 MHz, 298 K), containing H_3GePh, H_2GeEt_2, [(dmpe)$_2$MnH(=GeHPh)] (**3a**), *mer*-[(dmpe)$_2$MnH(GeH$_2$Ph)$_2$] (**4a**), and *trans*-[(dmpe)$_2$Mn(GeH$_2$Ph)(HGeH$_2$Ph)] (**5a**). Labelled peaks arise from Mn*H* environments. * indicates peaks arising from decomposition products.

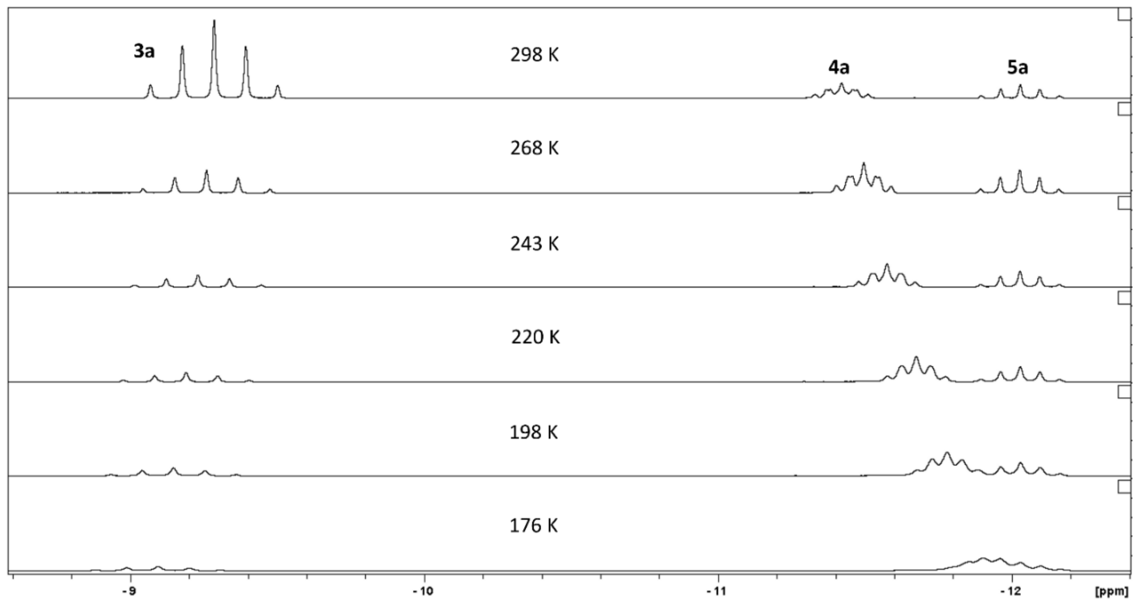

Figure S41. Expanded metal hydride region of variable temperature ^{1}H NMR spectra of a mixture formed from the reaction of [(dmpe)$_2$MnH(=GeEt$_2$)] (**2b**) and an excess of H_3GePh in *d*$_8$-toluene (500 MHz), containing H_3GePh, H_2GeEt_2, [(dmpe)$_2$MnH(=GeHPh)] (**3a**), *mer*-[(dmpe)$_2$MnH(GeH$_2$Ph)$_2$] (**4a**), and *trans*-[(dmpe)$_2$Mn(GeH$_2$Ph)(HGeH$_2$Ph)] (**5a**). Labelled peaks arise from Mn*H* environments.

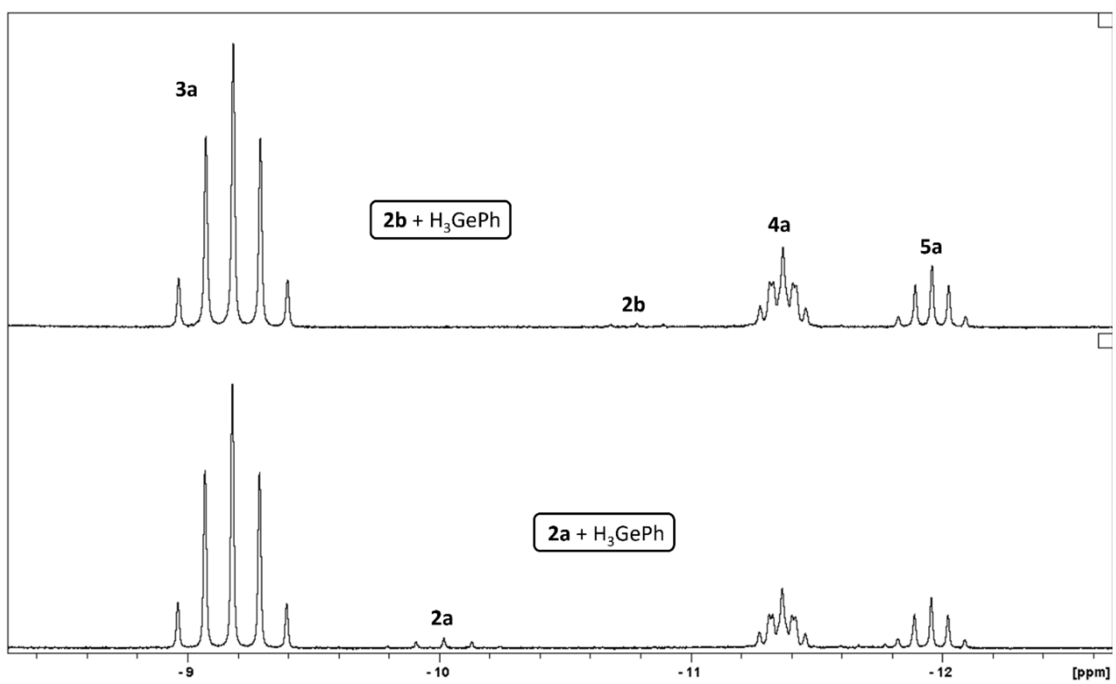

Figure S42. Expanded metal hydride region of the ^{1}H NMR spectrum of a mixture formed from the reaction of (top) [(dmpe)$_2$MnH(=GeEt$_2$)] (**2b**) or (bottom) [(dmpe)$_2$MnH(=GePh$_2$)] (**2a**) and an excess of H_3GePh in C_6D_6 (500 MHz, 298 K), containing H_3GePh, H_2GeEt_2 (top) or H_2GePh_2 (bottom), [(dmpe)$_2$MnH(=GeEt$_2$)] (**2b**; top) or [(dmpe)$_2$MnH(=GePh$_2$)] (**2a**; bottom), [(dmpe)$_2$MnH(=GeHPh)] (**3a**), *mer*-[(dmpe)$_2$MnH(GeH$_2$Ph)$_2$] (**4a**), and *trans*-[(dmpe)$_2$Mn(GeH$_2$Ph)(HGeH$_2$Ph)] (**5a**). Labelled peaks arise from Mn*H* environments.

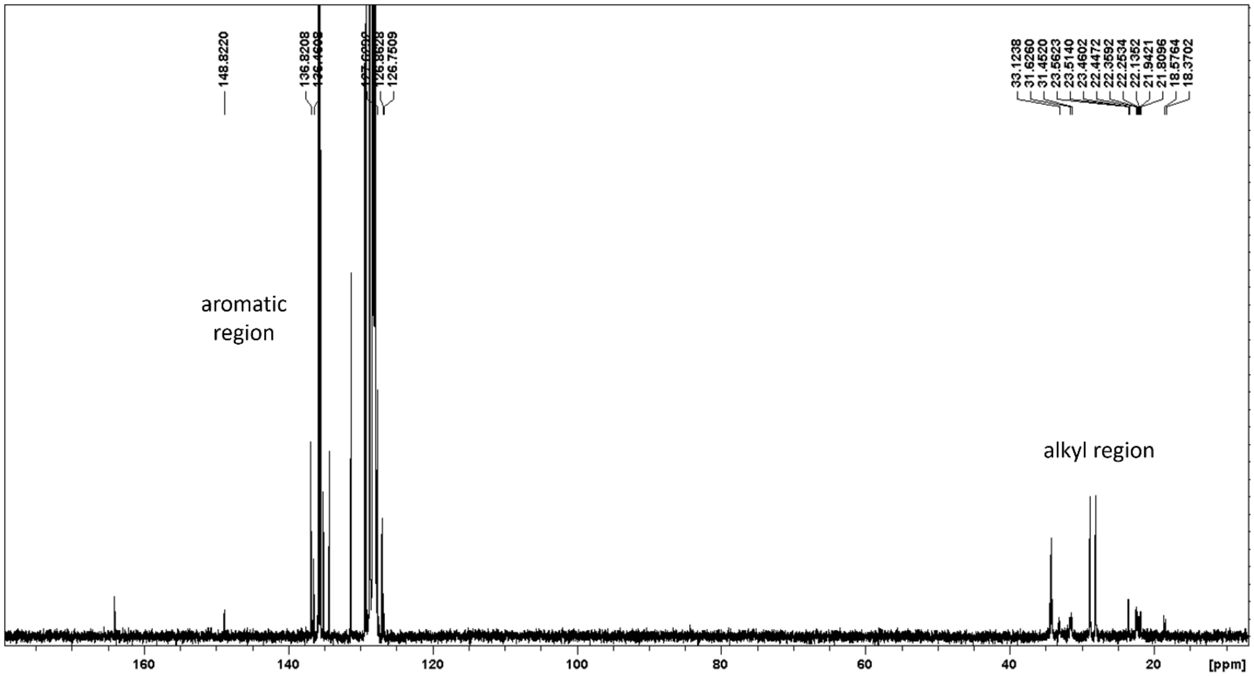

Figure S43. $^{13}C\{^{1}H\}$ NMR spectrum of a mixture formed from the reaction of [(dmpe)$_2$MnH(=GePh$_2$)] (**2a**) and an excess of H_3GePh in C_6D_6 (126 MHz, 298 K), containing H_3GePh, H_2GePh$_2$, [(dmpe)$_2$MnH(=GeHPh)] (**3a**), *mer*-[(dmpe)$_2$MnH(GeH$_2$Ph)$_2$] (**4a**), and *trans*-[(dmpe)$_2$Mn(GeH$_2$Ph)(HGeH$_2$Ph)] (**5a**).

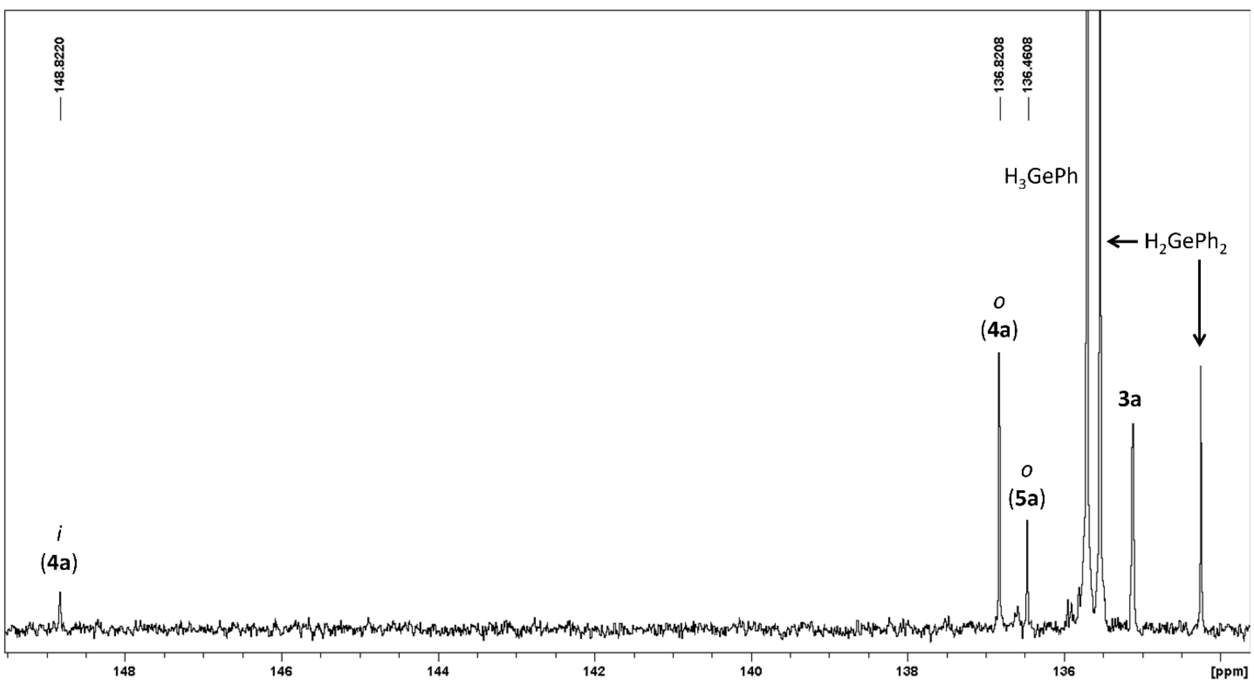

Figure S44. Expanded higher frequency aromatic region of the $^{13}C\{^{1}H\}$ NMR spectrum of a mixture formed from the reaction of [(dmpe)$_2$MnH(=GePh$_2$)] (**2a**) and an excess of H_3GePh in C_6D_6 (126 MHz, 298 K), containing H_3GePh, H_2GePh$_2$, [(dmpe)$_2$MnH(=GeHPh)] (**3a**), *mer*-[(dmpe)$_2$MnH(GeH$_2$Ph)$_2$] (**4a**), and *trans*-[(dmpe)$_2$Mn(GeH$_2$Ph)(HGeH$_2$Ph)] (**5a**).

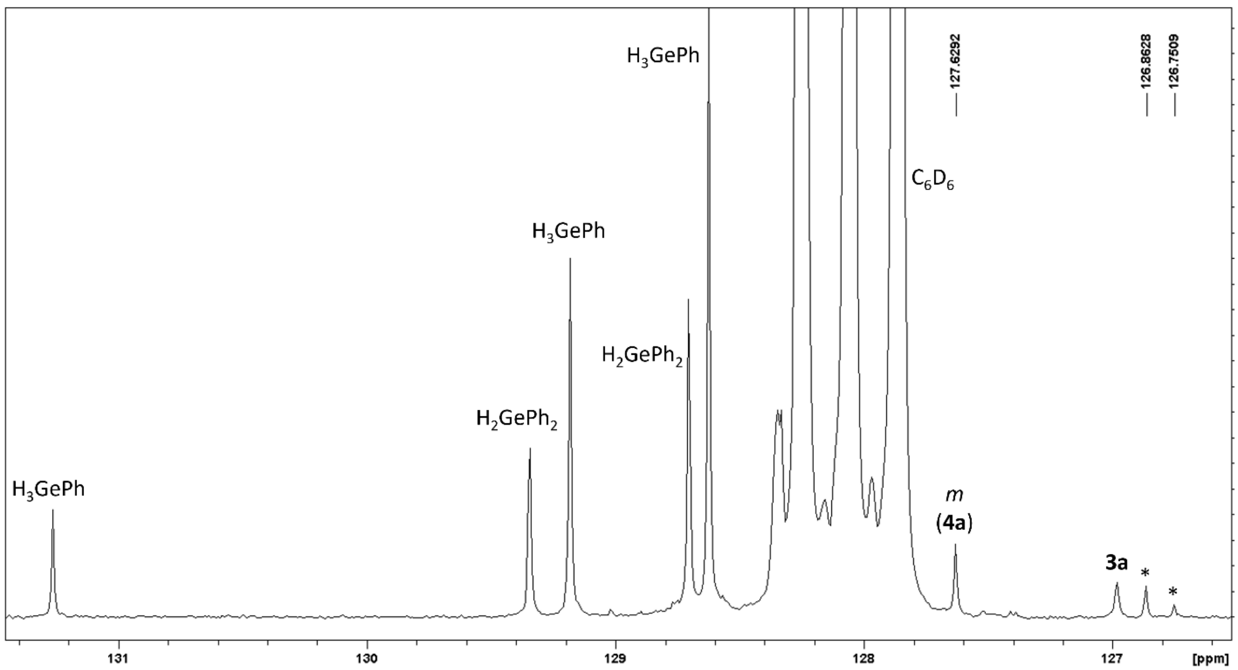

Figure S45. Expanded lower frequency aromatic region of the $^{13}C\{^1H\}$ NMR spectrum of a mixture formed from the reaction of [(dmpe)$_2$MnH(=GePh$_2$)] (**2a**) and an excess of H_3GePh in C_6D_6 (126 MHz, 298 K), containing H_3GePh, H_2GePh_2, [(dmpe)$_2$MnH(=GeHPh)] (**3a**), *mer*-[(dmpe)$_2$MnH(GeH$_2$Ph)$_2$] (**4a**), and *trans*-[(dmpe)$_2$Mn(GeH$_2$Ph)(HGeH$_2$Ph)] (**5a**). * indicates peaks which could not be assigned definitively to **4a** or **5a**, but were confirmed as arising from these species.

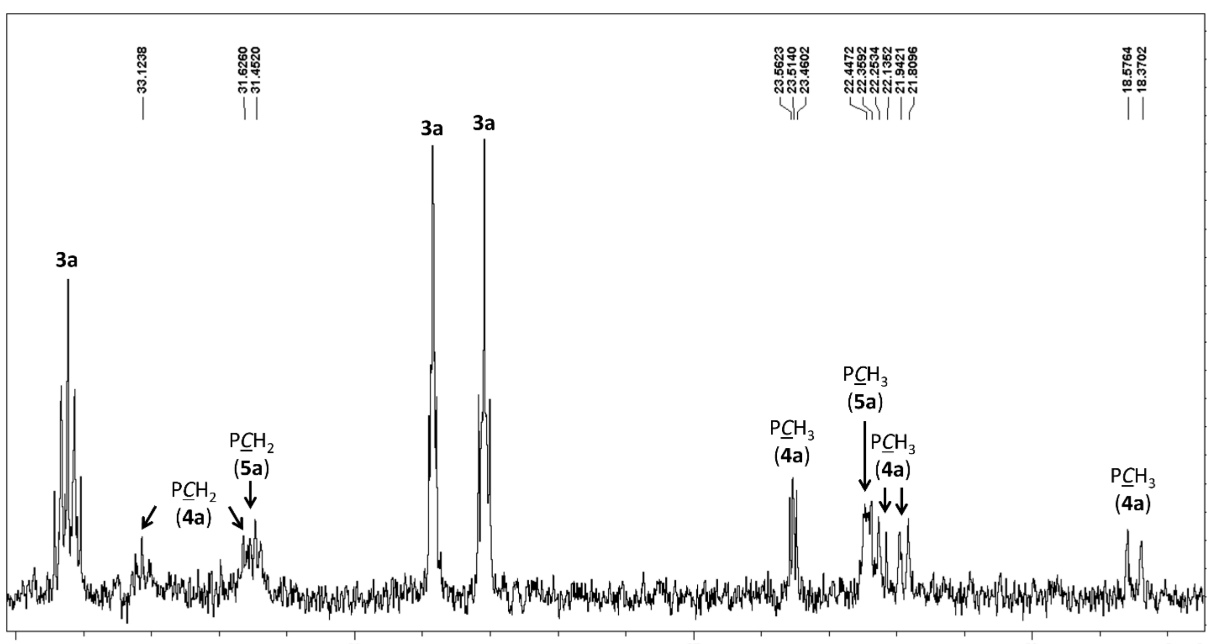

Figure S46. Expanded alkyl region of the $^{13}C\{^1H\}$ NMR spectrum of a mixture formed from the reaction of [(dmpe)$_2$MnH(=GePh$_2$)] (**2a**) and an excess of H_3GePh in C_6D_6 (126 MHz, 298 K), containing H_3GePh, H_2GePh_2, [(dmpe)$_2$MnH(=GeHPh)] (**3a**), *mer*-[(dmpe)$_2$MnH(GeH$_2$Ph)$_2$] (**4a**), and *trans*-[(dmpe)$_2$Mn(GeH$_2$Ph)(HGeH$_2$Ph)] (**5a**).

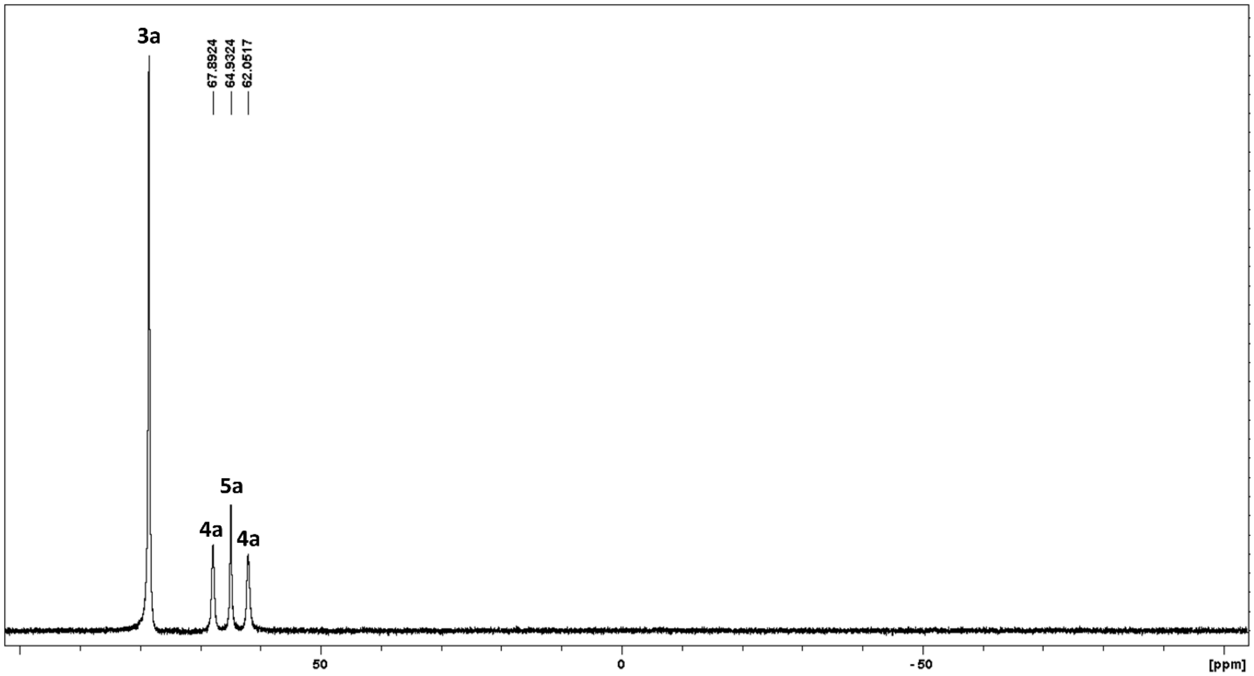

Figure S47. $^{31}P\{^{1}H\}$ NMR spectrum of a mixture formed from the reaction of [(dmpe)$_2$MnH(=GeEt$_2$)] (**2b**) and an excess of H_3GePh in C_6D_6 (202 MHz, 298 K), containing H_3GePh, H_2GeEt_2, [(dmpe)$_2$MnH(=GeHPh)] (**3a**), *mer*-[(dmpe)$_2$MnH(GeH$_2$Ph)$_2$] (**4a**), and *trans*-[(dmpe)$_2$Mn(GeH$_2$Ph)(HGeH$_2$Ph)] (**5a**).

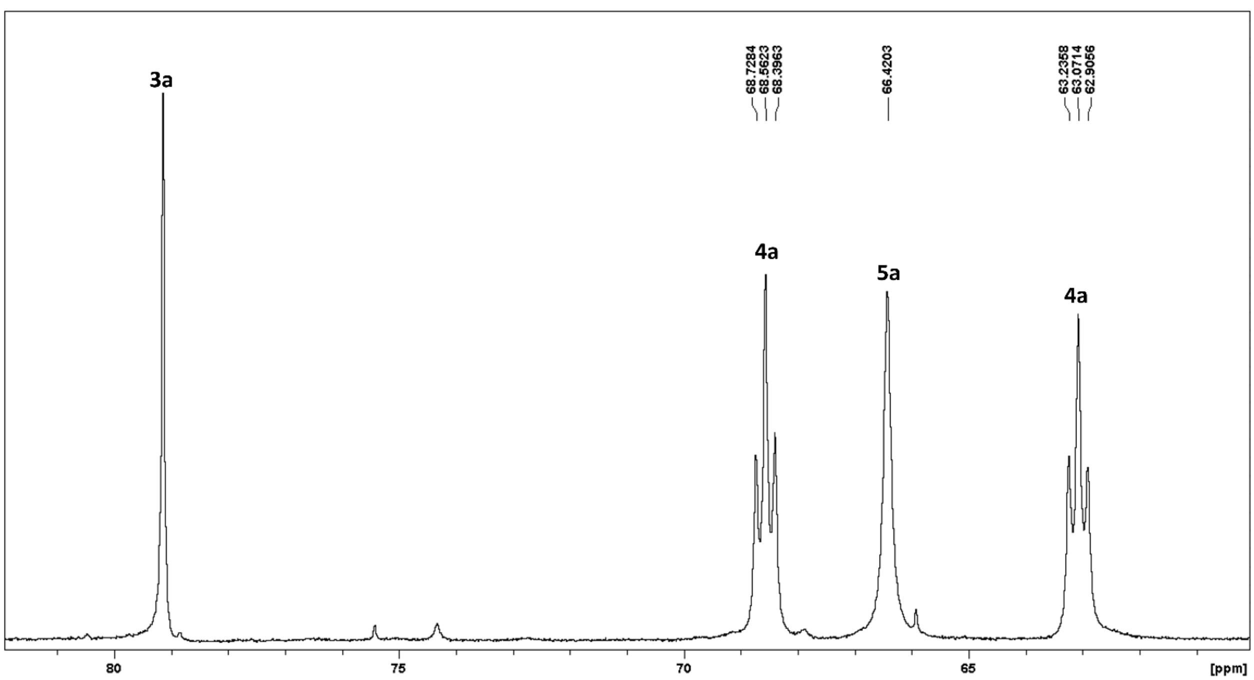

Figure S48. $^{31}P\{^{1}H\}$ NMR spectrum of a mixture formed from the reaction of [(dmpe)$_2$MnH(=GeEt$_2$)] (**2b**) and an excess of H_3GePh in d_8-toluene (202 MHz, 198 K), containing H_3GePh, H_2GeEt_2, [(dmpe)$_2$MnH(=GeHPh)] (**3a**), *mer*-[(dmpe)$_2$MnH(GeH$_2$Ph)$_2$] (**4a**), and *trans*-[(dmpe)$_2$Mn(GeH$_2$Ph)(HGeH$_2$Ph)] (**5a**).

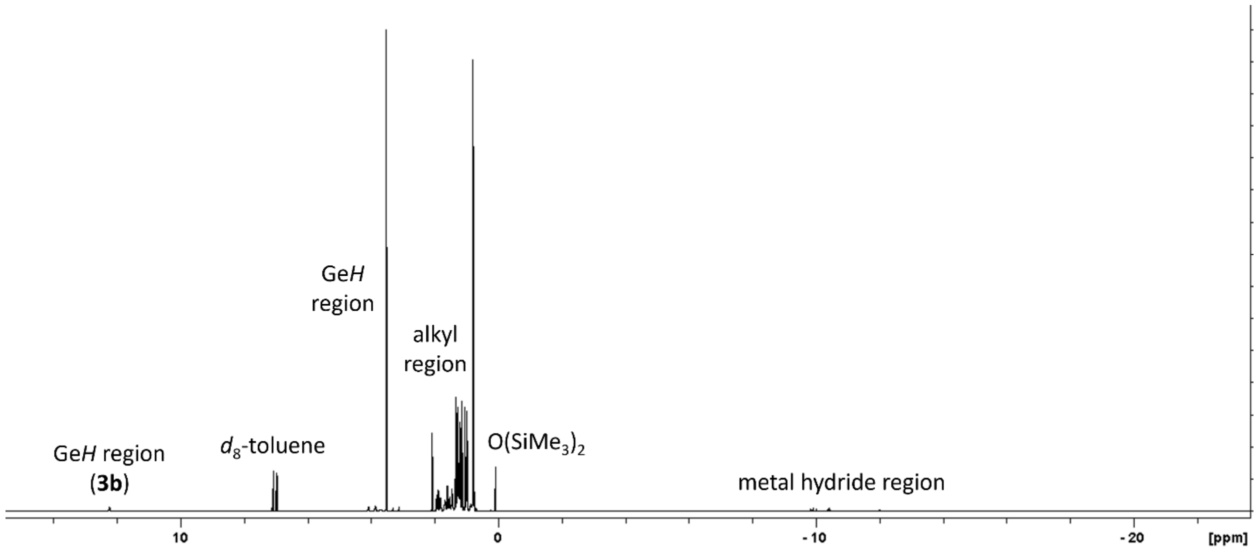

Figure S49. [1]H NMR spectrum of a mixture formed from the reaction of [(dmpe)$_2$MnH(=GeH^{n}Bu)] (**3b**) and an excess of H$_3$Ge^{n}Bu in d_8-toluene (600 MHz, 298 K), containing H$_3$Ge^{n}Bu, [(dmpe)$_2$MnH(=GeH^{n}Bu)] (**3b**), *mer*-[(dmpe)$_2$MnH(GeH$_2$^{n}Bu)$_2$] (**4b**), and *trans*-[(dmpe)$_2$Mn(GeH$_2$^{n}Bu)(HGeH$_2$^{n}Bu)] (**5b**).

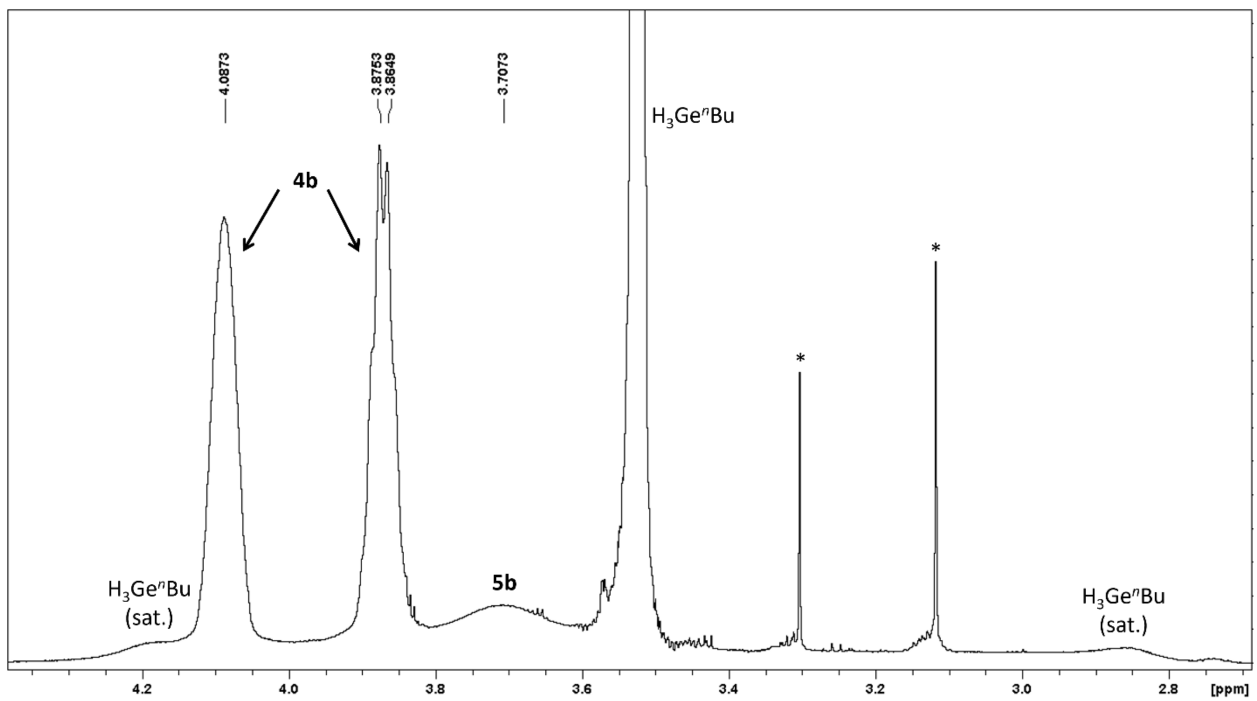

Figure S50. Expanded Ge*H* region of the [1]H NMR spectrum of a mixture formed from the reaction of [(dmpe)$_2$MnH(=GeH^{n}Bu)] (**3b**) and an excess of H$_3$Ge^{n}Bu in d_8-toluene (600 MHz, 298 K), containing H$_3$Ge^{n}Bu, [(dmpe)$_2$MnH(=GeH^{n}Bu)] (**3b**), *mer*-[(dmpe)$_2$MnH(GeH$_2$^{n}Bu)$_2$] (**4b**), and *trans*-[(dmpe)$_2$Mn(GeH$_2$^{n}Bu)(HGeH$_2$^{n}Bu)] (**5b**). Labelled peaks arise from Ge*H* environments, and * indicates peaks from impurities in the H$_3$Ge^{n}Bu used.

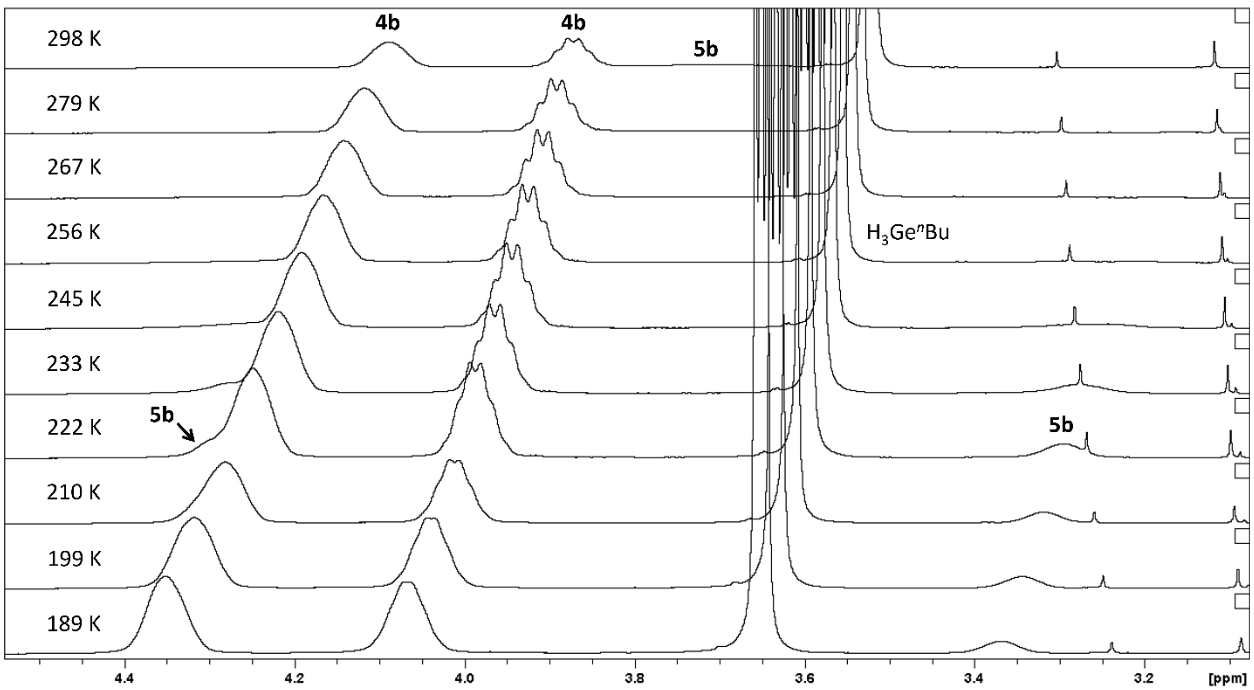

Figure S51. Expanded Ge*H* region of variable temperture ^{1}H NMR spectra of a mixture formed from the reaction of [(dmpe)$_2$MnH(=GeH^{n}Bu)] (**3b**) and an excess of H$_3$Ge^{n}Bu in d_8-toluene (500 MHz), containing H$_3$Ge^{n}Bu, [(dmpe)$_2$MnH(=GeH^{n}Bu)] (**3b**), *mer*-[(dmpe)$_2$MnH(GeH$_2$^{n}Bu)$_2$] (**4b**), and *trans*-[(dmpe)$_2$Mn(GeH$_2$^{n}Bu)(HGeH$_2$^{n}Bu)] (**5b**). Labelled peaks arise from Ge*H* environments.

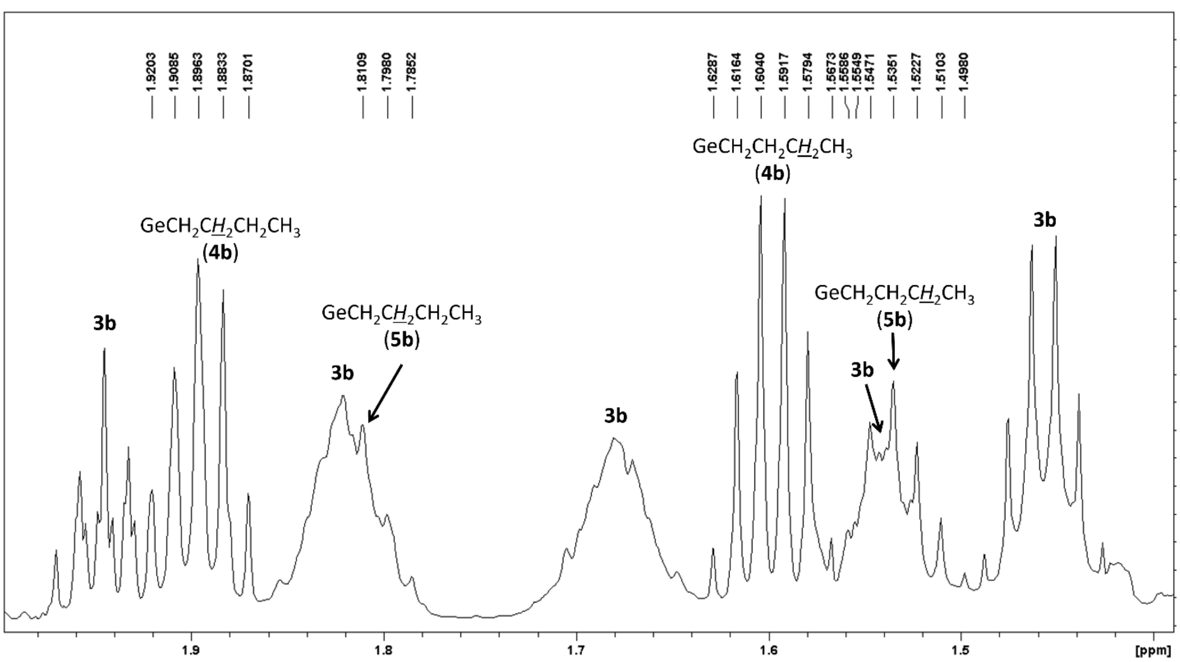

Figure S52. Expanded higher frequency alkyl region of the ^{1}H NMR spectrum of a mixture formed from the reaction of [(dmpe)$_2$MnH(=GeH^{n}Bu)] (**3b**) and an excess of H$_3$Ge^{n}Bu in d_8-toluene (600 MHz, 298 K), containing H$_3$Ge^{n}Bu, [(dmpe)$_2$MnH(=GeH^{n}Bu)] (**3b**), *mer*-[(dmpe)$_2$MnH(GeH$_2$^{n}Bu)$_2$] (**4b**), and *trans*-[(dmpe)$_2$Mn(GeH$_2$^{n}Bu)(HGeH$_2$^{n}Bu)] (**5b**).

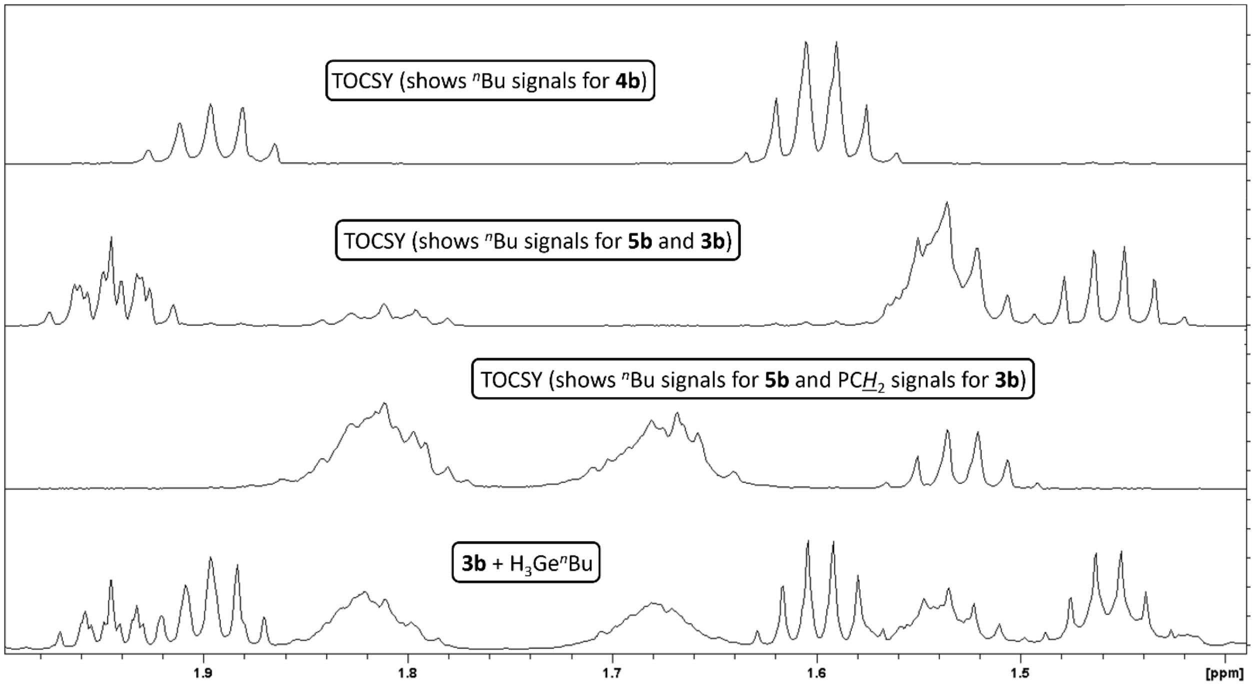

Figure S53. Bottom; expanded higher frequency alkyl region of the ^{1}H NMR spectrum of a mixture formed from the reaction of [(dmpe)$_2$MnH(=GeH^{n}Bu)] (**3b**) and an excess of H_3Ge^nBu in d_8-toluene (600 MHz, 298 K), containing H_3Ge^nBu, [(dmpe)$_2$MnH(=GeH^{n}Bu)] (**3b**), *mer*-[(dmpe)$_2$MnH(GeH$_2{}^n$Bu)$_2$] (**4b**), and *trans*-[(dmpe)$_2$Mn(GeH$_2{}^n$Bu)(HGeH$_2{}^n$Bu)] (**5b**). Top three; 1D TOCSY NMR spectra of the reaction mixture formed from the reaction of [(dmpe)$_2$MnH(=GePh$_2$)] (**2a**) and an excess of H_3Ge^nBu in d_8-toluene (500 MHz, 298 K), containing H_3Ge^nBu, H_2GePh_2, [(dmpe)$_2$MnH(=GeH^{n}Bu)] (**3b**), *mer*-[(dmpe)$_2$MnH(GeH$_2{}^n$Bu)$_2$] (**4b**), and *trans*-[(dmpe)$_2$Mn(GeH$_2{}^n$Bu)(HGeH$_2{}^n$Bu)] (**5b**), with excitation at 1.81 (second from the bottom), 1.54 (second from the top), or 1.61 (top) ppm. These spectra illustrate in the higher frequency region of *second from the bottom*; ^{n}Bu signals for **5b** and PC$\underline{H}_2$ signals for **3b**, *second from the top*; ^{n}Bu signals for **5b** and **3b**, and *top*; ^{n}Bu signals for **4b**.

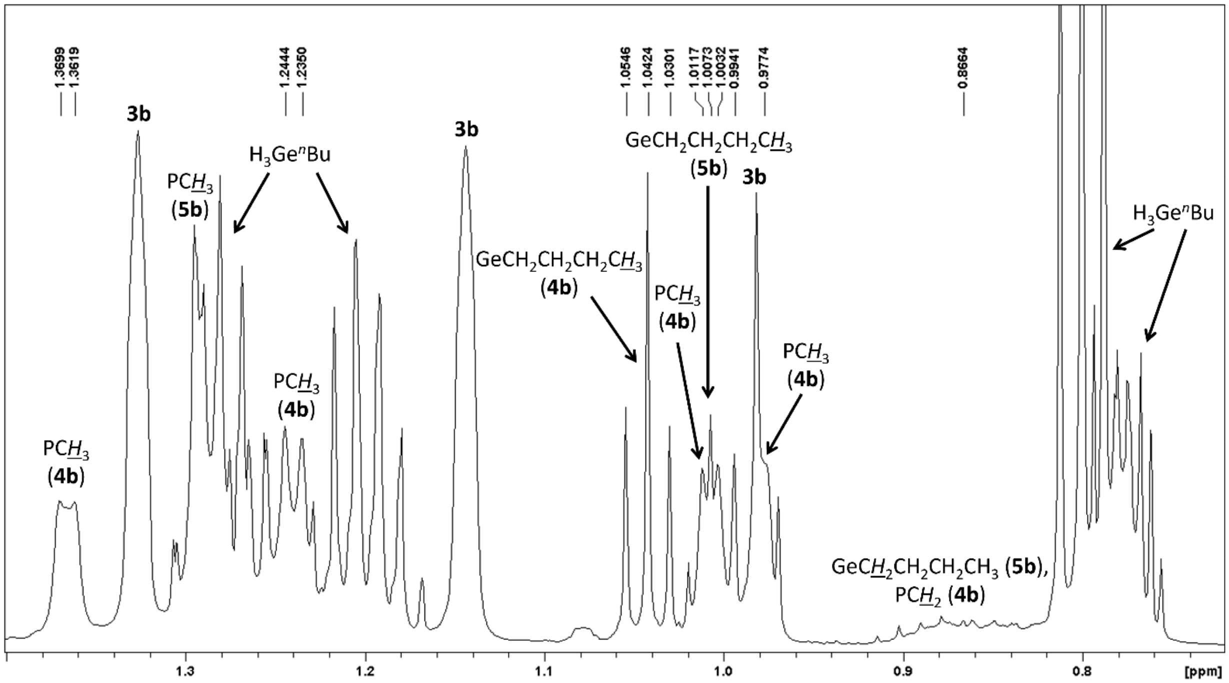

Figure S54. Expanded lower frequency alkyl region of the ^{1}H NMR spectrum of a mixture formed from the reaction of [(dmpe)$_2$MnH(=GeH^{n}Bu)] (**3b**) and an excess of H_3Ge^nBu in d_8-toluene (600 MHz, 298 K), containing H_3Ge^nBu, [(dmpe)$_2$MnH(=GeH^{n}Bu)] (**3b**), *mer*-[(dmpe)$_2$MnH(GeH$_2$^{n}Bu)$_2$] (**4b**), and *trans*-[(dmpe)$_2$Mn(GeH$_2$^{n}Bu)(HGeH$_2$^{n}Bu)] (**5b**).

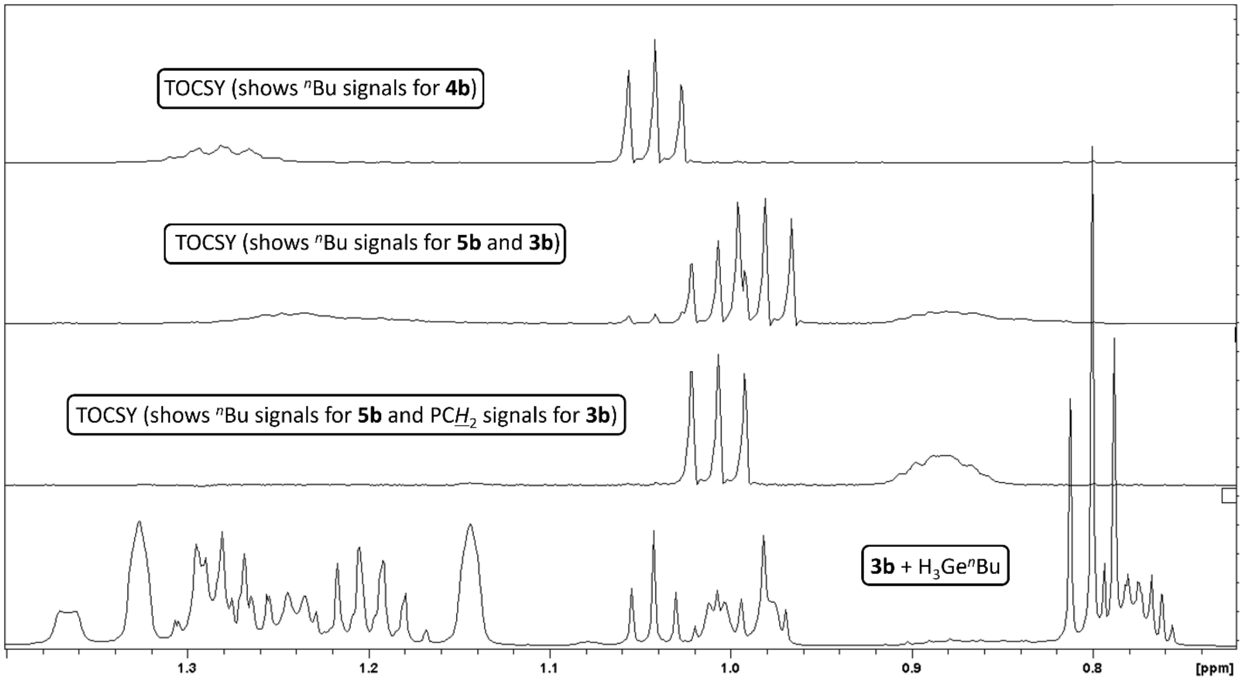

Figure S55. Bottom; expanded lower frequency alkyl region of the ^{1}H NMR spectrum of a mixture formed from the reaction of [(dmpe)$_2$MnH(=GeH^{n}Bu)] (**3b**) and an excess of H_3Ge^nBu in d_8-toluene (600 MHz, 298 K), containing H_3Ge^nBu, [(dmpe)$_2$MnH(=GeH^{n}Bu)] (**3b**), *mer*-[(dmpe)$_2$MnH(GeH$_2$^{n}Bu)$_2$] (**4b**), and *trans*-[(dmpe)$_2$Mn(GeH$_2$^{n}Bu)(HGeH$_2$^{n}Bu)] (**5b**). Top three; 1D TOCSY NMR spectra of the reaction mixture formed from the reaction of [(dmpe)$_2$MnH(=GePh$_2$)] (**2a**) and an excess of H_3Ge^nBu in d_8-toluene (500 MHz, 298 K), containing H_3Ge^nBu, H_2GePh_2, [(dmpe)$_2$MnH(=GeH^{n}Bu)] (**3b**), *mer*-[(dmpe)$_2$MnH(GeH$_2$^{n}Bu)$_2$] (**4b**), and *trans*-[(dmpe)$_2$Mn(GeH$_2$^{n}Bu)(HGeH$_2$^{n}Bu)] (**5b**), with excitation at 1.81 (second from the bottom), 1.54 (second from the top), or 1.61 (top) ppm. These spectra illustrate in the lower frequency region of *second from the bottom*; ^{n}Bu signals for **5b**, *second from the top*; ^{n}Bu signals for **5b** and **3b**, and *top*; ^{n}Bu signals for **4b**.

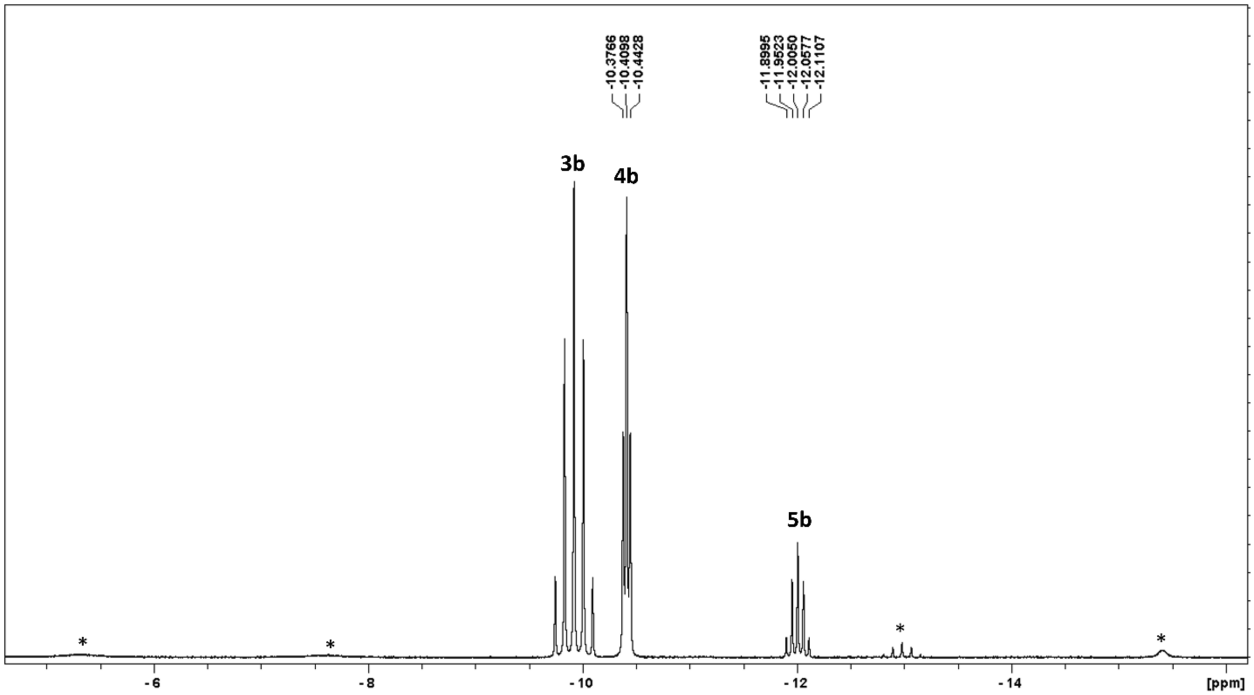

Figure S56. Expanded metal hydride region of the ^{1}H NMR spectrum of a mixture formed from the reaction of [(dmpe)$_2$MnH(=GeH^{n}Bu)] (**3b**) and an excess of H$_3$Ge^{n}Bu in d_8-toluene (600 MHz, 298 K), containing H$_3$Ge^{n}Bu, [(dmpe)$_2$MnH(=GeH^{n}Bu)] (**3b**), *mer*-[(dmpe)$_2$MnH(GeH$_2$^{n}Bu)$_2$] (**4b**), and *trans*-[(dmpe)$_2$Mn(GeH$_2$^{n}Bu)(HGeH$_2$^{n}Bu)] (**5b**). Labelled peaks arise from Mn<u>*H*</u> environments, and * indicates peaks arising from impurities in the reaction mixture.

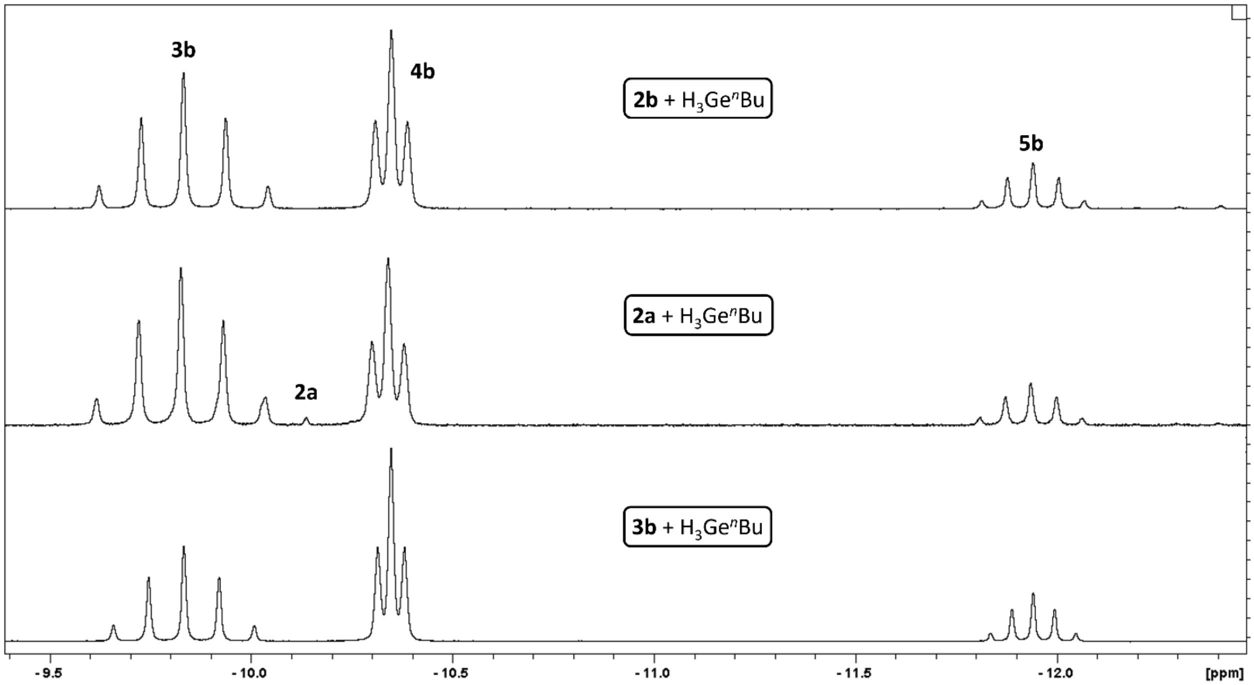

Figure S57. Expanded metal hydride region of the ^{1}H NMR spectrum of a mixture formed from the reaction of excess H_3Ge^nBu with [(dmpe)$_2$MnH(=GeH^{n}Bu)] (**3b**; bottom), [(dmpe)$_2$MnH(=GePh$_2$)] (**2a**; middle), or [(dmpe)$_2$MnH(=GeEt$_2$)] (**2b**; top) in C_6D_6 at 298 K (bottom; 500 MHz, middle and top; 600 MHz), containing H_3Ge^nBu, H_2GePh_2 (middle only) or H_2GeEt_2 (top only), **2a** (middle only), [(dmpe)$_2$MnH(=GeH^{n}Bu)] (**3b**), *mer*-[(dmpe)$_2$MnH(GeH$_2$^{n}Bu)$_2$] (**4b**), and *trans*-[(dmpe)$_2$Mn(GeH$_2$^{n}Bu)(HGeH$_2$^{n}Bu)] (**5b**). Labelled peaks arise from Mn*H* environments.

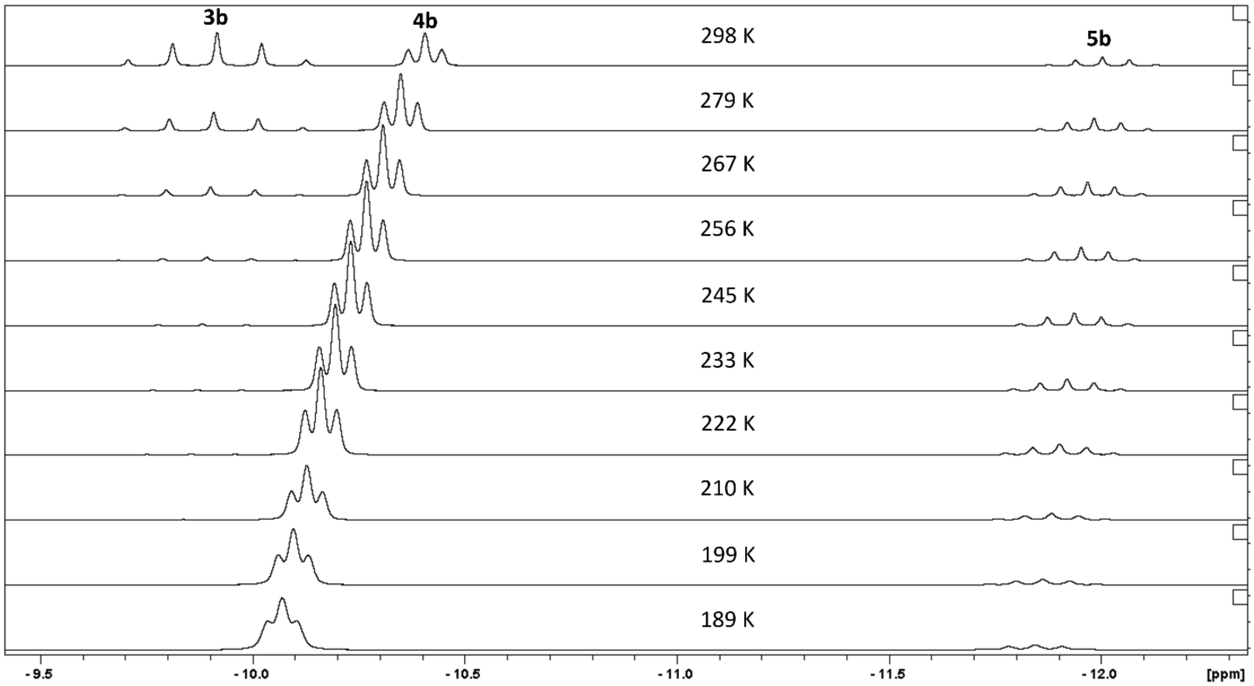

Figure S58. Expanded metal hydride region of variable temperature ^{1}H NMR spectra of a mixture formed from the reaction of [(dmpe)$_2$MnH(=GeH^{n}Bu)] (**3b**) and an excess of H$_3$Ge^{n}Bu in d_8-toluene (500 MHz), containing H$_3$Ge^{n}Bu, [(dmpe)$_2$MnH(=GeH^{n}Bu)] (**3b**), *mer*-[(dmpe)$_2$MnH(GeH$_2$^{n}Bu)$_2$] (**4b**), and *trans*-[(dmpe)$_2$Mn(GeH$_2$^{n}Bu)(HGeH$_2$^{n}Bu)] (**5b**). Labelled peaks arise from Mn*<u>H</u>* environments.

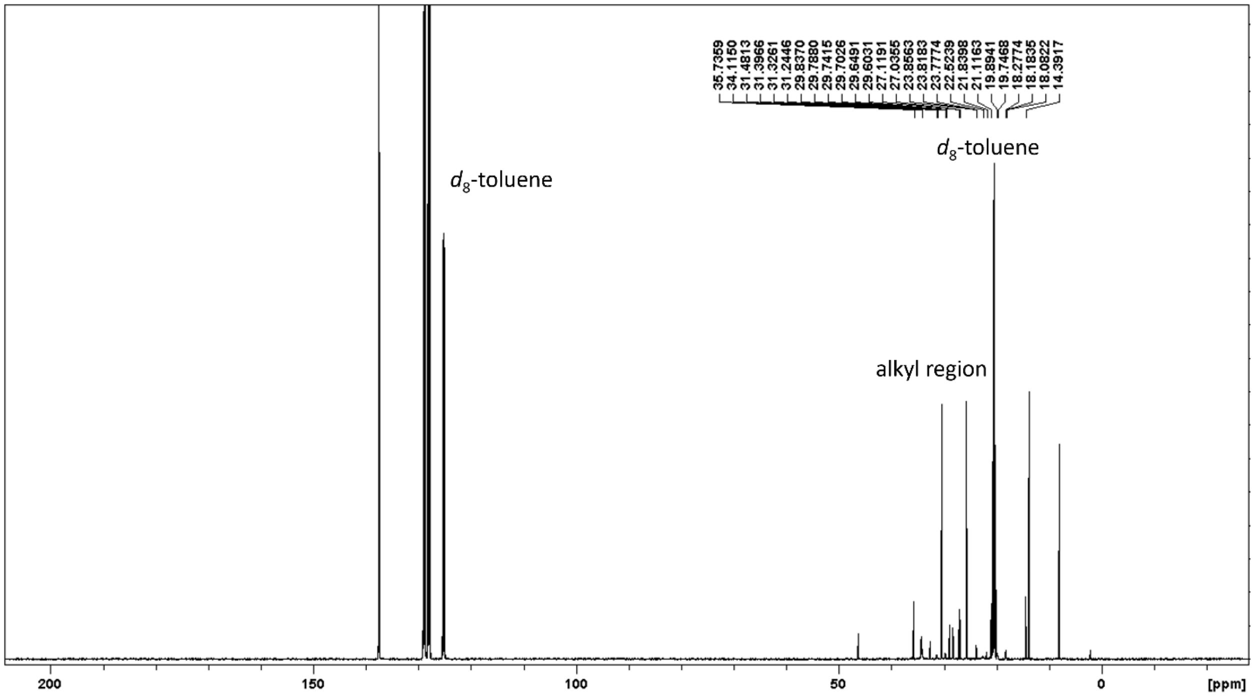

Figure S59. ^{31}C{^{1}H} NMR spectrum of a mixture formed from the reaction of [(dmpe)$_2$MnH(=GeH^{n}Bu)] (**3b**) and an excess of H_3Ge^nBu in d_8-toluene (151 MHz, 298 K), containing H_3Ge^nBu, [(dmpe)$_2$MnH(=GeH^{n}Bu)] (**3b**), *mer*-[(dmpe)$_2$MnH(GeH$_2{}^n$Bu)$_2$] (**4b**), and *trans*-[(dmpe)$_2$Mn(GeH$_2{}^n$Bu)(HGeH$_2{}^n$Bu)] (**5b**).

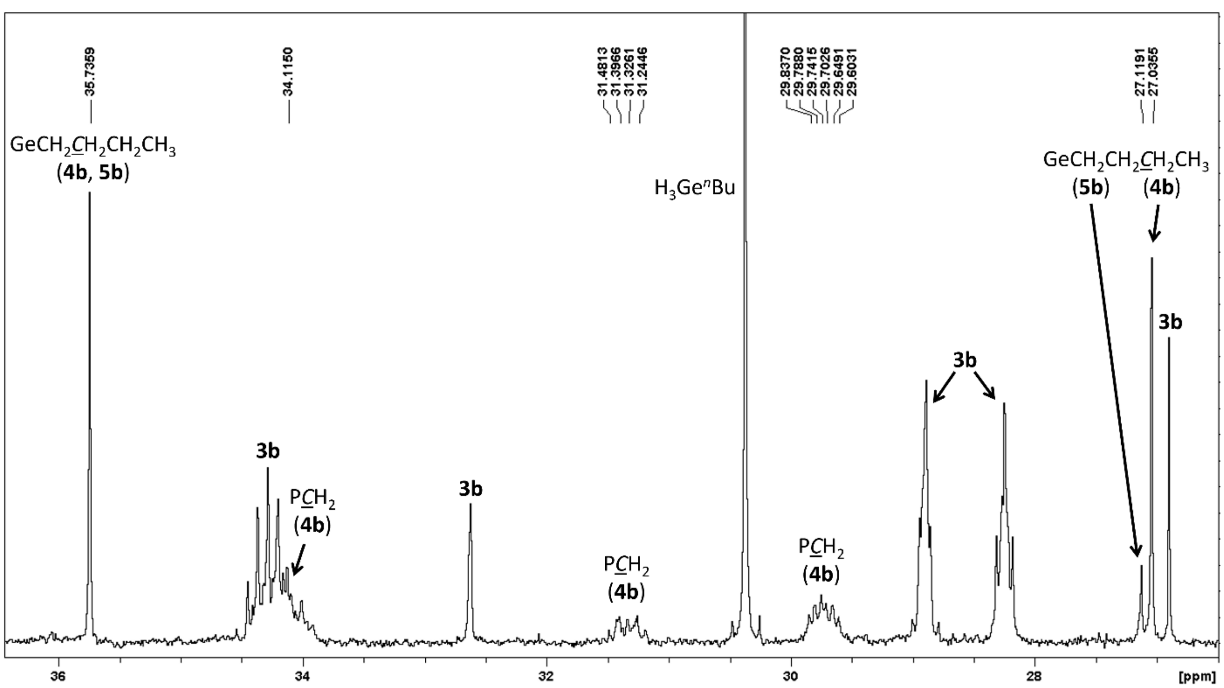

Figure S60. Expanded higher frequency alkyl region of the ^{31}C{^{1}H} NMR spectrum of a mixture formed from the reaction of [(dmpe)$_2$MnH(=GeH^{n}Bu)] (**3b**) and an excess of H_3Ge^nBu in d_8-toluene (151 MHz, 298 K), containing H_3Ge^nBu, [(dmpe)$_2$MnH(=GeH^{n}Bu)] (**3b**), *mer*-[(dmpe)$_2$MnH(GeH$_2{}^n$Bu)$_2$] (**4b**), and *trans*-[(dmpe)$_2$Mn(GeH$_2{}^n$Bu)(HGeH$_2{}^n$Bu)] (**5b**).

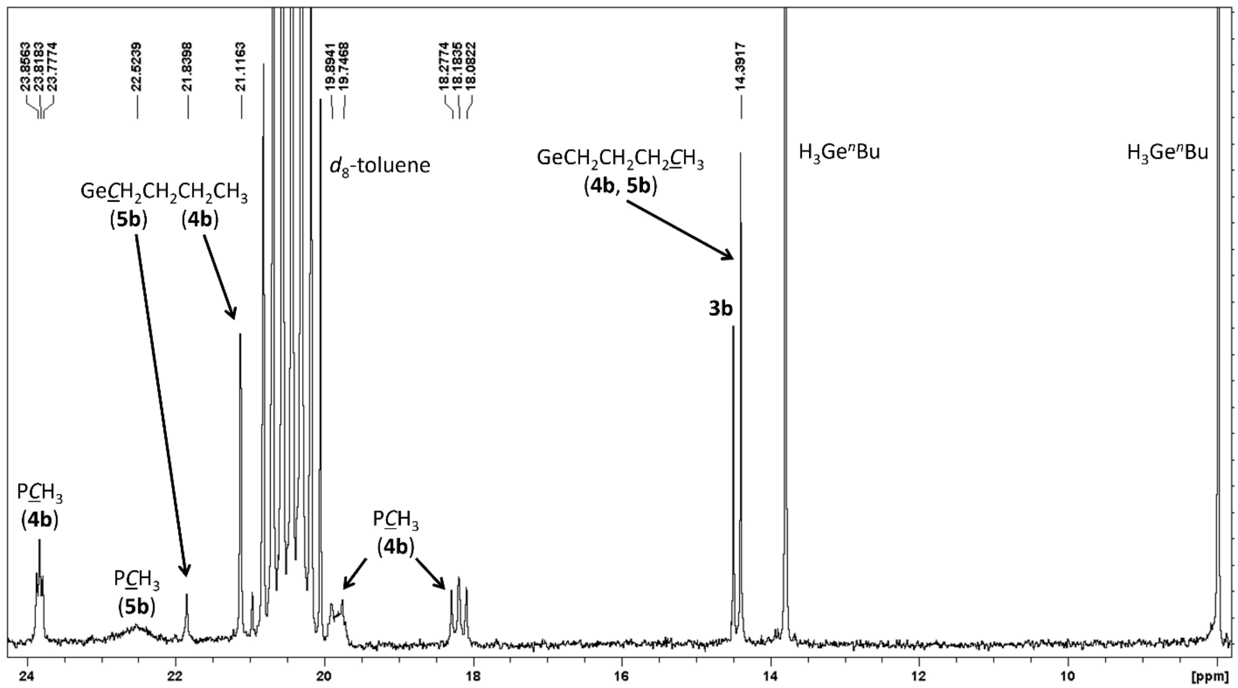

Figure S61. Expanded lower frequency alkyl region of the $^{31}C\{^1H\}$ NMR spectrum of a mixture formed from the reaction of $[(dmpe)_2MnH(=GeH^nBu)]$ (**3b**) and an excess of H_3Ge^nBu in d_8-toluene (151 MHz, 298 K), containing H_3Ge^nBu, $[(dmpe)_2MnH(=GeH^nBu)]$ (**3b**), *mer*-$[(dmpe)_2MnH(GeH_2{}^nBu)_2]$ (**4b**), and *trans*-$[(dmpe)_2Mn(GeH_2{}^nBu)(HGeH_2{}^nBu)]$ (**5b**).

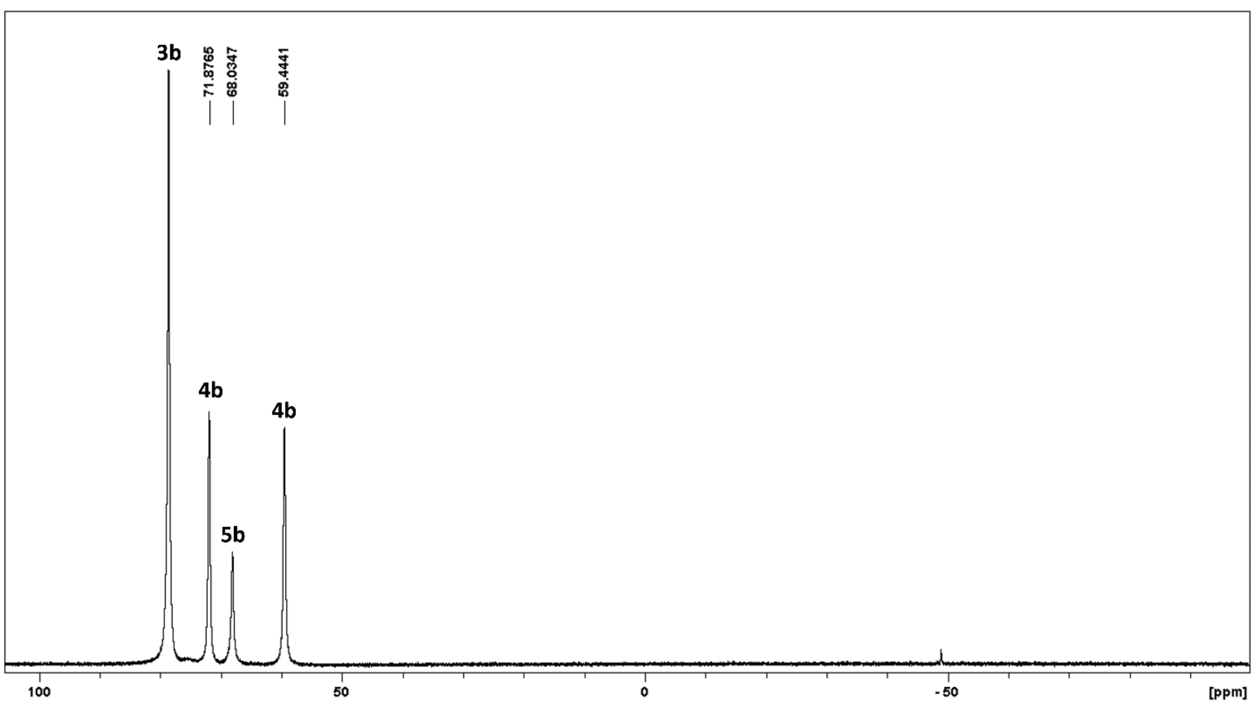

Figure S62. $^{31}P\{^1H\}$ NMR spectrum of a mixture formed from the reaction of $[(dmpe)_2MnH(=GeH^nBu)]$ (**3b**) and an excess of H_3Ge^nBu in d_8-toluene (243 MHz, 298 K), containing H_3Ge^nBu, $[(dmpe)_2MnH(=GeH^nBu)]$ (**3b**), *mer*-$[(dmpe)_2MnH(GeH_2{}^nBu)_2]$ (**4b**), and *trans*-$[(dmpe)_2Mn(GeH_2{}^nBu)(HGeH_2{}^nBu)]$ (**5b**).

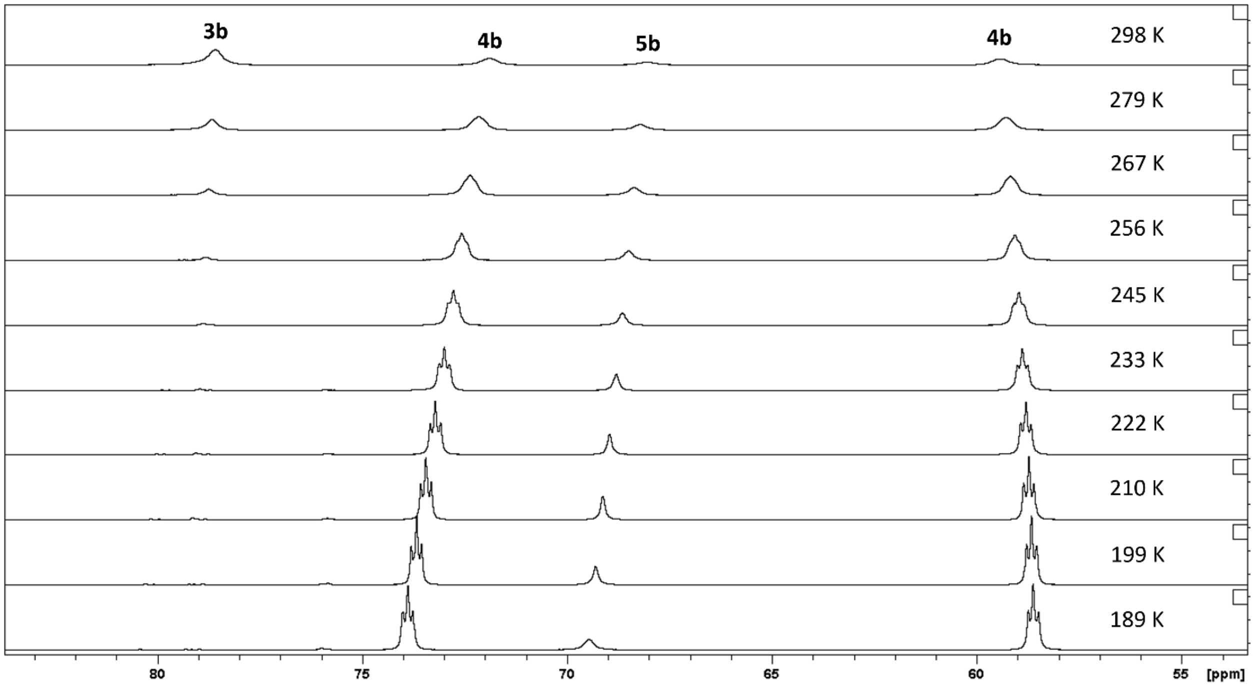

Figure S63. Variable temperature $^{31}P\{^1H\}$ NMR spectra of a mixture formed from the reaction of [(dmpe)$_2$MnH(=GeH^{n}Bu)] (**3b**) and an excess of H_3Ge^nBu in d_8-toluene (202 MHz), containing H_3Ge^nBu, [(dmpe)$_2$MnH(=GeH^{n}Bu)] (**3b**), *mer*-[(dmpe)$_2$MnH(GeH$_2{}^n$Bu)$_2$] (**4b**), and *trans*-[(dmpe)$_2$Mn(GeH$_2{}^n$Bu)(HGeH$_2{}^n$Bu)] (**5b**).

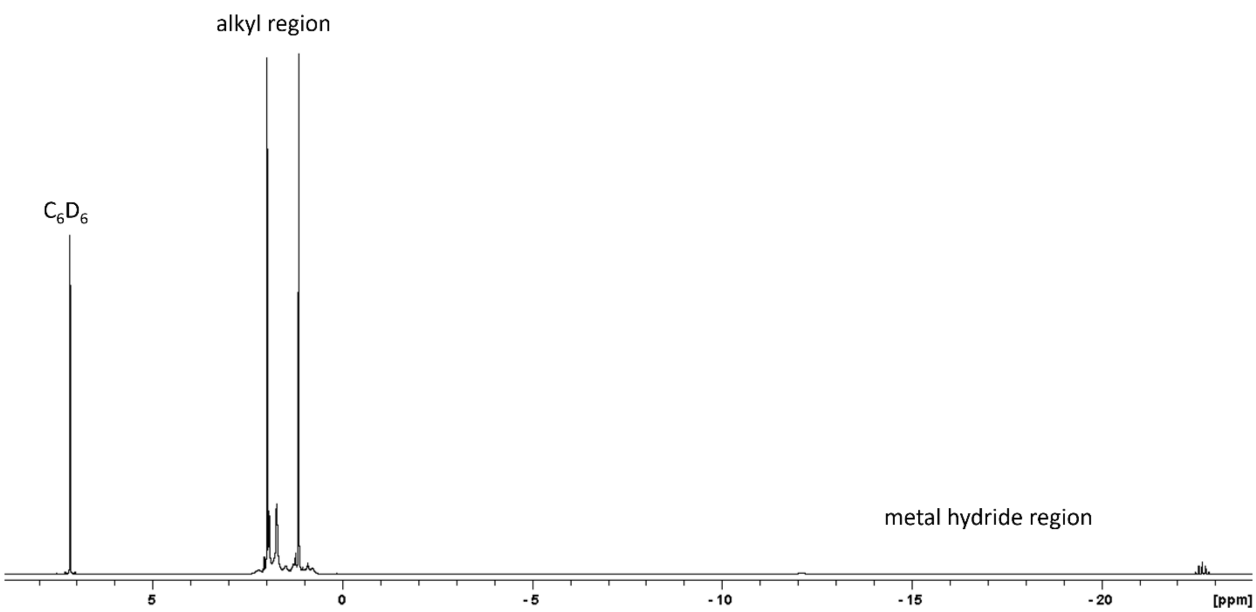

Figure S64. ^{1}H NMR spectrum of [{(dmpe)$_2$MnH}$_2$(μ-Ge)] (**6**) in C_6D_6 (600 MHz, 298 K).

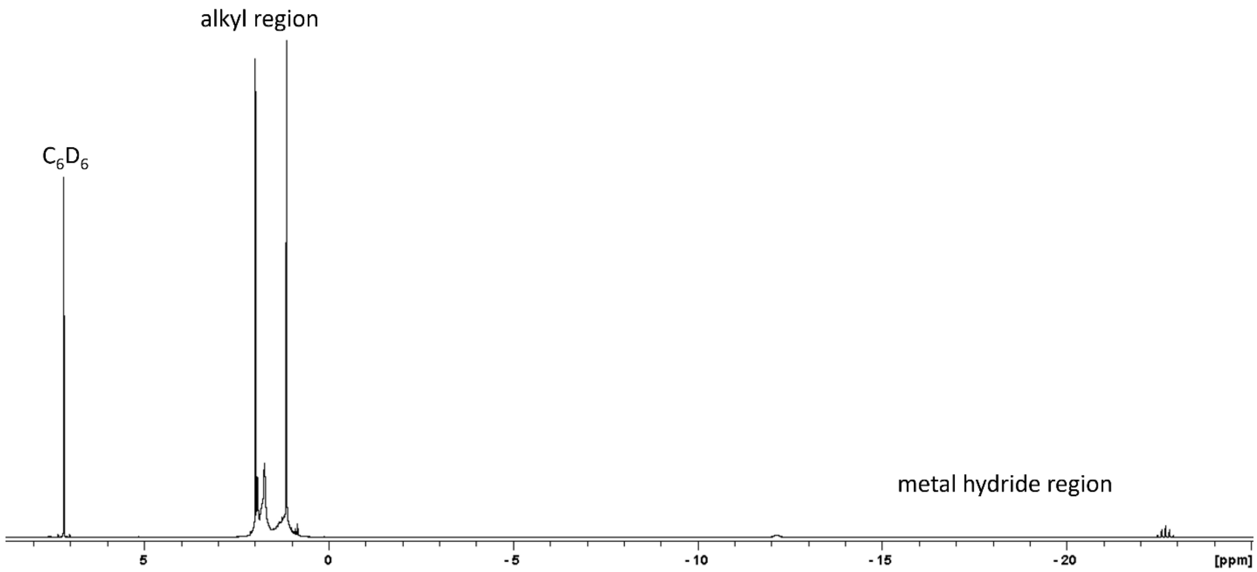

Figure S65. ^{1}H NMR spectrum of [{(dmpe)$_2$MnH}$_2$(μ-Ge)] (**6**) in C_6D_6 (500 MHz, 334 K).

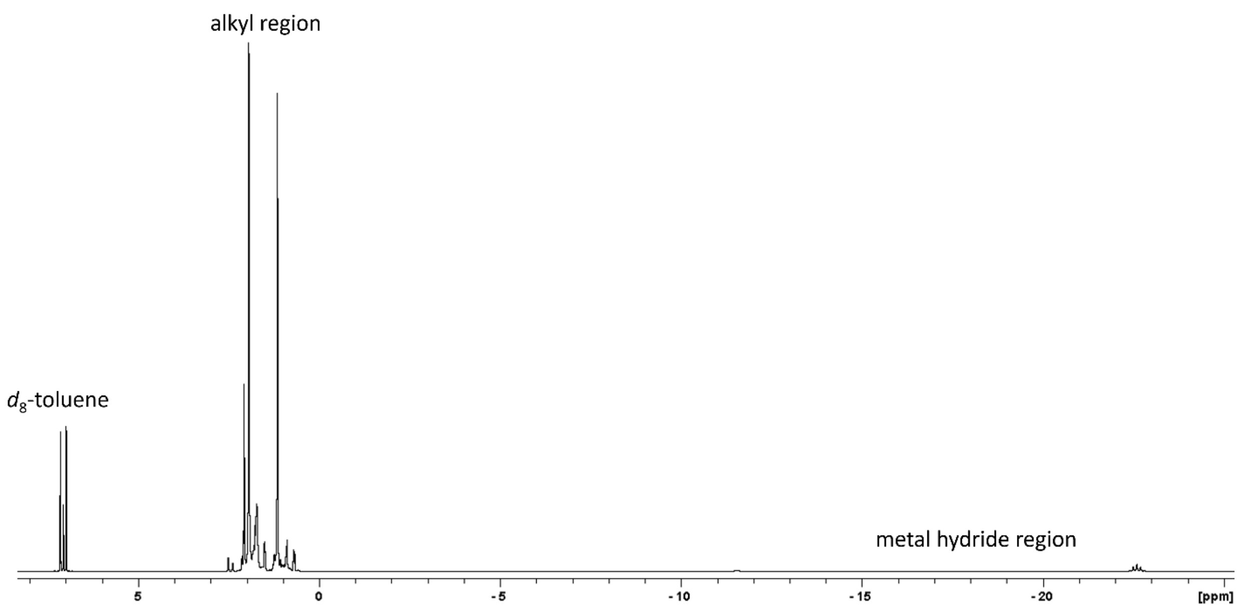

Figure S66. ^{1}H NMR spectrum of [{(dmpe)$_2$MnH}$_2$(μ-Ge)] (**6**) in d_8-toluene (500 MHz, 189 K).

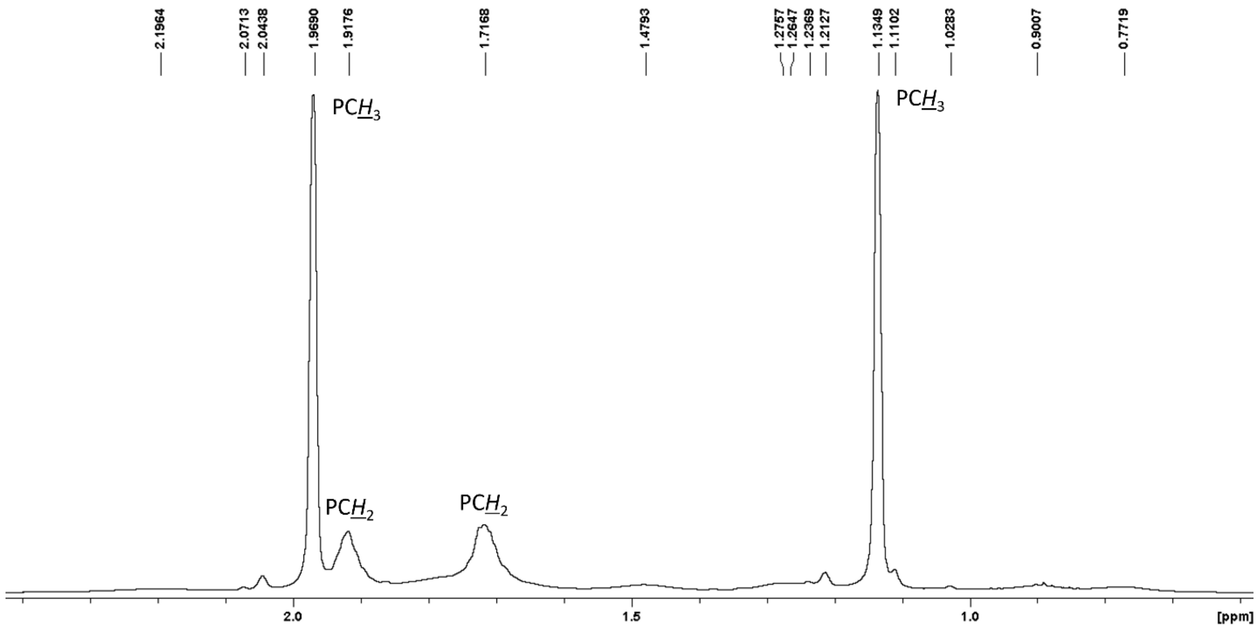

Figure S67. Expanded alkyl region of the ^{1}H NMR spectrum of [{(dmpe)$_2$MnH}$_2$(μ-Ge)] (**6**) in C_6D_6 (600 MHz, 298 K). Labelled peaks arise from the *trans*,*trans* isomer.

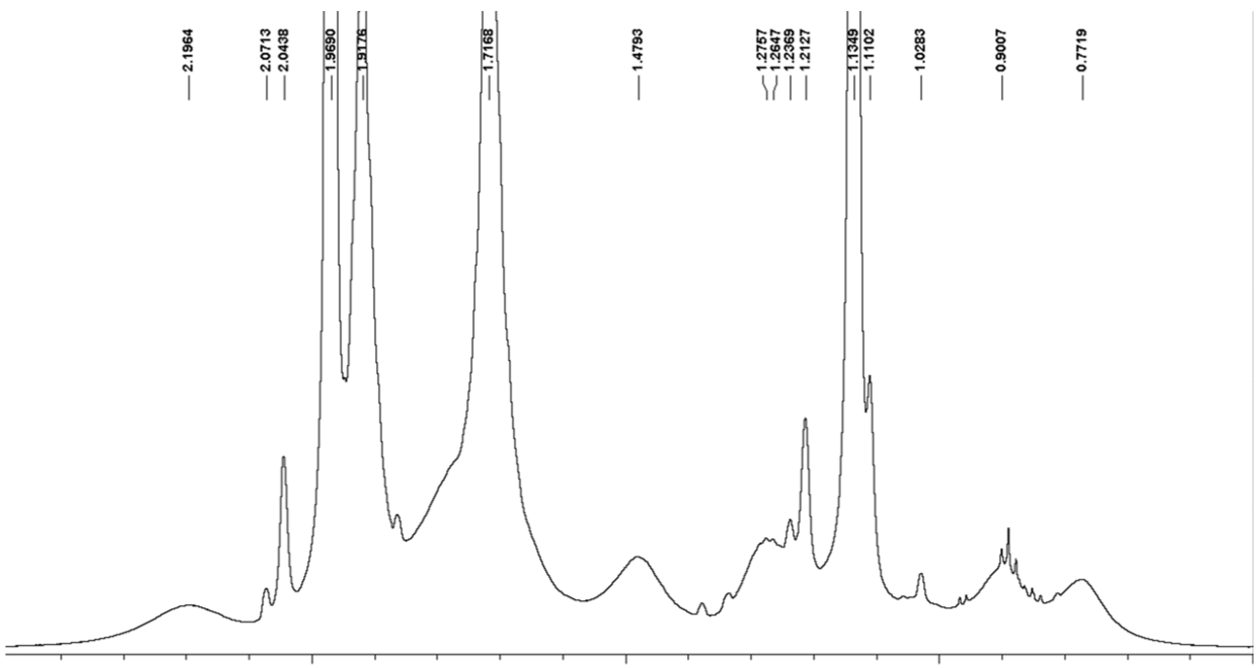

Figure S68. Zoomed-in view of the expanded alkyl region of the ^{1}H NMR spectrum of [{(dmpe)$_2$MnH}$_2$(μ-Ge)] (**6**) in C_6D_6 (600 MHz, 298 K). Cut off peaks arise from the *trans*,*trans* isomer, and others arise from the *cis*,*trans* or *cis*,*cis* isomers.

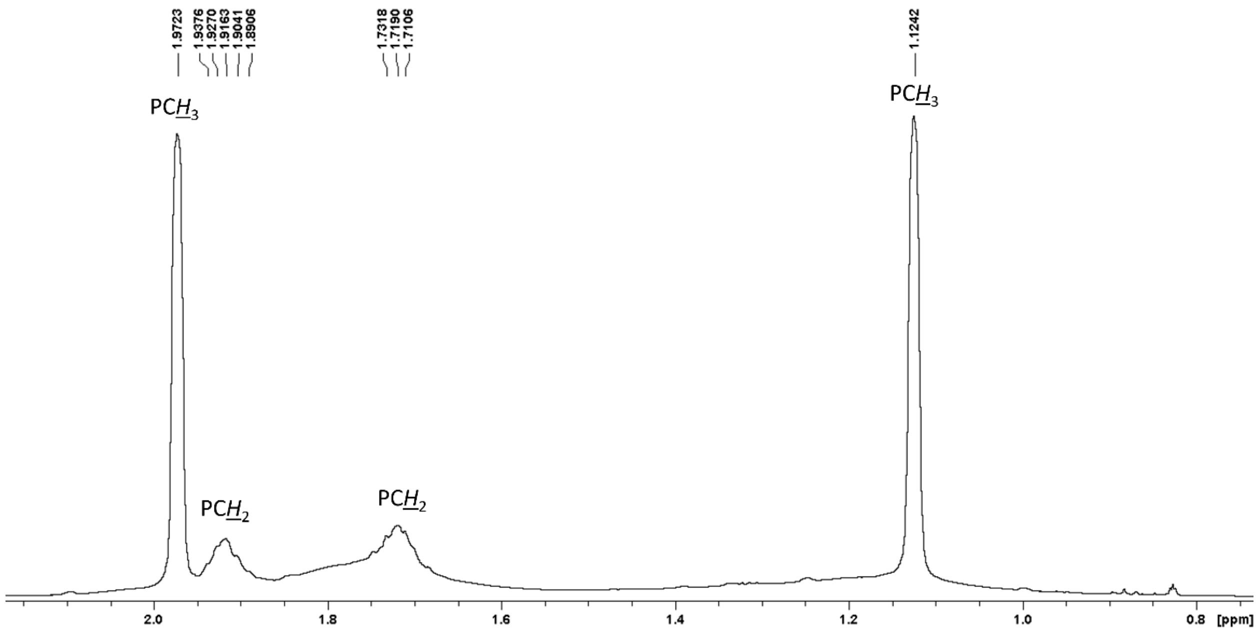

Figure S69. Expanded alkyl region of the ^{1}H NMR spectrum of [{(dmpe)$_2$MnH}$_2$(μ-Ge)] (**6**) in C_6D_6 (500 MHz, 334 K). Labelled peaks arise from the *trans*,*trans* isomer.

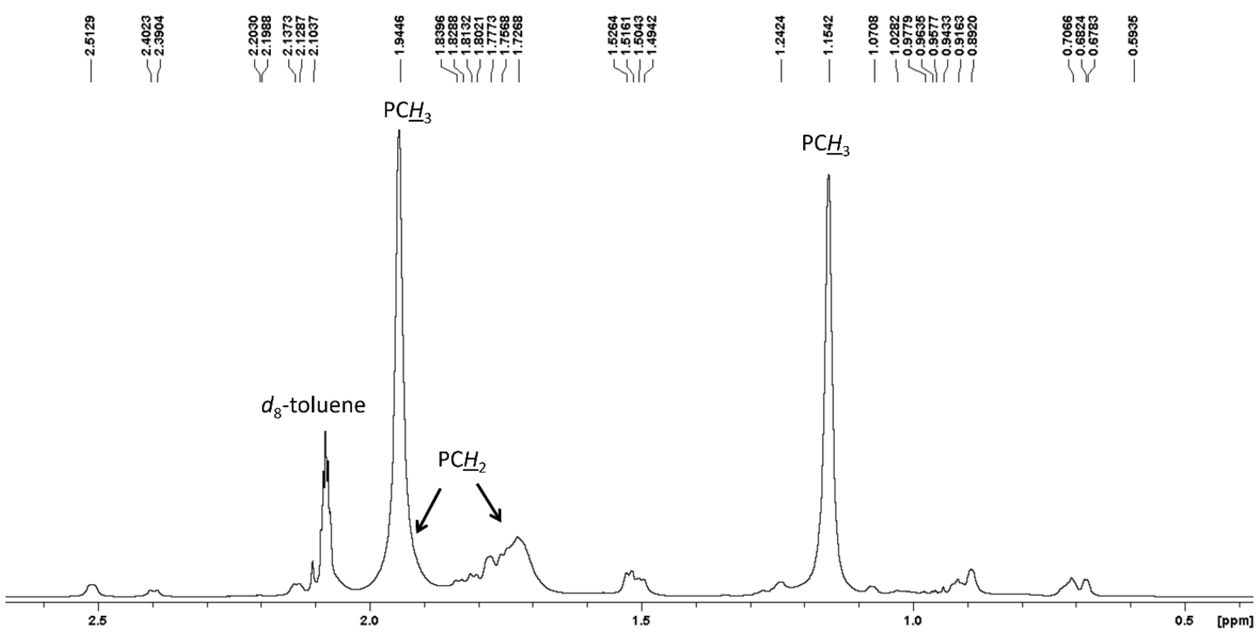

Figure S70. Expanded alkyl region of the ^{1}H NMR spectrum of [{(dmpe)$_2$MnH}$_2$(μ-Ge)] (**6**) in d_8-toluene (500 MHz, 189 K). Labelled peaks arise from the *trans*,*trans* isomer.

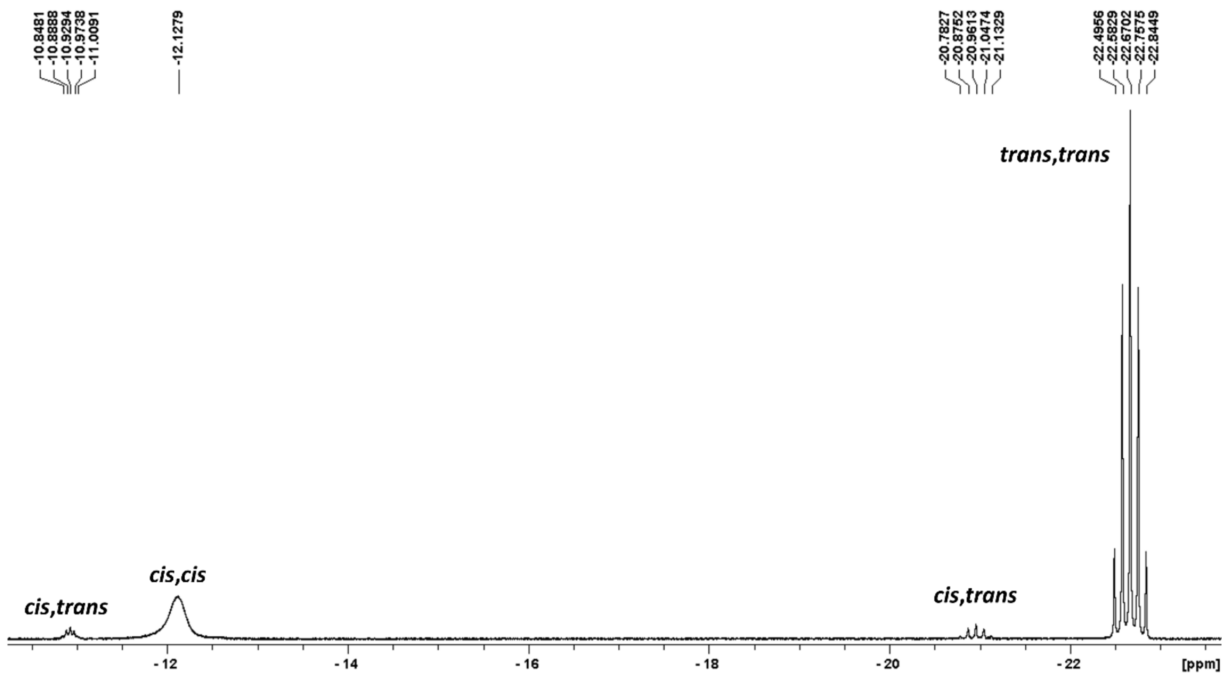

Figure S71. Expanded metal hydride region of the [1]H NMR spectrum of [{(dmpe)$_2$MnH}$_2$(μ-Ge)] (**6**) in C_6D_6 (600 MHz, 298 K). Labelled peaks arise from Mn*__H__* environments.

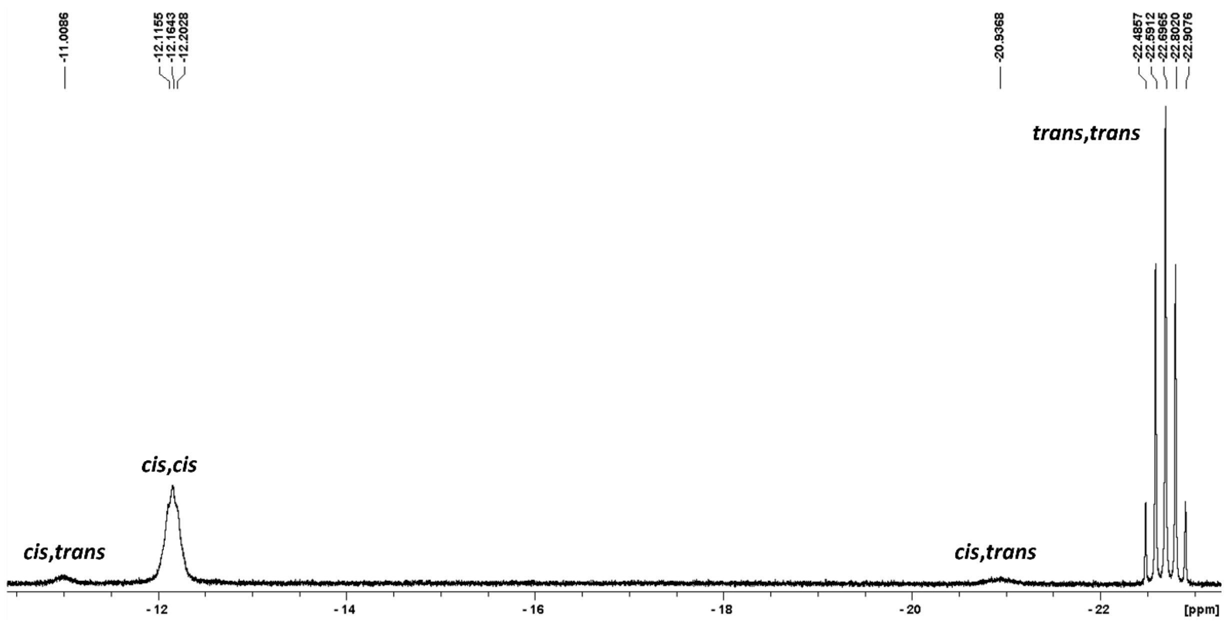

Figure S72. Expanded metal hydride region of the [1]H NMR spectrum of [{(dmpe)$_2$MnH}$_2$(μ-Ge)] (**6**) in C_6D_6 (500 MHz, 334 K). Labelled peaks arise from Mn*__H__* environments.

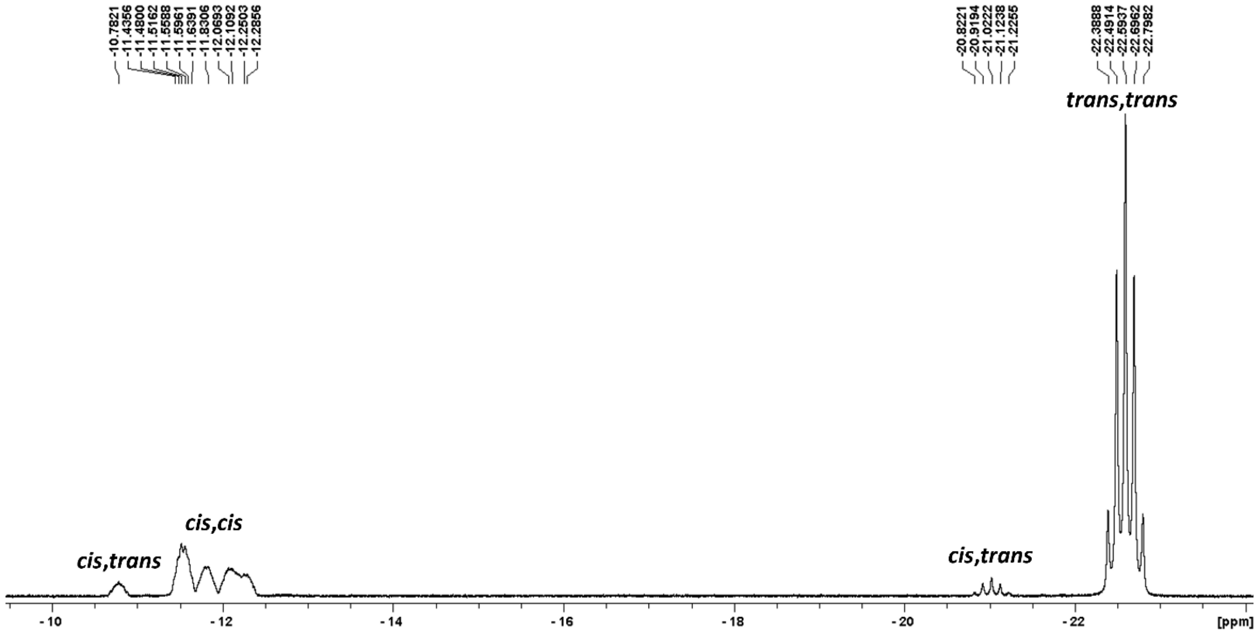

Figure S73. Expanded metal hydride region of the ^{1}H NMR spectrum of [{(dmpe)$_2$MnH}$_2$(μ-Ge)] (**6**) in d_8-toluene (500 MHz, 189 K). Labelled peaks arise from Mn*H* environments.

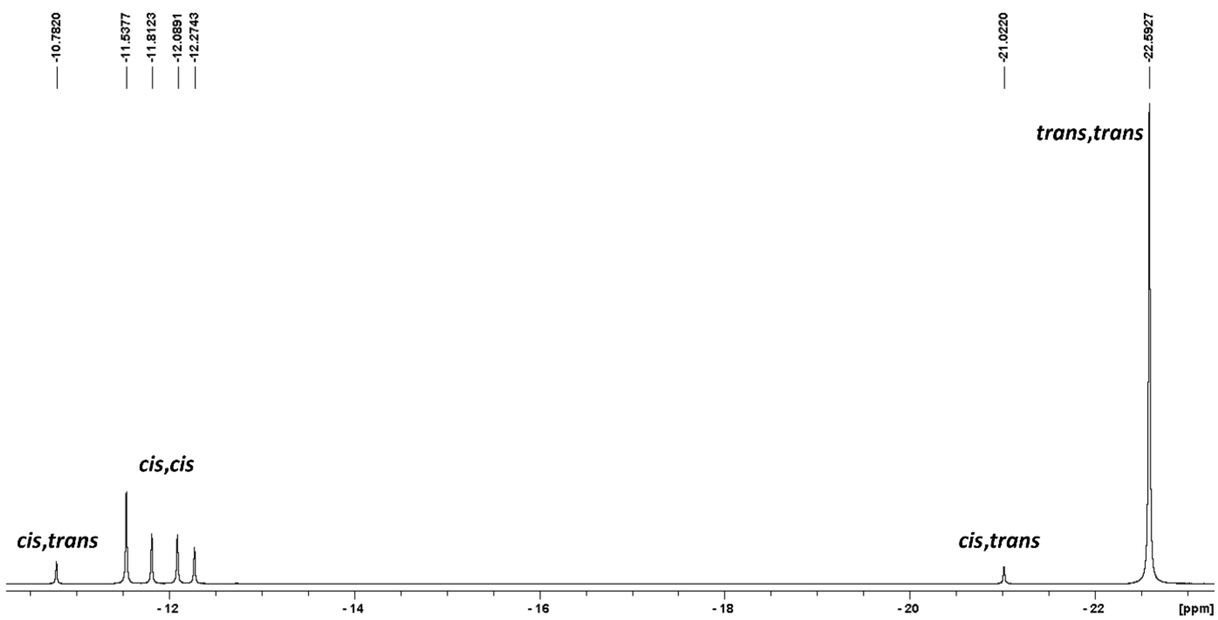

Figure S74. Expanded metal hydride region of the $^{1}H\{^{31}P\}$ NMR spectrum of [{(dmpe)$_2$MnH}$_2$(μ-Ge)] (**6**) in d_8-toluene (500 MHz, 189 K). Labelled peaks arise from Mn*H* environments.

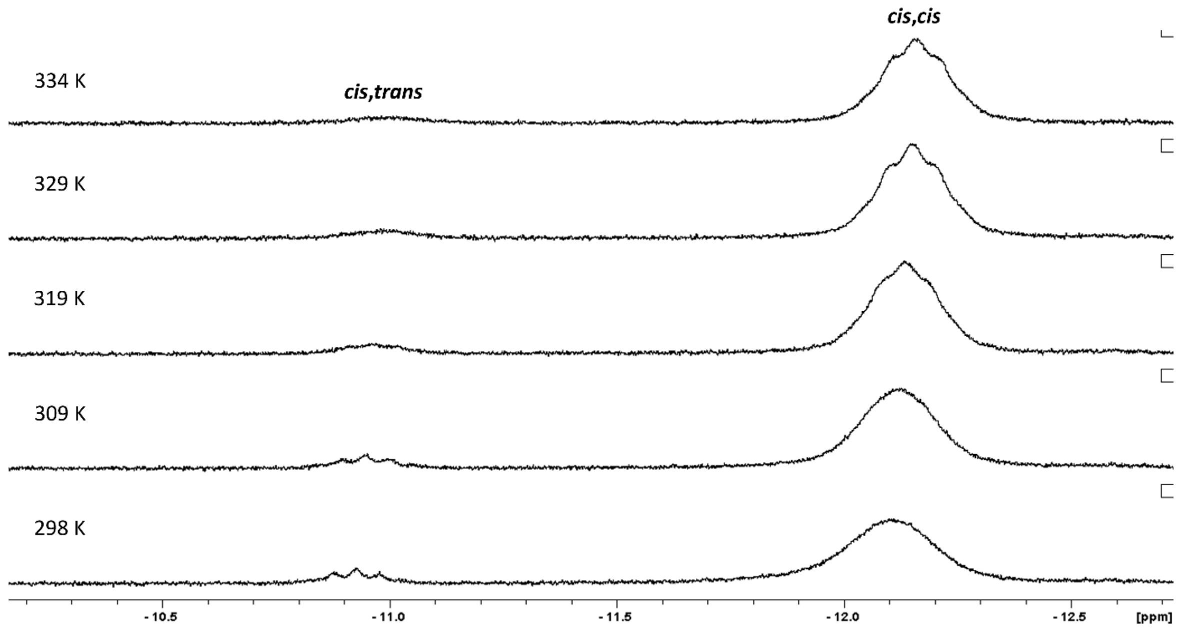

Figure S75. Expanded higher frequency metal hydride region of variable temperature ^{1}H NMR spectra of [{(dmpe)$_2$MnH}$_2$(μ-Ge)] (**6**) in C_6D_6 (500 MHz). Labelled peaks arise from Mn*H* environments.

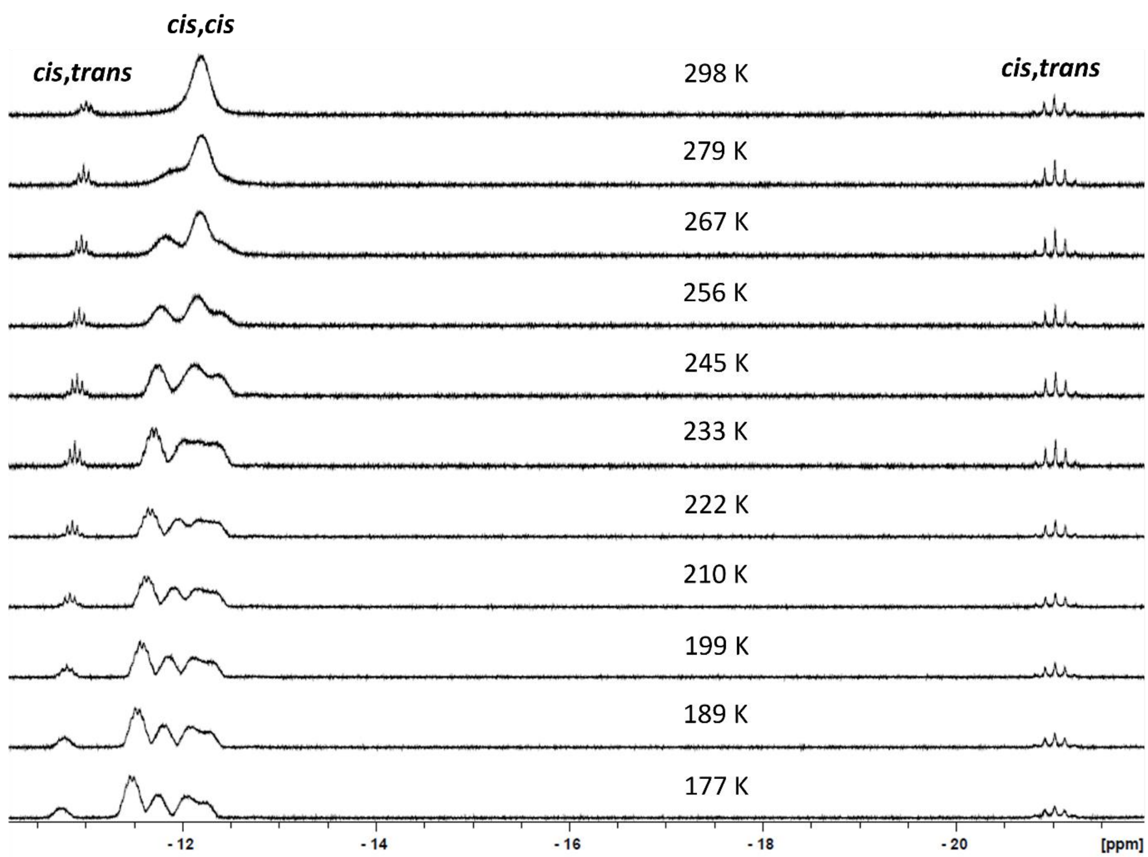

Figure S76. Expanded metal hydride region of variable temperature ^{1}H NMR spectra of [{(dmpe)$_2$MnH}$_2$(μ-Ge)] (**6**) in d_8-toluene (500 MHz). Labelled peaks arise from Mn*H* environments.

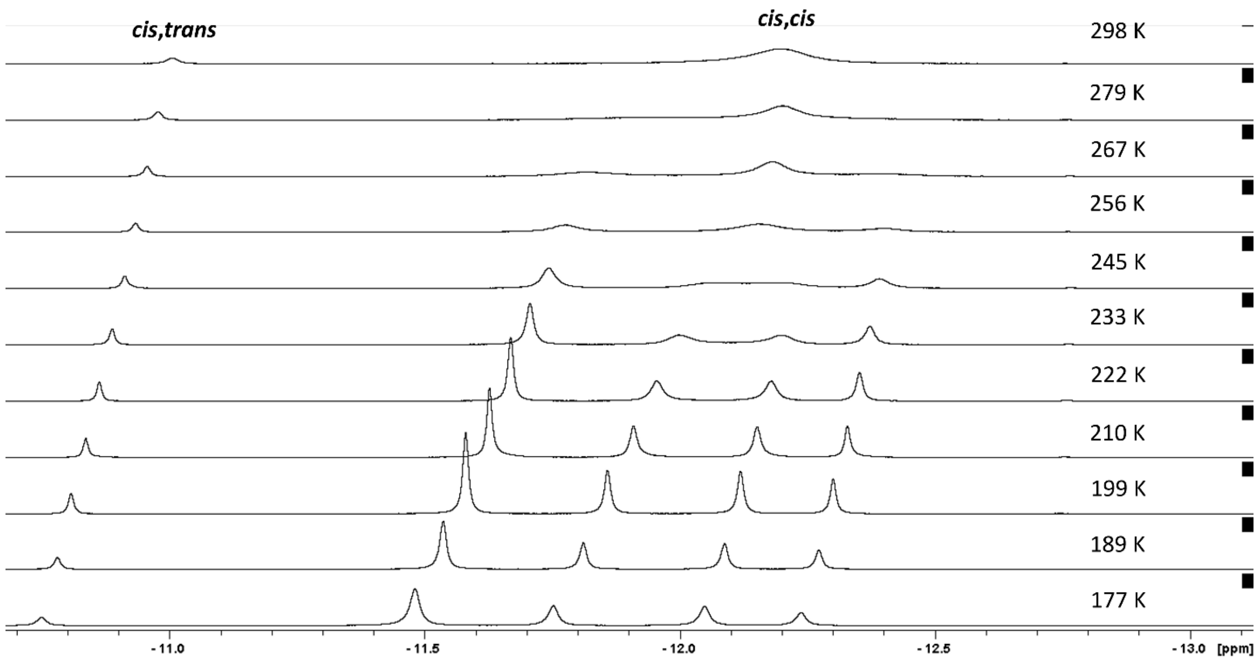

Figure S77. Expanded higher frequency metal hydride region of variable temperature $^{1}H\{^{31}P\}$ NMR spectra of [{(dmpe)$_2$MnH}$_2$(μ-Ge)] (**6**) in d_8-toluene (500 MHz). Labelled peaks arise from Mn*<u>H</u>* environments.

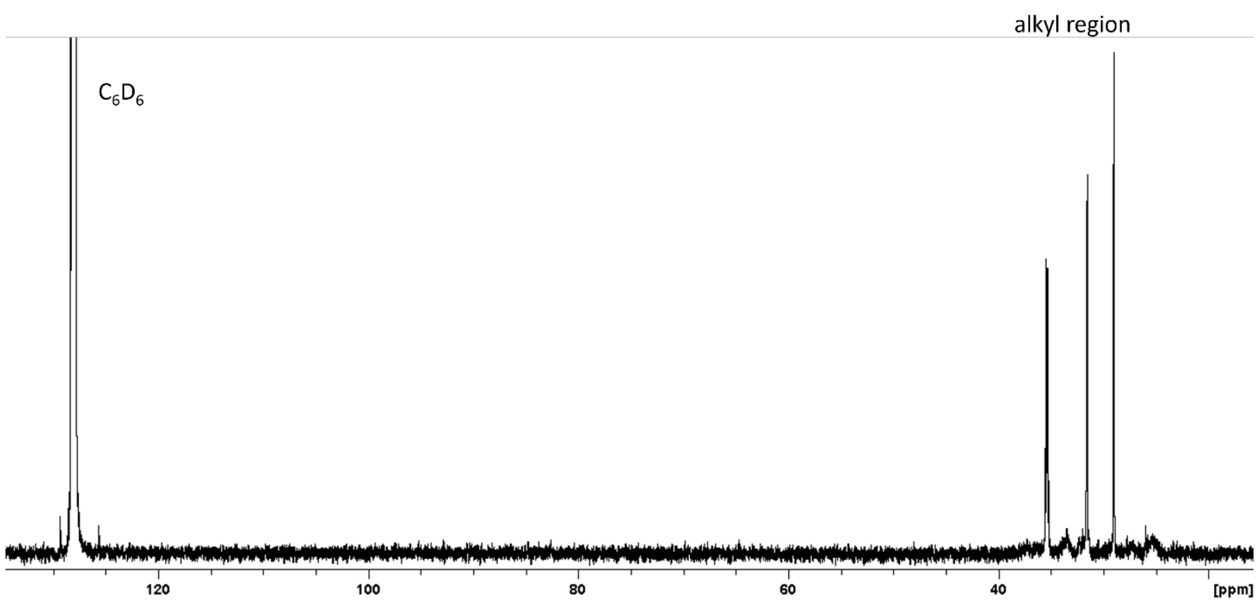

Figure S78. $^{13}C\{^{1}H\}$ NMR spectrum of [{(dmpe)$_2$MnH}$_2$(μ-Ge)] (**6**) in C_6D_6 (151 MHz, 298 K).

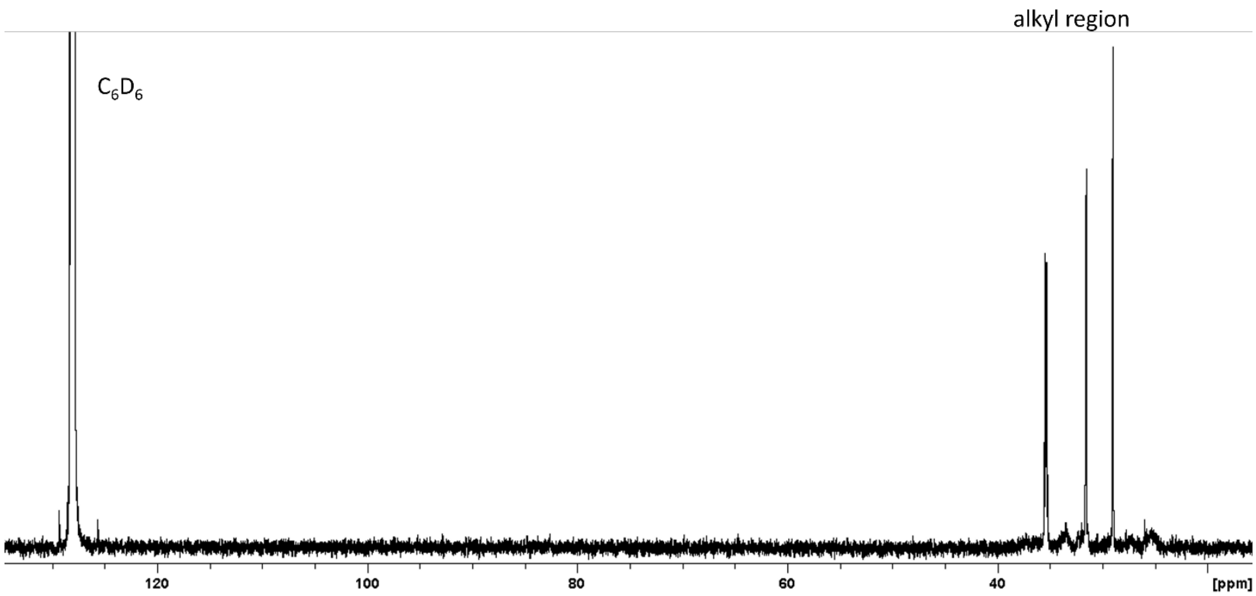

Figure S79. $^{13}C\{^1H\}$ NMR spectrum of $[\{(dmpe)_2MnH\}_2(\mu\text{-}Ge)]$ (**6**) in d_8-toluene (126 MHz, 189 K).

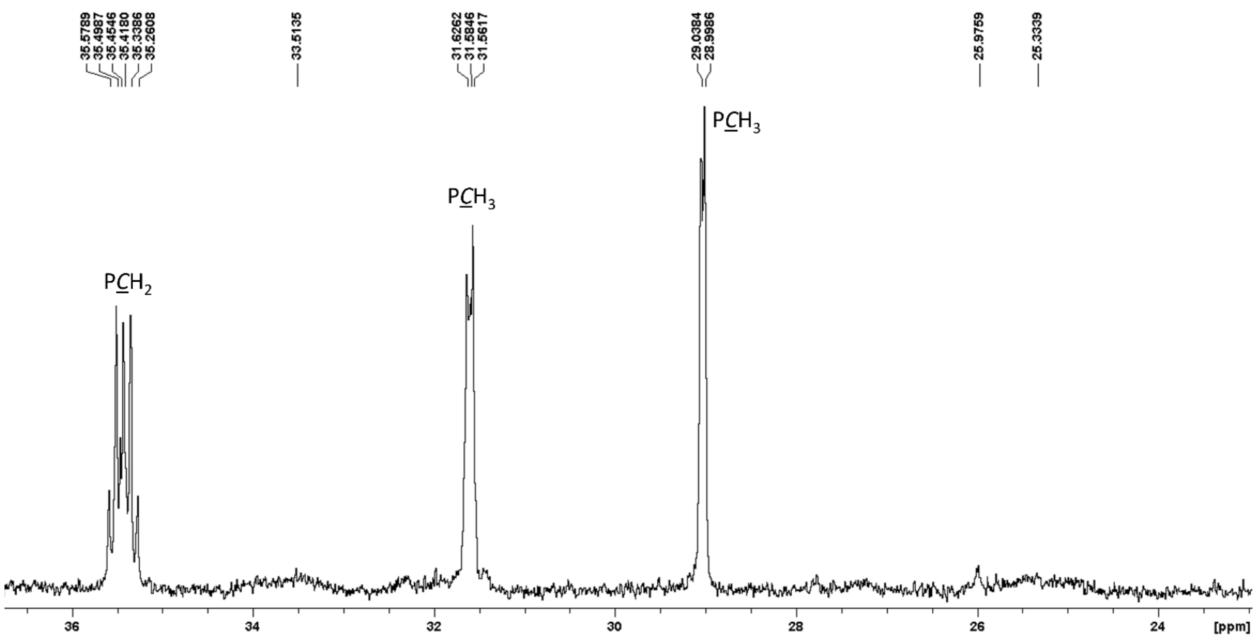

Figure S80. Expanded alkyl region of the $^{13}C\{^1H\}$ NMR spectrum of $[\{(dmpe)_2MnH\}_2(\mu\text{-}Ge)]$ (**6**) in C_6D_6 (151 MHz, 298 K). Labelled peaks arise from the *trans*,*trans* isomer.

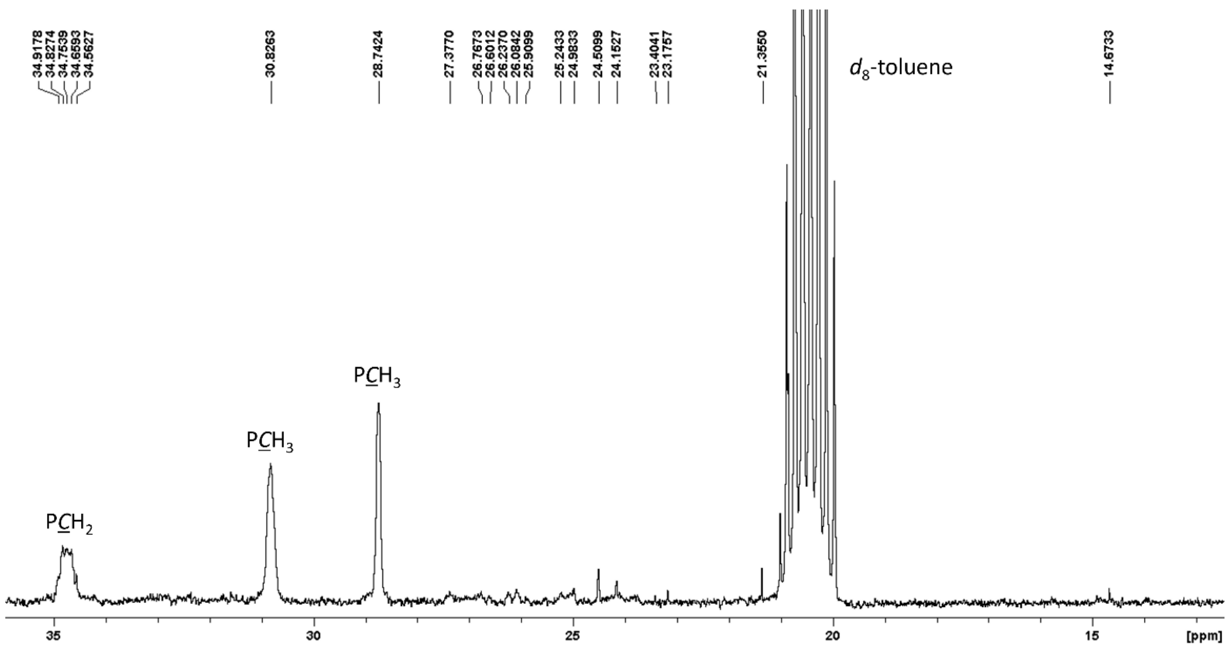

Figure S81. Expanded alkyl region of the $^{13}C\{^1H\}$ NMR spectrum of [{(dmpe)$_2$MnH}$_2$(μ-Ge)] (**6**) in d_8-toluene (126 MHz, 189 K). Labelled peaks arise from the *trans*,*trans* isomer.

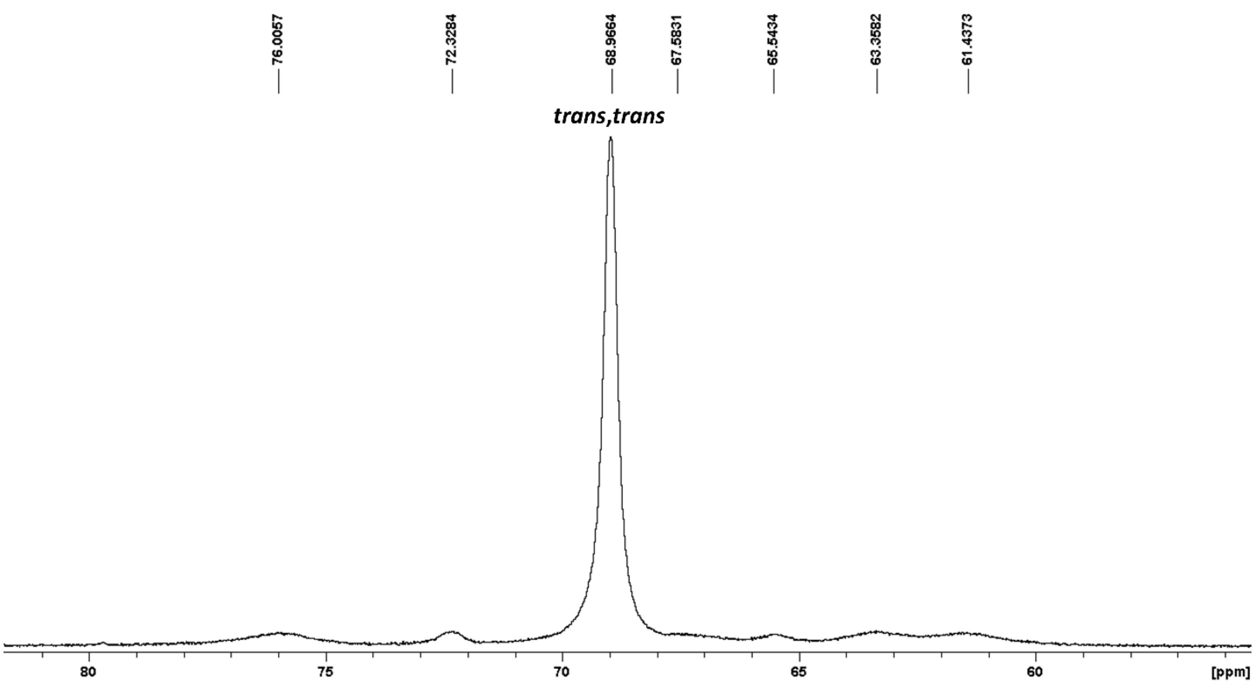

Figure S82. $^{31}P\{^1H\}$ NMR spectrum of [{(dmpe)$_2$MnH}$_2$(μ-Ge)] (**6**) in C_6D_6 (243 MHz, 298 K). Unlabelled peaks arise from the *cis*,*trans* or *cis*,*cis* isomers.

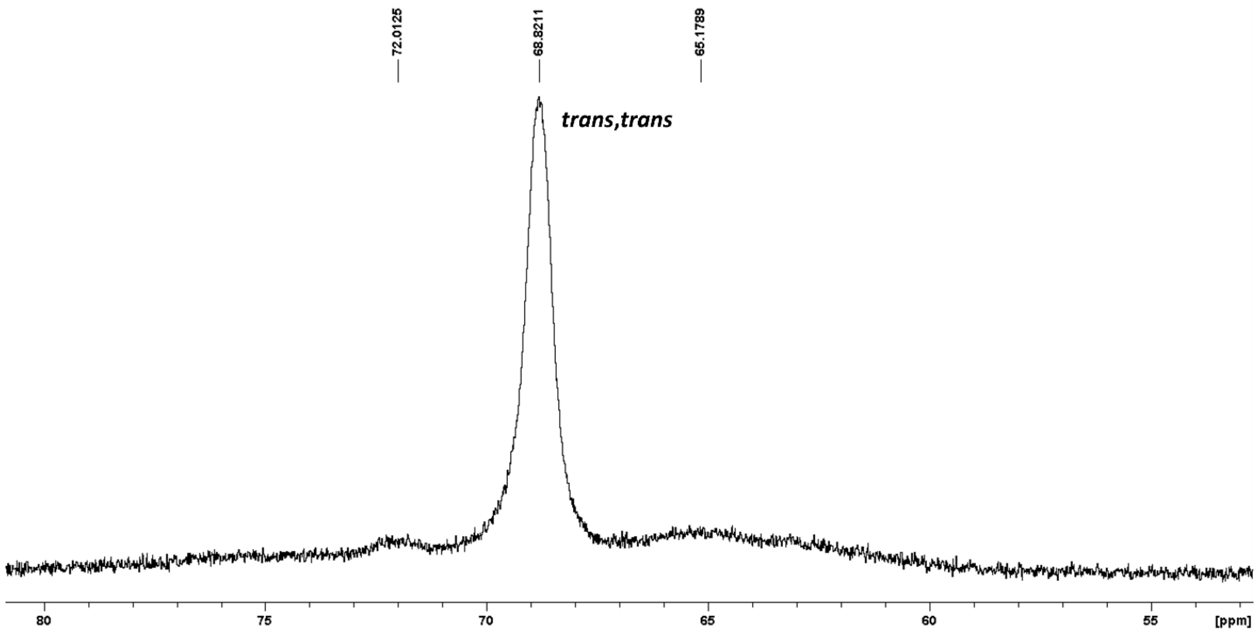

Figure S83. $^{31}P\{^{1}H\}$ NMR spectrum of [{(dmpe)$_2$MnH}$_2$(μ-Ge)] (**6**) in C_6D_6 (202 MHz, 334 K). Unlabelled peaks arise from the *cis*,*trans* or *cis*,*cis* isomers.

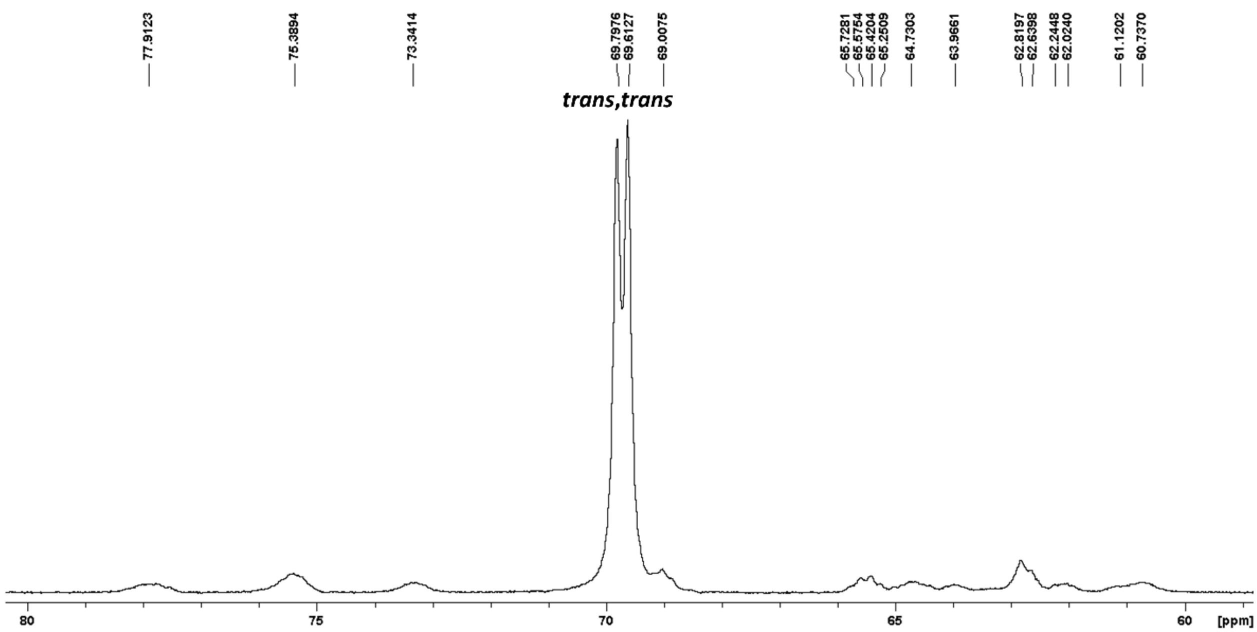

Figure S84. $^{31}P\{^{1}H\}$ NMR spectrum of [{(dmpe)$_2$MnH}$_2$(μ-Ge)] (**6**) in d_8-toluene (202 MHz, 189 K). Unlabelled peaks arise from the *cis*,*trans* or *cis*,*cis* isomers.

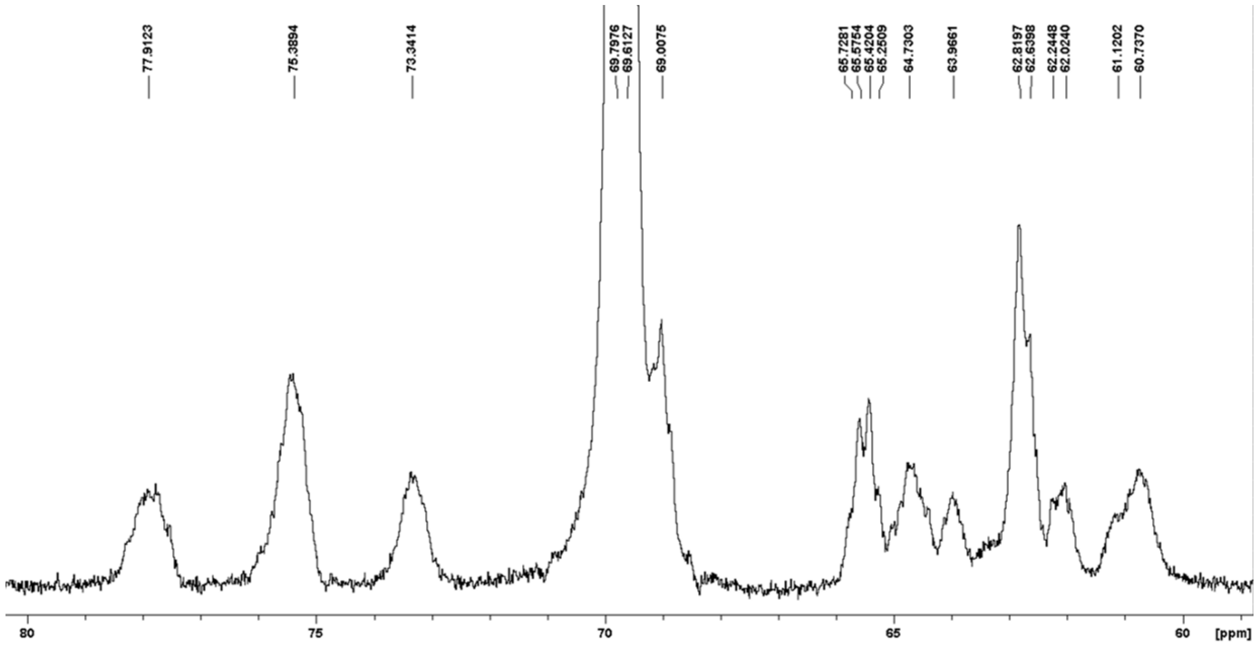

Figure S85. Zoomed-in view of the $^{31}P\{^{1}H\}$ NMR spectrum of $[\{(dmpe)_2MnH\}_2(\mu\text{-}Ge)]$ (**6**) in d_8-toluene (202 MHz, 189 K). Unlabelled peaks arise from the *cis*,*trans* or *cis*,*cis* isomers, while the cut-off peak is from the *trans*,*trans* isomer.

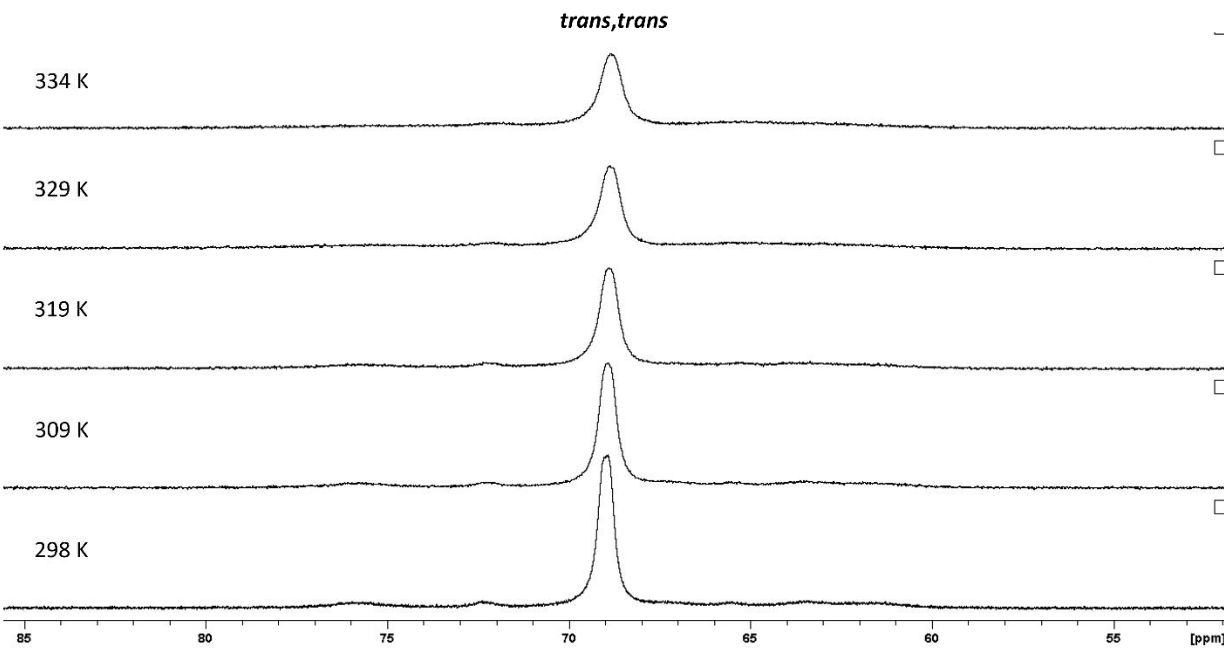

Figure S86. Variable temperature $^{31}P\{^{1}H\}$ NMR spectra of $[\{(dmpe)_2MnH\}_2(\mu\text{-}Ge)]$ (**6**) in C_6D_6 (202 MHz). Unlabelled peaks arise from the *cis*,*trans* or *cis*,*cis* isomers.

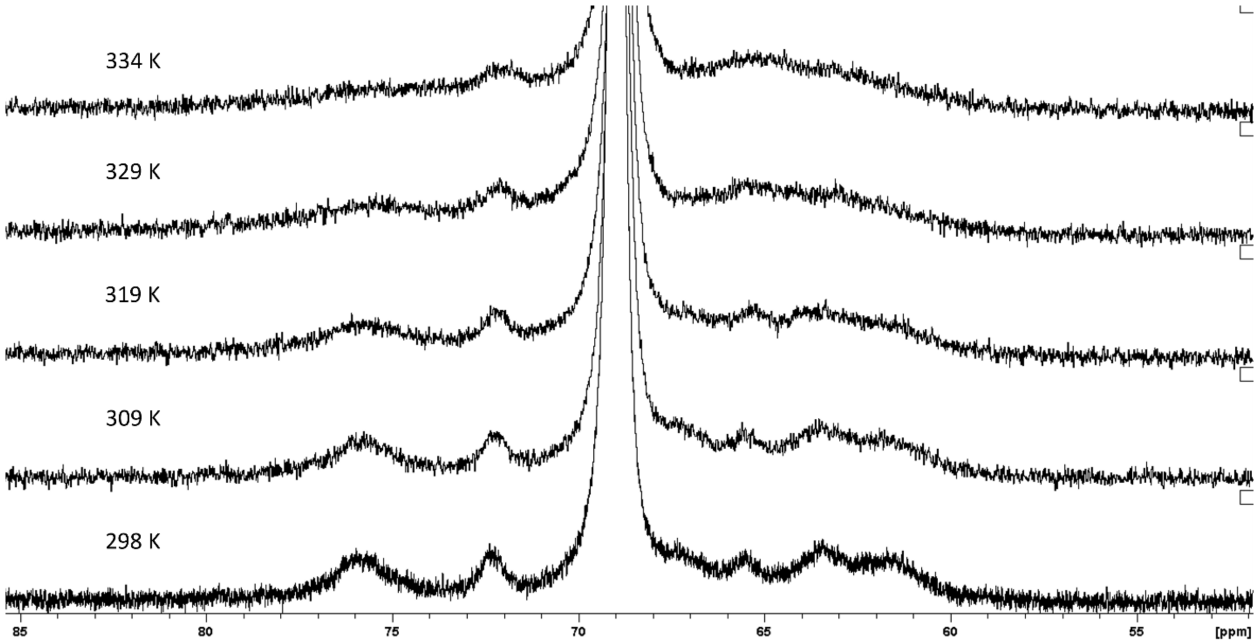

Figure S87. Zoomed-in views of variable temperature $^{31}P\{^{1}H\}$ NMR spectra of [{(dmpe)$_2$MnH}$_2$(μ-Ge)] (**6**) in C_6D_6 (202 MHz). Unlabelled peaks arise from the *cis*,*trans* or *cis*,*cis* isomers, while the cut-off peak is from the *trans*,*trans* isomer.

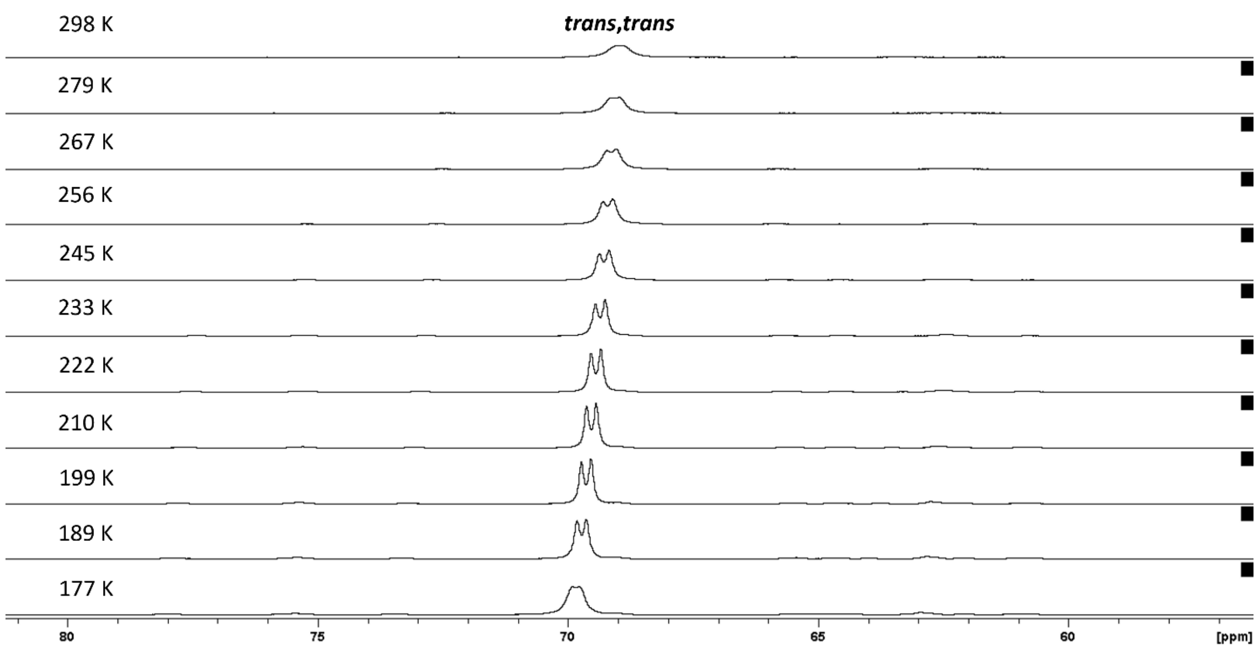

Figure S88. Variable temperature $^{31}P\{^{1}H\}$ NMR spectra of [{(dmpe)$_2$MnH}$_2$(μ-Ge)] (**6**) in d_8-toluene (202 MHz). Unlabelled peaks arise from the *cis*,*trans* or *cis*,*cis* isomers.

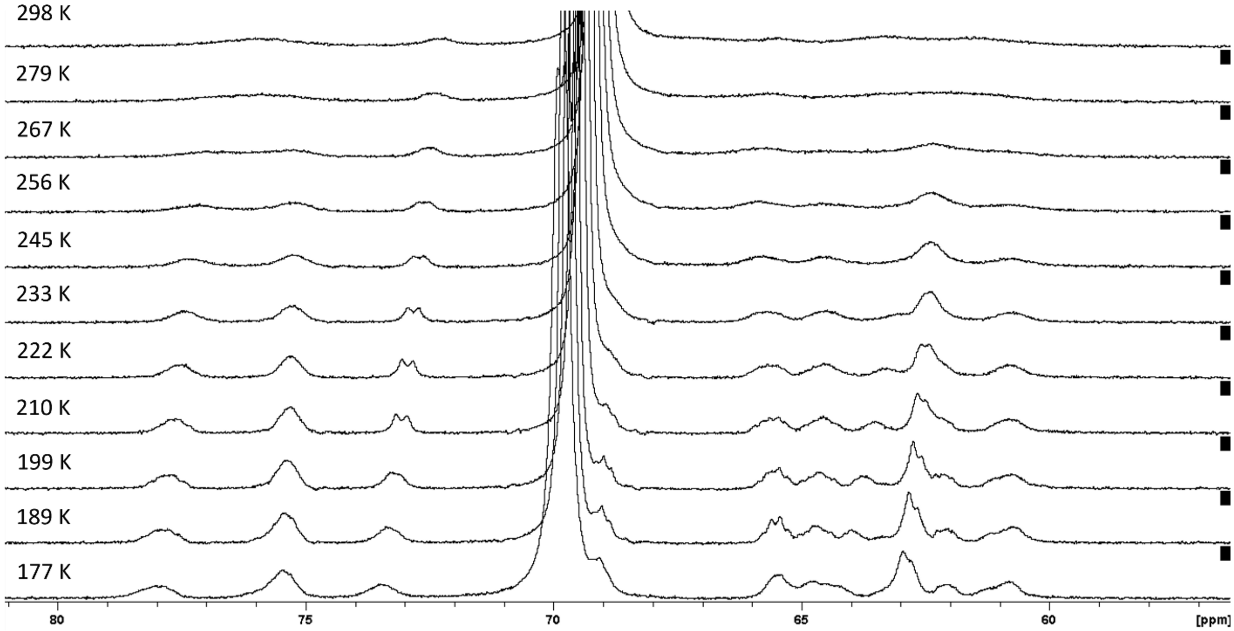

Figure S89. Zoomed-in views of variable temperature $^{31}P\{^{1}H\}$ NMR spectra of $[\{(dmpe)_2MnH\}_2(\mu\text{-}Ge)]$ (**6**) in d_8-toluene (202 MHz). Unlabelled peaks arise from the *cis*,*trans* or *cis*,*cis* isomers, while the cut-off peak is from the *trans*,*trans* isomer.

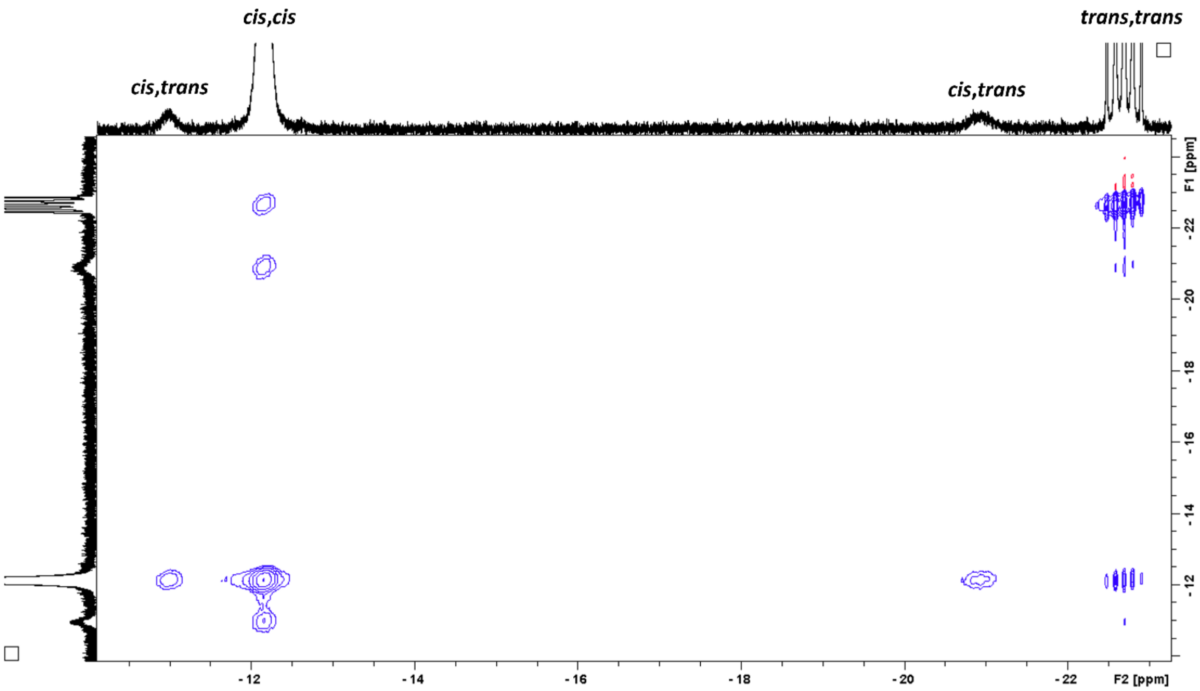

Figure S90. Expanded metal hydride region of the NOESY NMR spectrum of $[\{(dmpe)_2MnH\}_2(\mu\text{-}Ge)]$ (**6**) in d_8-toluene (500 MHz, 334 K). To allow visualization of the minor *cis*,*trans* isomer on the 1D spectra, the 1D spectra on the x- and y- axes have been zoomed in to the extent that peaks arising from the *cis*,*cis* and *trans*,*trans* isomers are cut off. Cross-peaks indicate chemical exchange between all four Mn*H* environments of the three isomers.

Graphs Showing Relative Concentrations of Manganese-containing Species in Mixtures Containing 3a-b, 4a-b, and 5a-b.

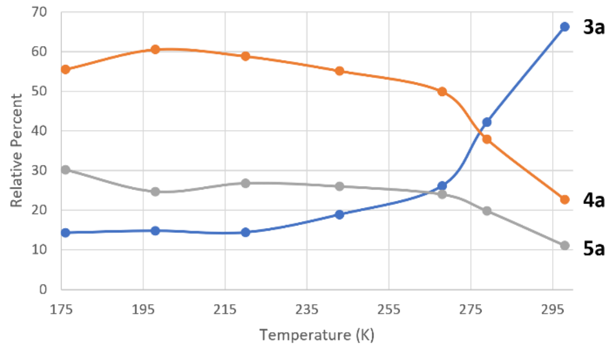

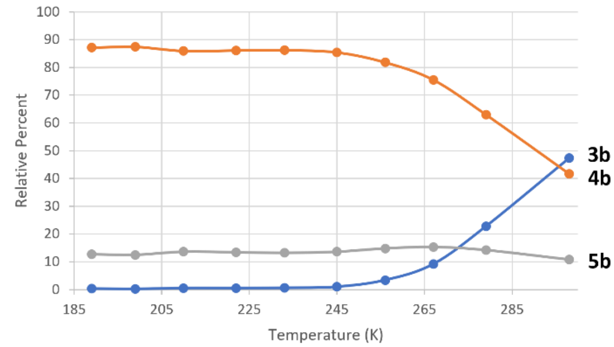

Figure S91. Graphs showing relative concentration over temperature of (left) [(dmpe)$_2$MnH(GeHPh)] (**3a**), *mer*-[(dmpe)$_2$MnH(GeH$_2$Ph)$_2$] (**4a**), and *trans*-[(dmpe)$_2$Mn(GeH$_2$Ph)(HGeH$_2$Ph)] (**5a**), or (right) [(dmpe)$_2$MnH(GeH^{n}Bu)] (**3b**), *mer*-[(dmpe)$_2$MnH(GeH$_2$^{n}Bu)$_2$] (**4b**), and *trans*-[(dmpe)$_2$Mn(GeH$_2$^{n}Bu)(HGeH$_2$^{n}Bu)] (**5b**), in mixtures generated in d_8-toluene by (for the phenyl analogue) exposure of [(dmpe)$_2$MnH(=GeEt$_2$)] (**2b**) to 5 equivalents of H$_3$GePh or (for the butyl analogue) exposure of [(dmpe)$_2$MnH(GeH^{n}Bu)] (**3b**) to 4 equivalents of H$_3$Ge^{n}Bu. Blue = **3a-b**, orange = **4a-b**, grey = **5a-b**. Relative concentrations of species in solution were determined by ^{1}H NMR spectroscopy at 500 MHz.

2D Powder X-ray Diffractogram of Crystal Structure of [{(dmpe)$_2$MnH}$_2$(μ-Ge)] (6)

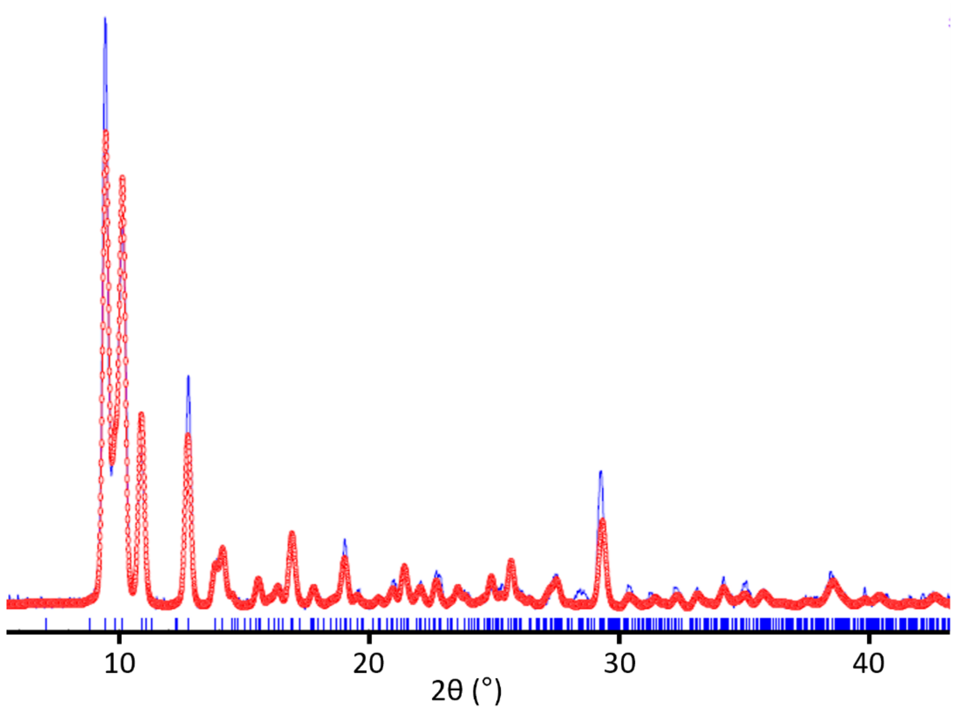

Figure S92. Overlay of (blue) the 2D power X-ray diffractogram of the isolated sample of [{(dmpe)$_2$MnH}$_2$(μ-Ge)] (**6**) and (red) the theoretical diffractogram calculated form the single crystal X-ray structure of *trans*,*trans*-[{(dmpe)$_2$MnH}$_2$(μ-Ge)] (***trans*,*trans*-6**), indicating that the bulk sample of **6** exists exclusively as the *trans*,*trans* isomer in the solid state. λ = 1.54056 Å, T = 298 K.

Figure of X-ray Crystal Structure of [O{^{n}BuGe=MnH(dmpe)$_2$}$_2$] (7).

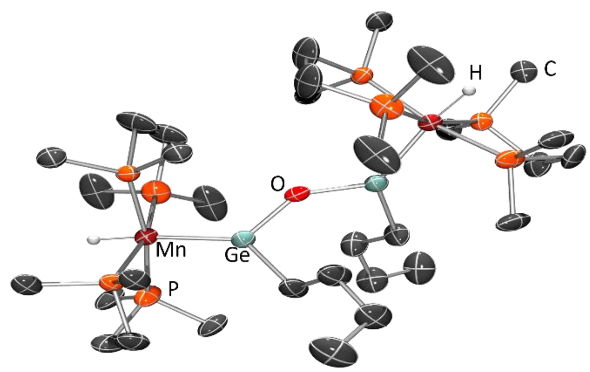

Figure S93. X-ray crystal structure of [O{^{n}BuGe=MnH(dmpe)$_2$}$_2$] (**7**), with ellipsoids at 50 % probability. Most hydrogen atoms have been omitted for clarity. Hydrogen atoms on Mn were located from the difference map and refined isotropically.

Tables of X-ray Crystal Data and Crystal Structure Refinement.

Table S1. Crystal and structure refinement data for [$(dmpe)_2MnH(=GePh_2)$] (**2a**).

dentification code	MnHGePh2
Empirical formula	$C_{24}H_{43}GeMnP_4$
Formula weight	582.99
Temperature/K	100
Crystal system	monoclinic
Space group	$P2_1/c$
a/Å	15.9001(17)
b/Å	14.3514(16)
c/Å	12.5626(12)
α/°	90
β/°	103.094(4)
γ/°	90
Volume/$Å^3$	2792.1(5)
Z	4
$\rho_{calc}g/cm^3$	1.387
μ/mm^{-1}	1.768
F(000)	1216.0
Crystal size/mm^3	0.3 × 0.3 × 0.15
Radiation	MoKα (λ = 0.71073)
2Θ range for data collection/°	3.87 to 59.022
Index ranges	$-21 \leq h \leq 21$, $-19 \leq k \leq 19$, $-17 \leq l \leq 17$
Reflections collected	32261
Independent reflections	7772 [R_{int} = 0.0334, R_{sigma} = 0.0499]
Data/restraints/parameters	7772/0/283
Goodness-of-fit on F^2	1.045
Final R indexes [I>=2σ (I)]	R_1 = 0.0247, wR_2 = 0.0643
Final R indexes [all data]	R_1 = 0.0302, wR_2 = 0.0664
Largest diff. peak/hole / e $Å^{-3}$	0.95/-0.46

Table S2. Crystal and structure refinement data for [(dmpe)$_2$MnH(=GeHPh)] (**3a**).

Identification code	MnHGeHPh
Empirical formula	$C_{18}H_{39}GeMnP_4$
Formula weight	506.90
Temperature/K	100
Crystal system	monoclinic
Space group	$P2_1/n$
a/Å	8.9471(17)
b/Å	16.251(8)
c/Å	16.702(4)
α/°	90
β/°	96.35(2)
γ/°	90
Volume/Å^3	2413.6(14)
Z	4
ρ_{calc}g/cm^3	1.395
μ/mm^{-1}	2.034
F(000)	1056.0
Crystal size/mm^3	0.2 × 0.15 × 0.15
Radiation	MoKα (λ = 0.71073)
2Θ range for data collection/°	3.508 to 59.228
Index ranges	$-12 \le h \le 12$, $-22 \le k \le 22$, $-23 \le l \le 20$
Reflections collected	28443
Independent reflections	6780 [R_{int} = 0.0488, R_{sigma} = 0.0595]
Data/restraints/parameters	6780/0/233
Goodness-of-fit on F^2	1.024
Final R indexes [I>=2σ (I)]	R_1 = 0.0301, wR_2 = 0.0705
Final R indexes [all data]	R_1 = 0.0438, wR_2 = 0.0741
Largest diff. peak/hole / e Å^{-3}	0.48/-0.73

Table S3. Crystal and structure refinement data for *trans,trans*-[{(dmpe)$_2$MnH}$_2$(μ-Ge)] (***trans,trans*-6**).

Identification code	Mn2Ge
Empirical formula	$C_{24}H_{66}GeMn_2P_8$
Formula weight	784.99
Temperature/K	100.00
Crystal system	monoclinic
Space group	$P2_1/c$
a/Å	17.673(2)
b/Å	17.979(7)
c/Å	11.970(3)
α/°	90
β/°	101.283(18)
γ/°	90
Volume/Å^3	3729.7(18)
Z	4
ρ_{calc}g/cm^3	1.398
μ/mm^{-1}	1.825
F(000)	1648.0
Crystal size/mm^3	0.4 × 0.4 × 0.25
Radiation	MoKα (λ = 0.71073)
2Θ range for data collection/°	3.264 to 59.126
Index ranges	$-24 \leq h \leq 22$, $-24 \leq k \leq 24$, $-16 \leq l \leq 16$
Reflections collected	46413
Independent reflections	10386 [R_{int} = 0.0346, R_{sigma} = 0.0386]
Data/restraints/parameters	10386/0/341
Goodness-of-fit on F^2	1.185
Final R indexes [I>=2σ (I)]	R_1 = 0.0321, wR_2 = 0.0732
Final R indexes [all data]	R_1 = 0.0397, wR_2 = 0.0751
Largest diff. peak/hole / e Å^{-3}	0.46/-0.51

Table S4. Crystal and structure refinement data for [O{^{n}BuGe=MnH(dmpe)$_2$}$_2$] (**7**).

Identification code	MnGenBuO
Empirical formula	$C_{32}H_{84}Ge_2Mn_2OP_8$
Formula weight	987.81
Temperature/K	100.00(10)
Crystal system	monoclinic
Space group	C2
a/Å	26.777(18)
b/Å	9.568(3)
c/Å	9.796(5)
α/°	90
β/°	109.100(10)
γ/°	90
Volume/Å^3	2372(2)
Z	2
ρ_{calc}g/cm^3	1.383
μ/mm^{-1}	2.069
F(000)	1036.0
Crystal size/mm^3	0.3 × 0.2 × 0.1
Radiation	MoKα (λ = 0.71073)
2Θ range for data collection/°	4.4 to 59.09
Index ranges	-37 ≤ h ≤ 37, -13 ≤ k ≤ 13, -13 ≤ l ≤ 13
Reflections collected	6567
Independent reflections	6567 [R_{int} = ?, R_{sigma} = 0.1121]
Data/restraints/parameters	6567/157/216
Goodness-of-fit on F^2	0.950
Final R indexes [I>=2σ (I)]	R_1 = 0.0604, wR_2 = 0.1473
Final R indexes [all data]	R_1 = 0.1031, wR_2 = 0.1562
Largest diff. peak/hole / e Å^{-3}	1.22/-0.56
Flack parameter	0.17(2)

Figures Showing DFT Calculated Structures of 2a-b, 3a-b, 4b, 5b, and 6.

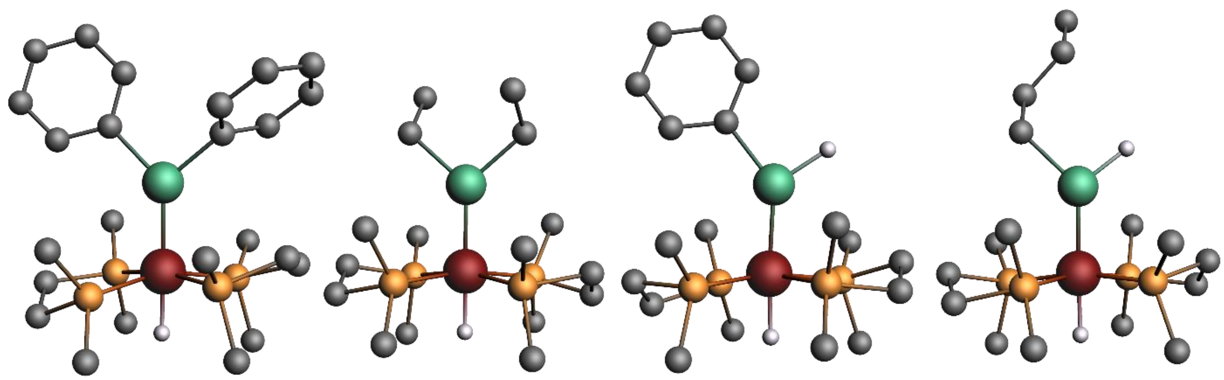

Figure S94. DFT-calculated structures of germylene complexes; [(dmpe)$_2$MnH(=GePh$_2$)] (**2a**; left), [(dmpe)$_2$MnH(=GeEt$_2$)] (**2b**; second from left), [(dmpe)$_2$MnH(=GeHPh)] (**3a**; second from right), and [(dmpe)$_2$MnH(=GeH^{n}Bu)] (**3b**; right). Most hydrogen atoms (those not on Mn or Ge) are not shown for clarity. Atom colours; Mn = red, Ge = green, P = orange, C = dark grey, H = light grey.

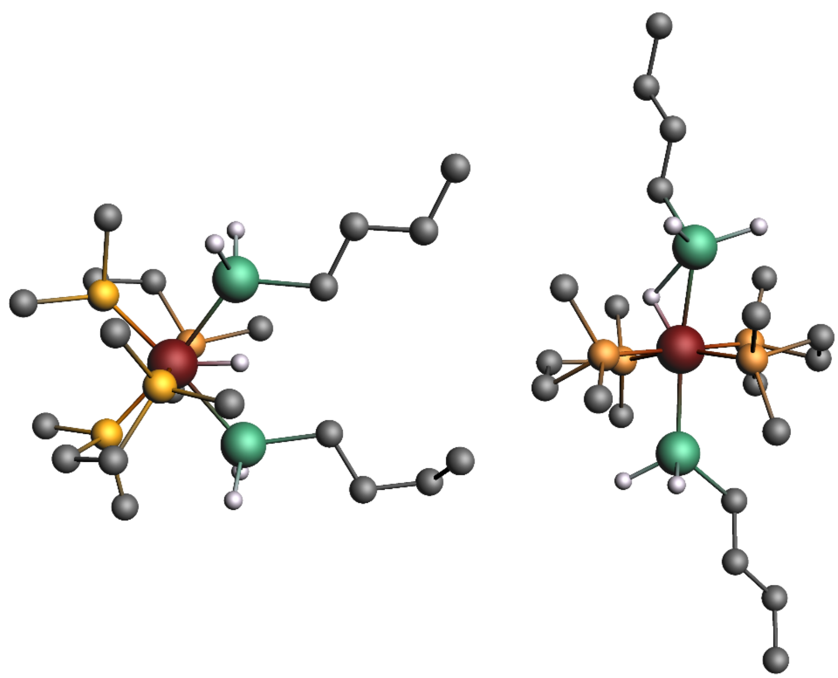

Figure S95. DFT-calculated structures of for digermyl hydride complexes; *mer*-[(dmpe)$_2$MnH(GeH$_2$^{n}Bu)$_2$] (**4b**; left) and *trans*-[(dmpe)$_2$Mn(GeH$_2$^{n}Bu)(HGeH$_2$^{n}Bu)] (**5b**; right). Most hydrogen atoms (those not on Mn or Ge) are not shown for clarity. Atom colours; Mn = red, Ge = green, P = orange, C = dark grey, H = light grey.

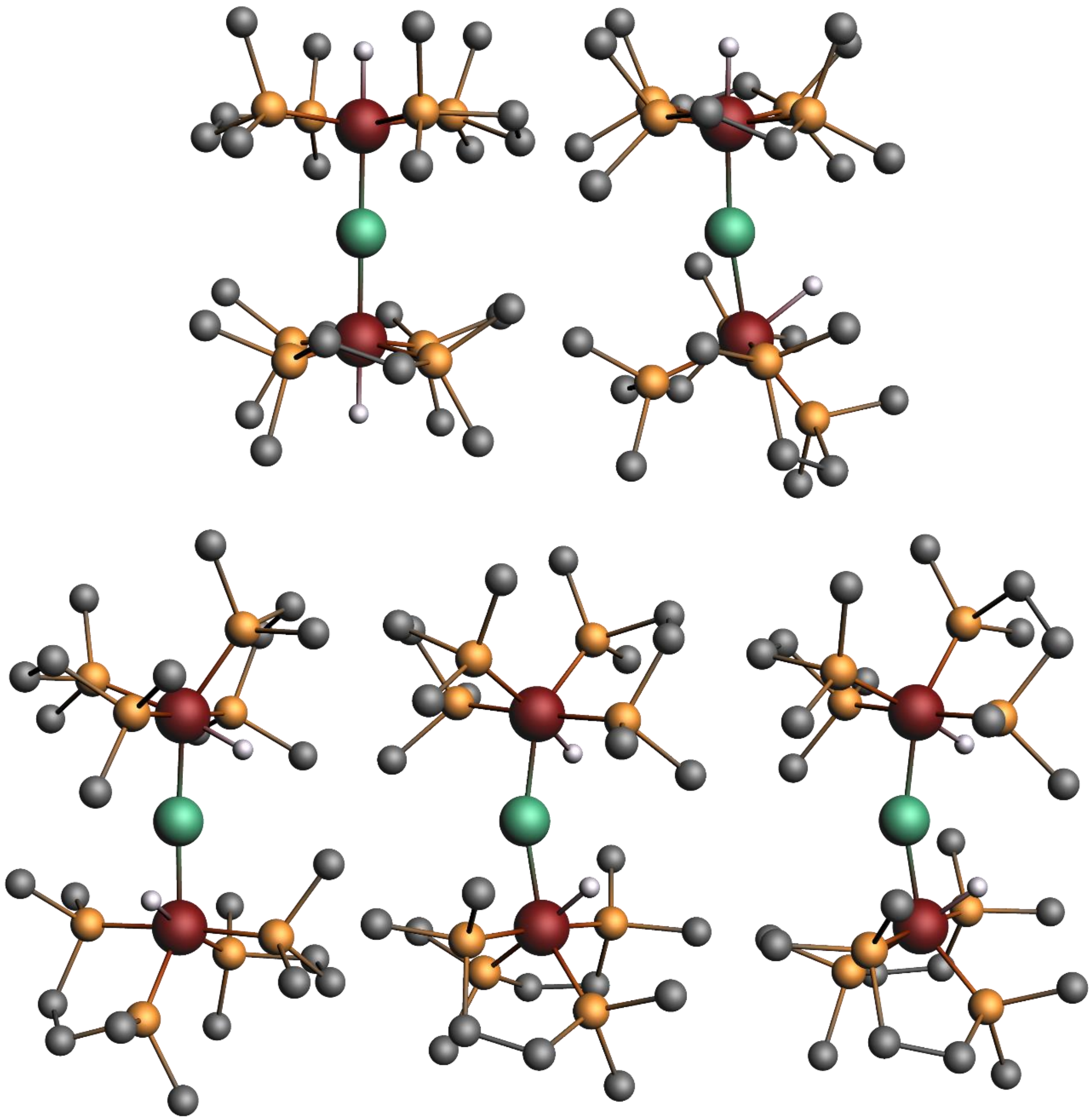

Figure S96. DFT-calculated structures of the isomers of the germanide complex [{(dmpe)$_2$MnH}$_2$(μ-Ge)] (**6**). Top; these are the lowest energy rotamers for the (top left) *trans*,*trans*- and (top right) *cis*,*trans*-isomers. Bottom; three structures of the *cis*,*cis* isomer with nearly identical energies corresponding to (bottom left) the *rac* isomer, (bottom middle) the lowest energy *meso* rotamer, and (bottom right) the second lowest energy *meso* rotamer. Most hydrogen atoms (those not on Mn) are not shown for clarity. Atom colours; Mn = red, Ge = green, P = orange, C = dark grey, H = light grey.

Figures Showing Superimposed Calculated and X-ray Structures of 2a, 3a, and *trans,trans*-6.

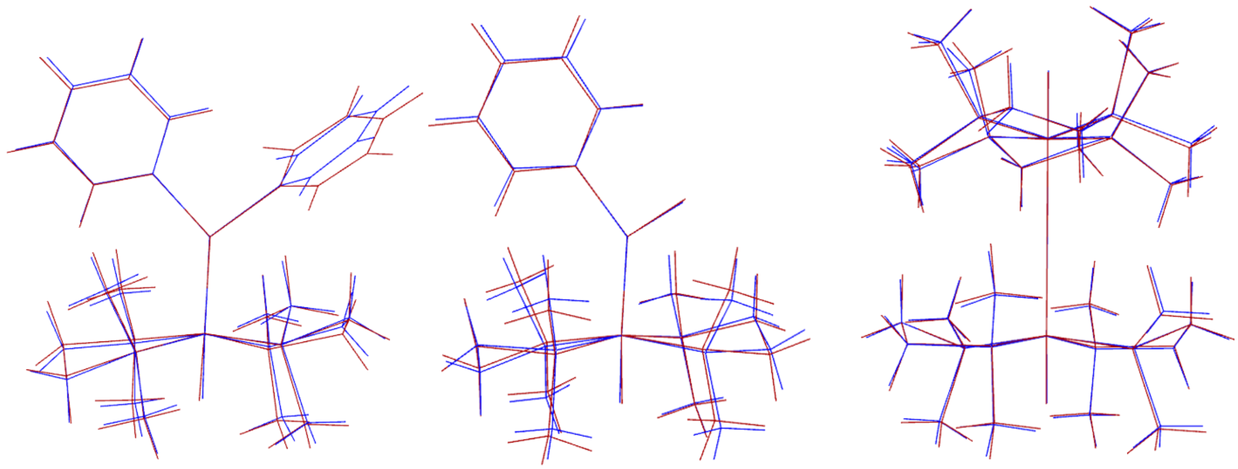

Figure S97. Superimposed DFT-calculated (red) and X-ray (blue) structure of, from left to right, $[(dmpe)_2MnH(=GePh_2)]$ (**2a**), $[(dmpe)_2MnH(=GeHPh)]$ (**3a**), and *trans*,*trans*-$[\{(dmpe)_2MnH\}_2(\mu\text{-}Ge)]$ (***trans*,*trans*-6**).

<u>Tables of DFT-calculated Bond Metrics, Mayer Bond Orders, and Hirshfeld Charges for 2a-b, 3a-b, 4a-b, 5a-b, and 6.</u>

Table S5. Selected calculated and crystallographically determined bond lengths (Å) and Mayer bond orders (b.o.) for germylene complexes; [(dmpe)$_2$MnH(=GePh$_2$)] (**2a**), [(dmpe)$_2$MnH(=GeEt$_2$)] (**2b**), [(dmpe)$_2$MnH(=GeHPh)] (**3a**), and [(dmpe)$_2$MnH(=GeH^{n}Bu)] (**3b**).

		2a	**2b**	**3a**	**3b**
Mn–Ge	d(XRD)	2.2636(4)	–	2.2462(6)	–
	d(DFT)	2.25	2.25	2.24	2.24
	Mayer b.o.	1.40	1.41	1.41	1.44
Mn–H	d(XRD)	1.50(2)	–	1.54(2)	–
	d(DFT)	1.57	1.58	1.58	1.58
	Mayer b.o.	0.81	0.83	0.82	0.83
Ge–H	d(XRD)	–	–	1.54(3)	–
	d(DFT)	–	–	1.6051	1.6044
	Mayer b.o.	–	–	0.83	0.84

Table S6. Selected calculated bond lengths (Å) and Mayer bond orders (b.o.) for digermyl hydride complexes; *mer*-[(dmpe)$_2$MnH(GeH$_2$Ph)$_2$] (**4a**), *mer*-[(dmpe)$_2$MnH(GeH$_2{}^n$Bu)$_2$] (**4b**), *trans*-[(dmpe)$_2$Mn(GeH$_2$Ph)(HGeH$_2$Ph)] (**5a**), and *trans*-[(dmpe)$_2$Mn(GeH$_2{}^n$Bu)(HGeH$_2{}^n$Bu)] (**5b**).

		4a	**4b**	**5a**	**5b**
Mn–Ge$_{H\mathit{Ge}H2R'}$	d	–	–	2.49	2.49
	b.o.	–	–	0.70	0.74
Mn–Ge$_{\mathit{Ge}H2R'}$	d	2.48	2.48, 2.49	2.49	2.48
	b.o.	0.79	0.80, 0.81	0.83	0.78
Mn–H	d	1.56	1.55	1.55	1.54
	b.o.	0.57	0.60	0.60	0.65
Ge–H$_{\mathit{H}GeH2R'}$	d	1.96	1.94, 1.95	1.91	1.91
	b.o.	0.2065, 0.2067	0.1901, 0.1950	0.2745	0.2368
Ge–H$_{term}$	d	1.57	1.57	1.56, 1.57	1.56, 1.57
	b.o.	0.87	0.86, 0.88	0.85, 0.86, 0.90, 0.91	0.86, 0.87, 0.89

Table S7. Selected calculated and crystallographically determined bond lengths (Å) and Mayer bond orders (b.o.) for the various isomers of [{(dmpe)$_2$MnH}$_2$(μ-Ge)] (**6**).

		trans,trans	***cis,trans***	***cis,cis*** (rac)	***cis,cis*** (meso); lowest energy rotamer	***cis,cis*** (meso); higher energy rotamer
HMnMnH torsion		–	–	83.8	101.9	73.7
Mn–Ge	d(XRD)	2.2806(7), 2.2817(7)	–	–	–	–
	d(DFT)	2.26	2.25 (*trans*), 2.27 (*cis*)	2.23	2.24	2.23, 2.24
	Mayer b.o.	1.38	1.25 (*trans*), 1.36 (*cis*)	1.30	1.26	1.23, 1.30
Mn–H	d(XRD)	1.53(3), 1.58(3)	–	–	–	–
	d(DFT)	1.57	1.58 (*trans*), 1.78 (*cis*)	1.59	1.59, 1.60	1.59
	Mayer b.o.	0.98	0.92 (*trans*), 0.69 (*cis*)	0.81	0.72, 0.76	0.75, 0.81
Ge–H (*cis*)	d(DFT)	–	2.10	2.20, 2.21	2.13, 2.14	2.08, 2.26
	Mayer b.o.	–	0.23	0.11	0.17, 0.20	0.11, 0.18

Table S8. Selected Hirshfeld charges for germylene complexes [(dmpe)$_2$MnH(=GePh$_2$)] (**2a**), [(dmpe)$_2$MnH(=GeEt$_2$)] (**2b**), [(dmpe)$_2$MnH(=GeHPh)] (**3a**), and [(dmpe)$_2$MnH(=GeH^{n}Bu)] (**3b**), as well as digermyl hydride complexes; *mer*-[(dmpe)$_2$MnH(GeH$_2$Ph)$_2$] (**4a**), *mer*-[(dmpe)$_2$MnH(GeH$_2{}^n$Bu)$_2$] (**4b**), *trans*-[(dmpe)$_2$Mn(GeH$_2$Ph)(HGeH$_2$Ph)] (**5a**), and *trans*-[(dmpe)$_2$Mn(GeH$_2{}^n$Bu)(HGeH$_2{}^n$Bu)] (**5b**).

	2a	**2b**	**3a**	**3b**	**4a**	**4b**	**5a**	**5b**
Ge	0.21	0.23	0.17	0.19	0.20	0.20	0.20 (HGeR$_3$), 0.15 (GeR$_3$)	0.20 (HGeR$_3$), 0.15 (GeR$_3$)
Mn	–0.26	–0.26	–0.26	–0.26	–0.25	–0.25	–0.24	–0.24
Mn*H*	–0.10	–0.11	–0.11	–0.11	–0.06	–0.06	–0.06	–0.06
Ge*H*	–	–	–0.11	–0.11	–0.08, –0.09	–0.09	–0.08 (HGeR$_3$), –0.09 (GeR$_3$)	–0.08, –0.09 (HGeR$_3$), –0.09, –0.10 (GeR$_3$)

Table S9. Selected Hirshfeld charges for the various isomers of [{(dmpe)$_2$MnH}$_2$(μ-Ge)] (**6**).

	trans,trans	***cis,trans***	***cis,cis*** (rac)	***cis,cis*** (meso); lowest energy rotamer	***cis,cis*** (meso); higher energy rotamer
Ge	0.06	0.10	0.14	0.13	0.14
Mn	–0.27	–0.27	–0.27	–0.27	–0.27, –0.28
Mn*H*	–0.10	–0.11 (*trans*), –0.09 (*cis*)	–0.09	–0.09	–0.09, –0.10

Table S10. Fragment Hirshfeld charges for the Ge-containing fragment from fragment interaction calculations {GeR_2 + $(dmpe)_2MnH$ or Ge + 2 × $(dmpe)_2MnH$)} on [$(dmpe)_2MnH(=GePh_2)$] (**2a**), [$(dmpe)_2MnH(=GeEt_2)$] (**2b**), [$(dmpe)_2MnH(=GeHPh)$] (**3a**), [$(dmpe)_2MnH(=GeH^{n}Bu)$] (**3b**), and *trans*,*trans*-[{$(dmpe)_2MnH$}$_2$(μ-Ge)] (***trans,trans*-6**).

$GePh_2$ (**2a**)	$GeEt_2$ (**2b**)	GeHPh (**3a**)	$GeH^{n}Bu$ (**3b**)	Ge (***trans,trans*-6**)
–0.32	–0.26	–0.31	–0.29	–0.55

Slater-type Molecular Orbitals Involved in Mn–Ge Bonding in 2a and 3a-b.

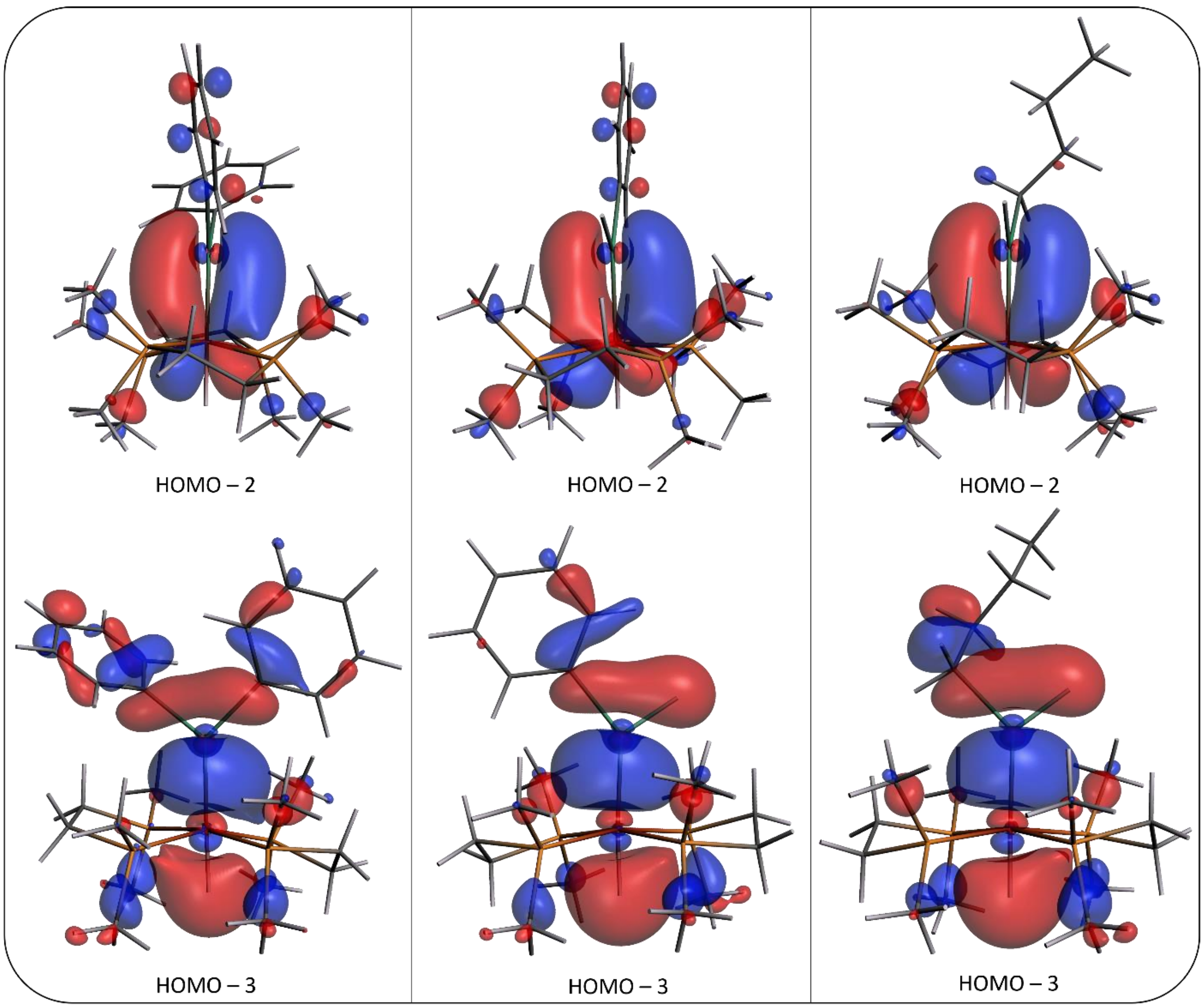

Figure S98. Slater-type σ (bottom) and π (top) molecular orbitals involved in Mn–Ge bonding in [$(dmpe)_2MnH(=GePh_2)$] (**2b**; left), [$(dmpe)_2MnH(=GeHPh)$] (**3a**; middle), and [$(dmpe)_2MnH(=GeH^{n}Bu)$] (**3b**; right), with isosurfaces set to 0.03.

Overall Deformation Densities of 2a-b, 3a-b, and *trans*,*trans*-6.

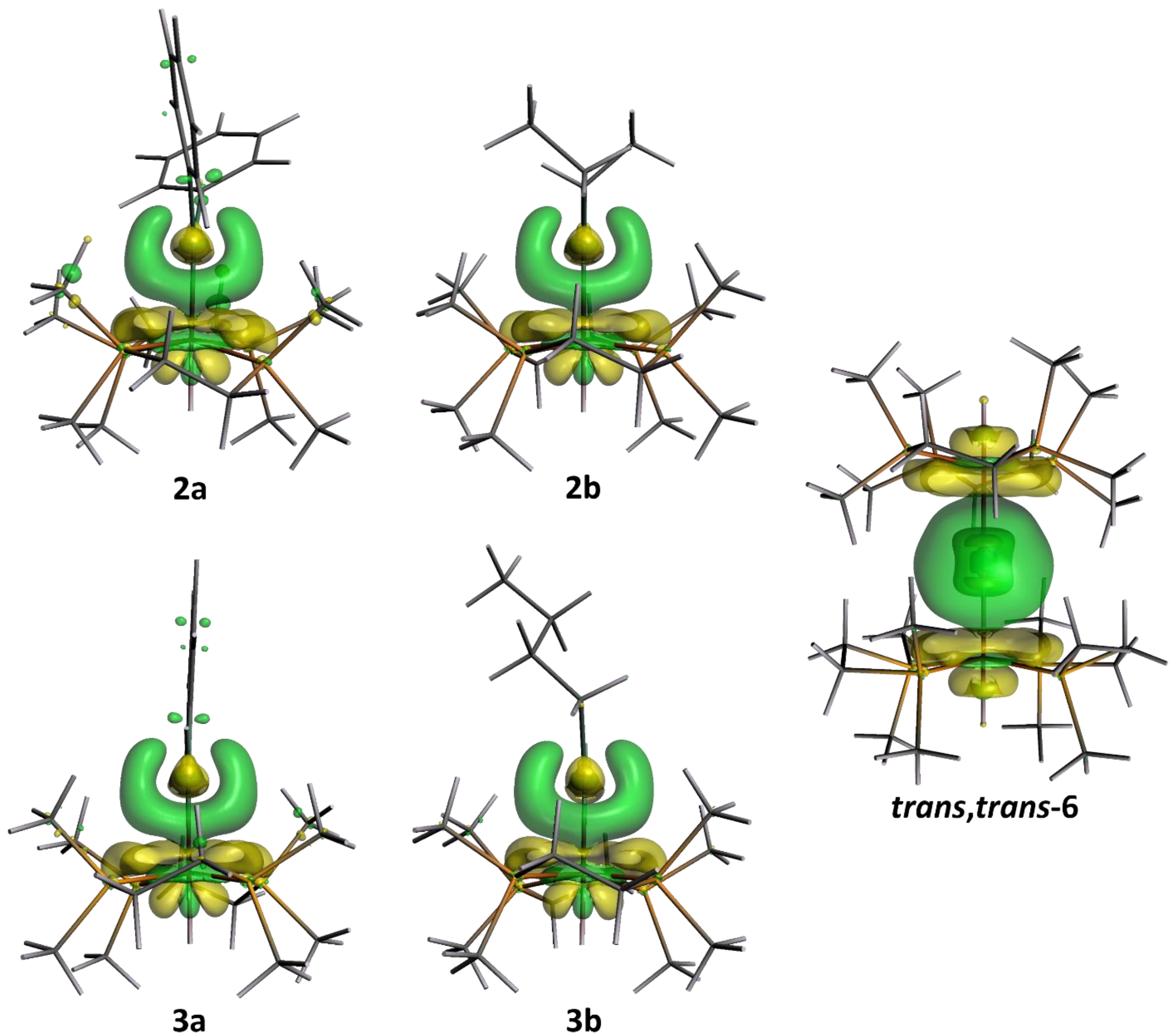

Figure S99. SCF deformation density isosurfaces from interaction calculations using neutral [(dmpe)$_2$MnH] and either germylene or Ge fragments for [(dmpe)$_2$MnH(=GePh$_2$)] (**2a**), [(dmpe)$_2$MnH(=GeEt$_2$)] (**2b**), [(dmpe)$_2$MnH(=GeHPh)] (**3a**), [(dmpe)$_2$MnH(=GeH^{n}Bu)] (**3b**), and *trans*,*trans*-[{(dmpe)$_2$MnH}$_2$(μ-Ge)] (***trans*,*trans*-6**), with isosurfaces set to 0.003. Increased (green) and decreased (yellow) electron density is presented relative to the fragments.

Selected ETS-NOCV Deformation Densities, NOCV Orbitals, and Fragment Orbital Contributors for 2a-b, 3a-b, and *trans*,*trans*-6.

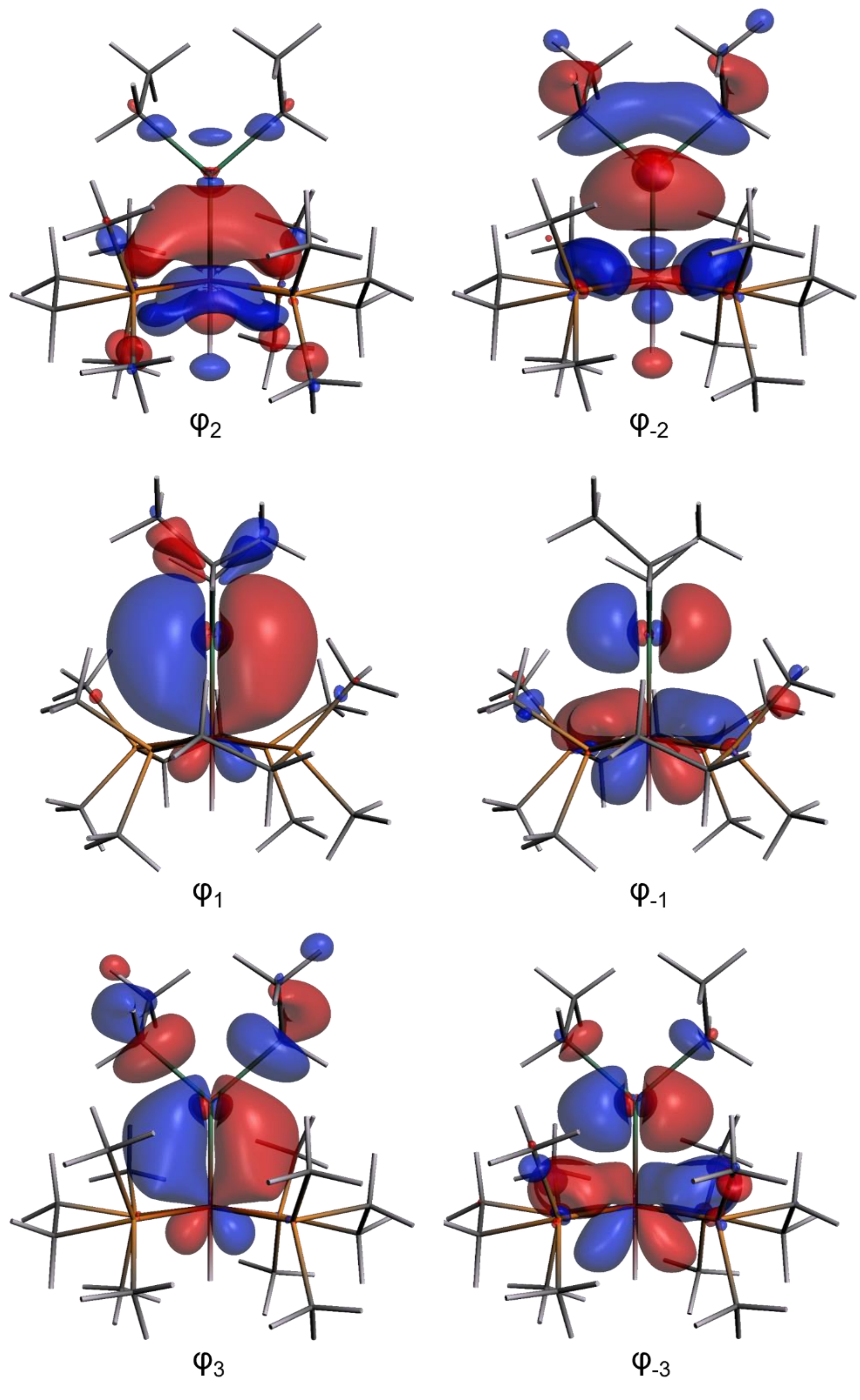

Figure S100. ETS-NOCV NOCV orbitals from interaction calculation using neutral [$(dmpe)_2MnH$] and $GeEt_2$ fragments for [$(dmpe)_2MnH(=GeEt_2)$] (**2b**), with isosurfaces set to 0.03. Associated deformation density contributions and main fragment orbitals can be found in Figure 7 (left).

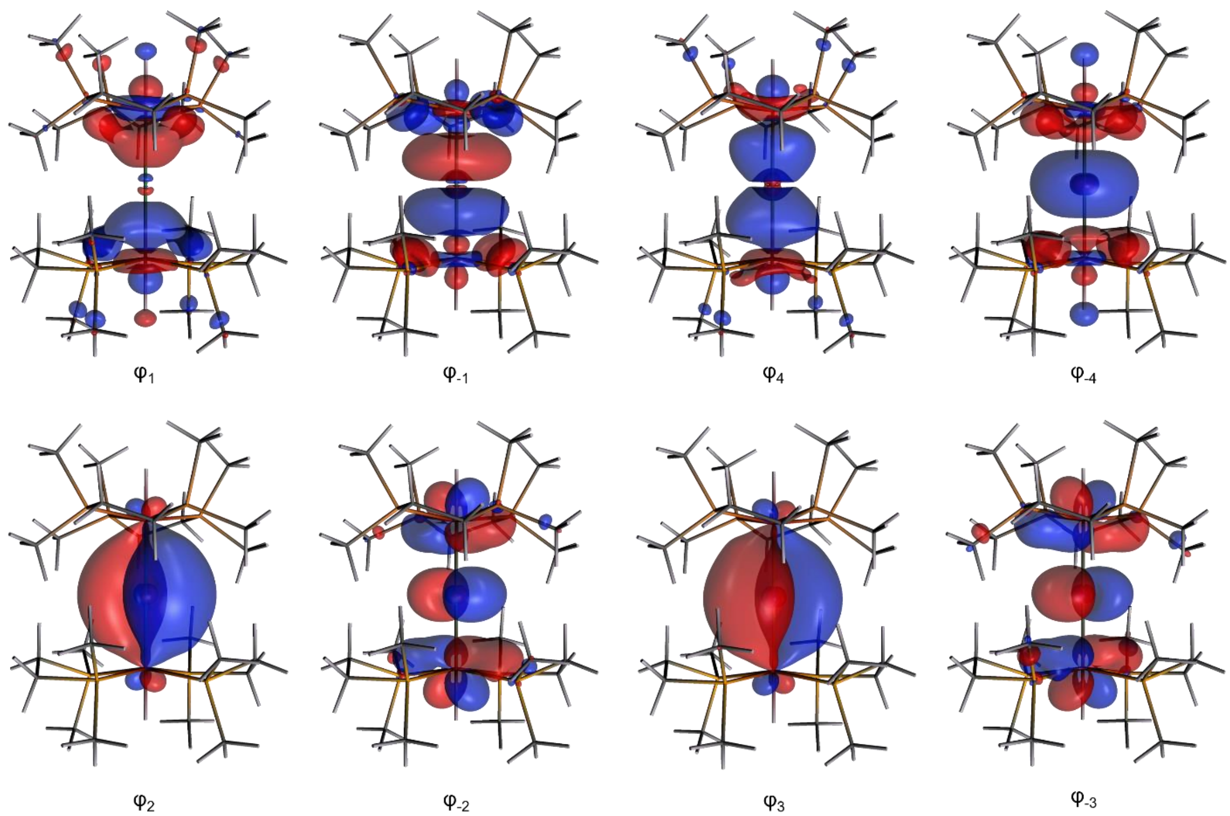

Figure S101. ETS-NOCV NOCV orbitals from interaction calculation using neutral [(dmpe)$_2$MnH] and Ge fragments for *trans*,*trans*-[{(dmpe)$_2$MnH}$_2$(μ-Ge)] (***trans*,*trans*-6**), with isosurfaces set to 0.03. Associated deformation density contributions and main fragment orbitals can be found in Figure 7 (right).

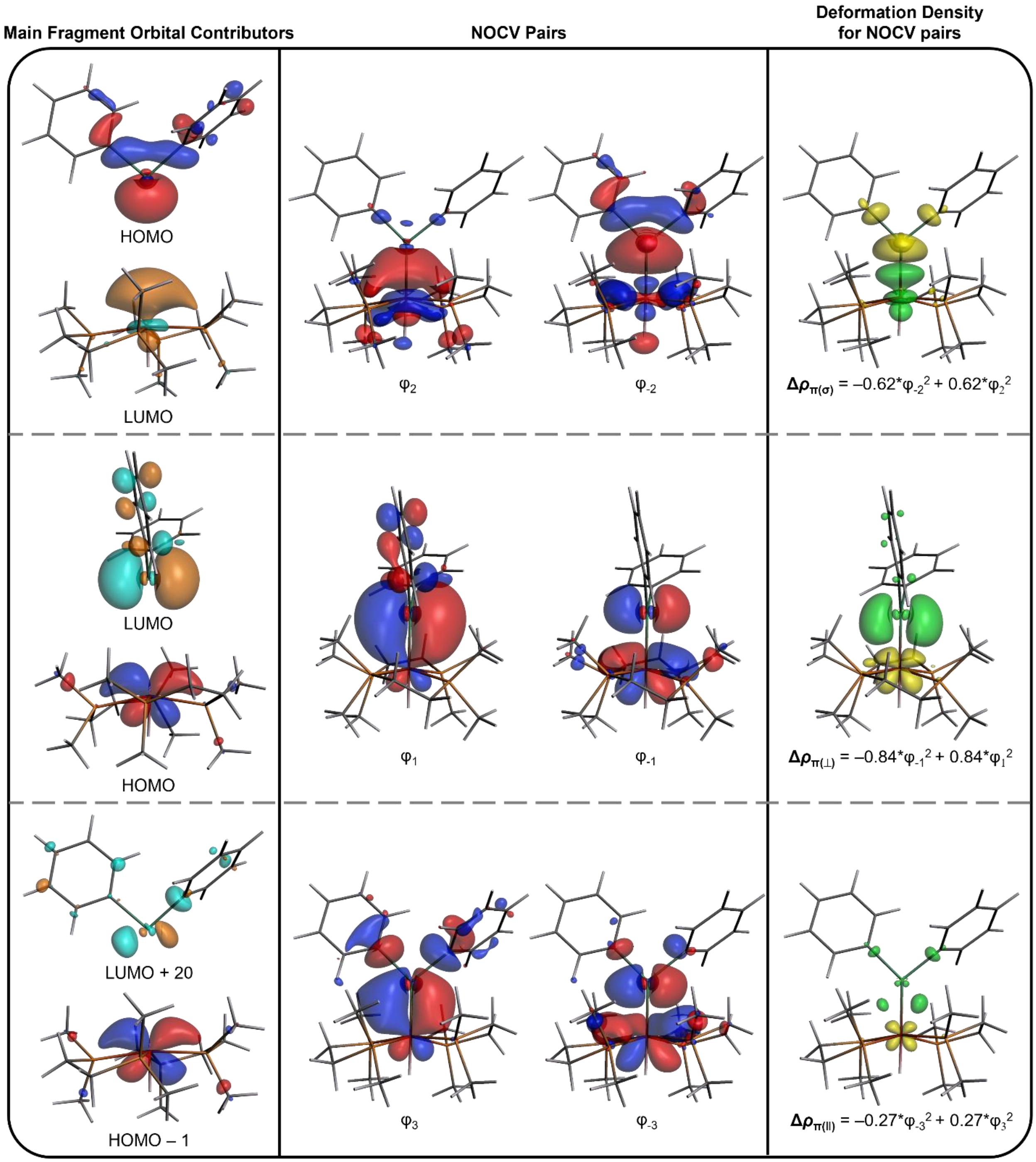

Figure S102. ETS-NOCV main fragment orbital contributors (left), NOCV orbitals (middle), and deformation densities (right) from interaction calculation using neutral [(dmpe)$_2$MnH] and GePh$_2$ fragments for [(dmpe)$_2$MnH(=GePh$_2$)] (**2a**), with isosurfaces set to 0.05, 0.03, and 0.003, respectively. Increased (green) and decreased (yellow) electron density is presented relative to the fragments.

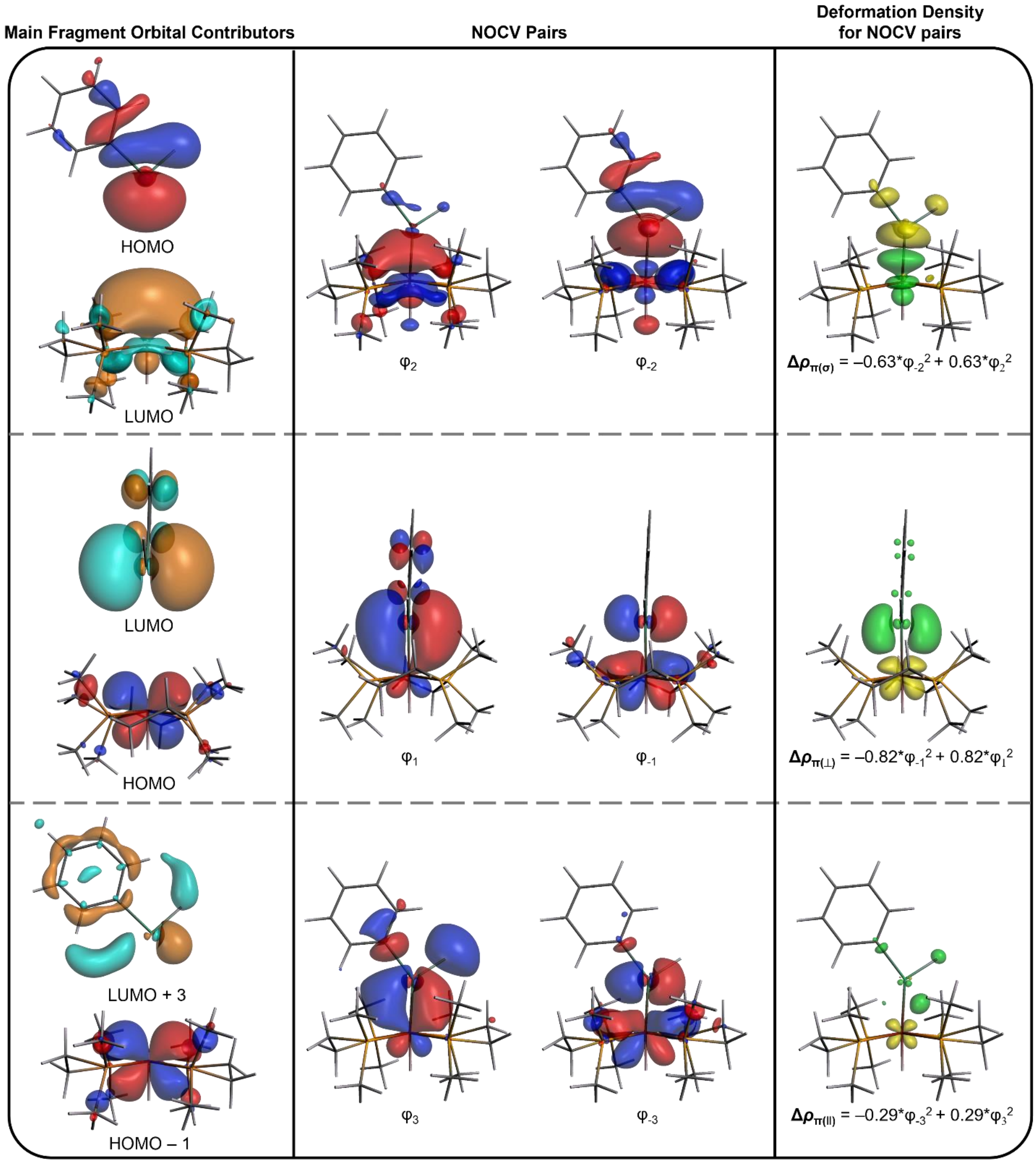

Figure S103. ETS-NOCV main fragment orbital contributors (left), NOCV orbitals (middle), and deformation densities (right) from interaction calculation using neutral [(dmpe)$_2$MnH] and GeHPh fragments for [(dmpe)$_2$MnH(=GeHPh)] (**3a**), with isosurfaces set to 0.03, 0.03, and 0.003, respectively. Increased (green) and decreased (yellow) electron density is presented relative to the fragments.

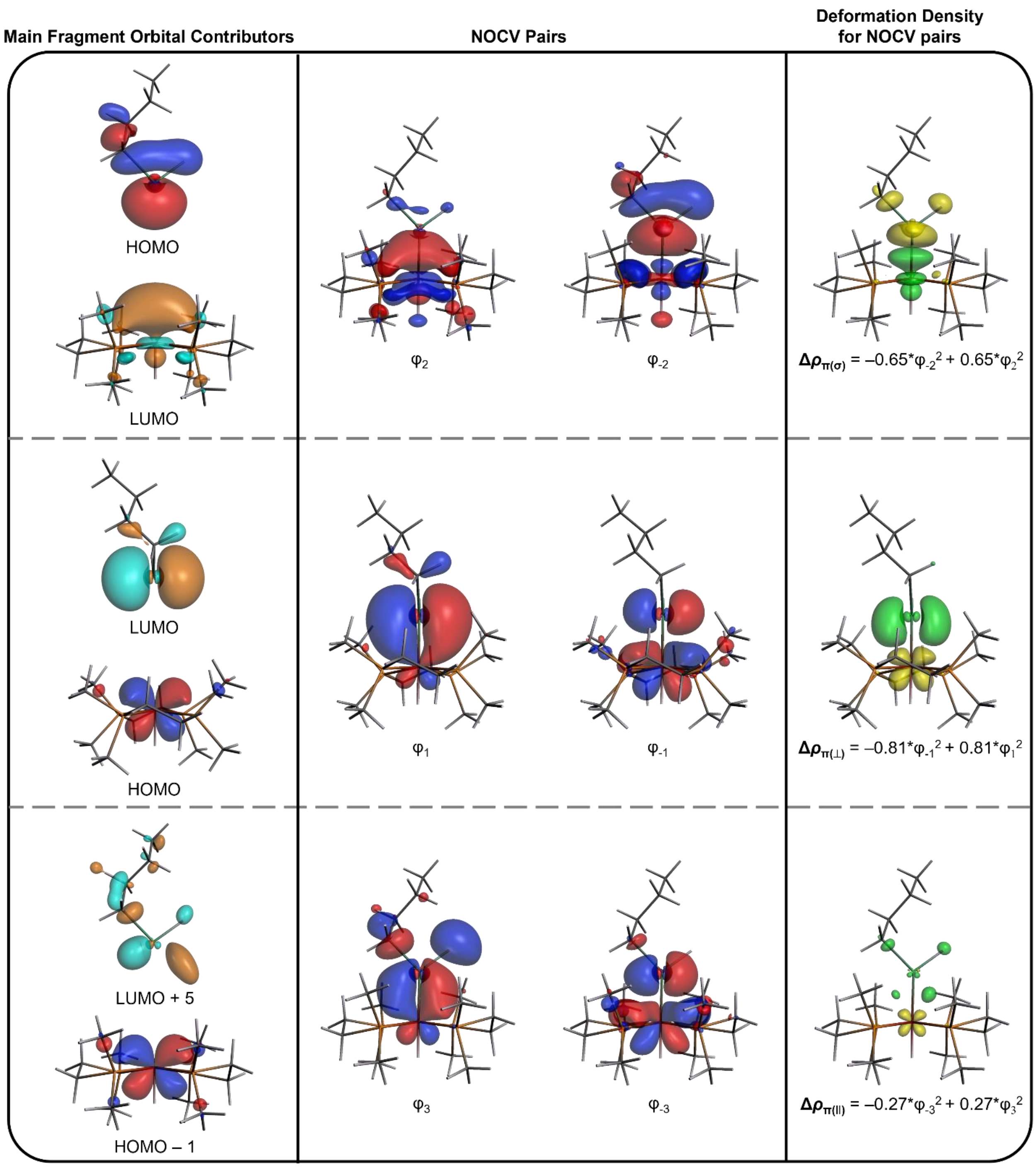

Figure S104. ETS-NOCV main fragment orbital contributors (left), NOCV orbitals (middle), and deformation densities (right) from interaction calculation using neutral [(dmpe)$_2$MnH] and GeH^{n}Bu fragments for [(dmpe)$_2$MnH(=GeH^{n}Bu)] (**3b**), with isosurfaces set to 0.04, 0.03, and 0.003, respectively. Increased (green) and decreased (yellow) electron density is presented relative to the fragments.

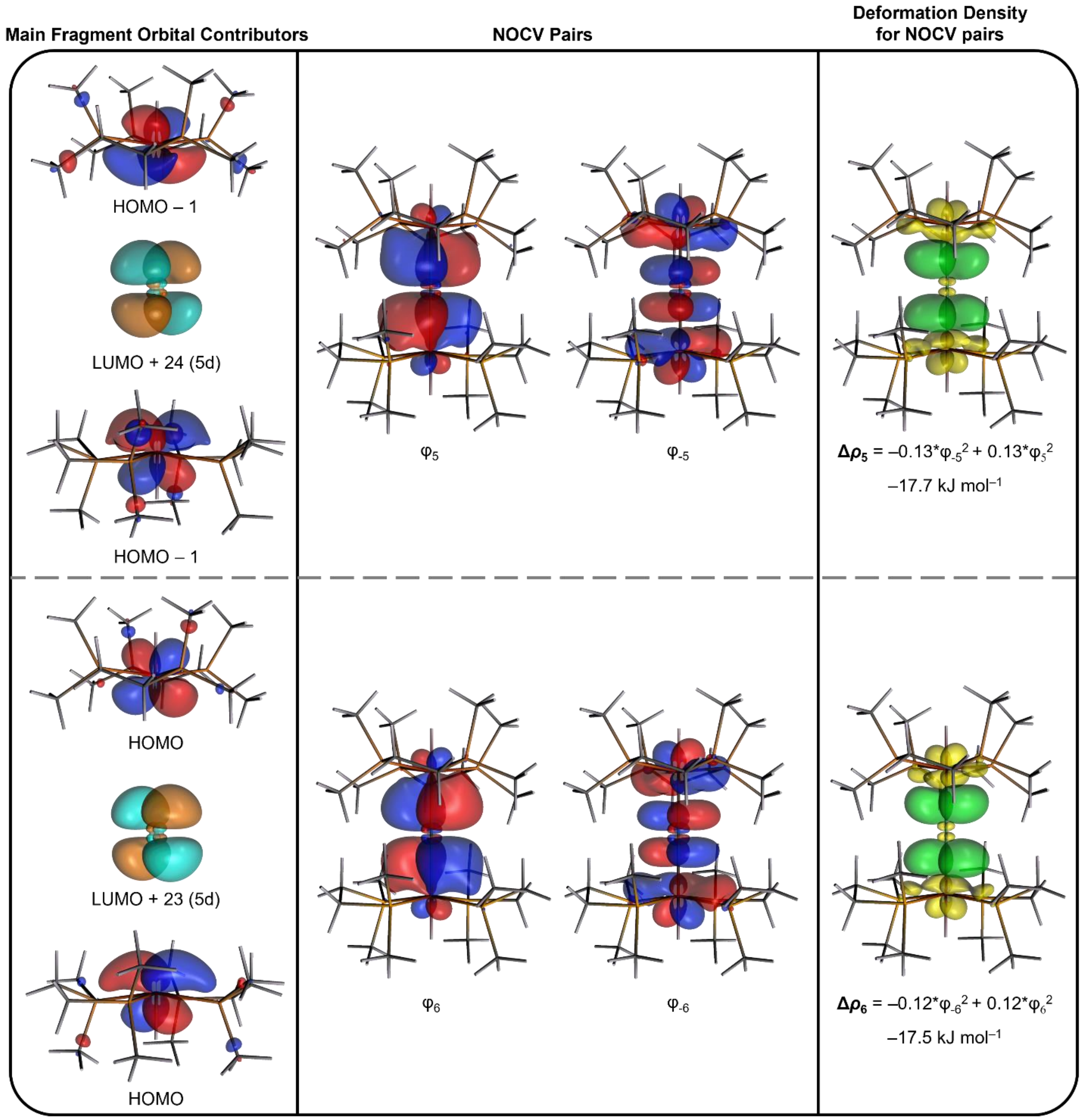

Figure S105. ETS-NOCV main fragment orbital contributors (left), NOCV orbitals (middle), and deformation densities (right) associated with polarization functions which enhance the Ge–Mn π backdonation interactions, from interaction calculation using neutral [(dmpe)$_2$MnH] and Ge fragments for *trans*,*trans*-[{(dmpe)$_2$MnH}$_2$(μ-Ge)] (***trans*,*trans*-6**), with isosurfaces set to 0.04, 0.03, and 0.003, respectively. Increased (green) and decreased (yellow) electron density is presented relative to the fragments. For the other four contributions to Mn–Ge–Mn bonding in ***trans*,*trans*-6**, the ETS-NOCV main fragment orbital contributors and deformation densities can be found in Figure 7 (right), and the NOCV orbitals can be found in Figure S101.

Miscellaneous

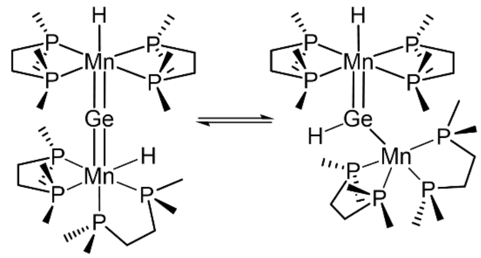

Scheme S1. Postulated reversible 1,1-insertion process for *cis*,*trans*-[{(dmpe)$_2$MnH}$_2$(μ-Ge)] (***cis,trans*-6**) to afford a fluxional 5-coordinate manganese centre, which could render all environments on the *cis*-[(dmpe)$_2$MnH] fragment equivalent on the NMR timescale, without causing *cis-trans* isomerization at manganese.

Table S11. Selected room temperature ^{1}H and ^{31}P NMR chemical shifts (ppm, C_6D_6 unless otherwise noted) for [(dmpe)$_2$MnH(=GePh$_2$)] (**2a**), [(dmpe)$_2$MnH(=GeEt$_2$)] (**2b**), [(dmpe)$_2$MnH(=GeHPh)] (**3a**), [(dmpe)$_2$MnH(=GeH^{n}Bu)] (**3b**), *mer*-[(dmpe)$_2$MnH(GeH$_2$Ph)$_2$] (**4a**), *mer*-[(dmpe)$_2$MnH(GeH$_2$^{n}Bu)$_2$] (**4b**), *trans*-[(dmpe)$_2$Mn(GeH$_2$Ph)(HGeH$_2$Ph)] (**5a**), *trans*-[(dmpe)$_2$Mn(GeH$_2$^{n}Bu)(HGeH$_2$^{n}Bu)] (**5b**), and the various isomers of [{(dmpe)$_2$MnH}$_2$(μ-Ge)] (**6**).

Complex	^{1}H NMR (Mn*H*)^a	^{1}H NMR (Ge*H*)	^{31}P NMR
2a	–10.02	–	79.67
2b	–10.79	–	79.90
3a	–9.18	12.68	78.64
3b	–9.82	12.38	78.55
4a	–11.37	4.94, 4.93	67.89, 62.05
4b^b	–10.41	4.09, 3.87	71.88, 59.44
5a	–11.96	4.72	64.93
5b^b	–12.01	3.71	68.03
***trans,trans*-6**	–22.67	–	68.97
***cis,trans*-6**	–10.93, –20.96	–	–
***cis,cis*-6**	–12.13	–	–

a This column includes hydrogen environments bridging between Mn and Ge.

b These spectra were obtained in *d*^{8}-toluene.